2011

SOLUTION PHASE AND MEMBRANE IMMOBILIZED IRON-BASED FREE RADICAL REACTIONS: FUNDAMENTALS AND APPLICATIONS FOR WATER TREATMENT

Scott Romak Lewis
University of Kentucky, romakulus@hotmail.com

ABSTRACT OF DISSERTATION

Scott Romak Lewis

The Graduate School

University of Kentucky

2011

SOLUTION PHASE AND MEMBRANE IMMOBILIZED IRON-BASED FREE RADICAL REACTIONS: FUNDAMENTALS AND APPLICATIONS FOR WATER TREATMENT

ABSTRACT OF DISSERTATION

A dissertation submitted in partial fulfillment of the
requirements for the degree of Doctor of Philosophy in the
College of Engineering
at the University of Kentucky

By
Scott Romak Lewis

Lexington, Kentucky

Director: Dr. Dibakar Bhattacharyya, Alumni Professor of Chemical Engineering

Lexington, Kentucky

2011

ABSTRACT OF DISSERTATION

SOLUTION PHASE AND MEMBRANE IMMOBILIZED IRON-BASED FREE RADICAL REACTIONS: FUNDAMENTALS AND APPLICATIONS FOR WATER TREATMENT

Membrane-based separation processes have been used extensively for drinking water purification, wastewater treatment, and numerous other applications. Reactive membranes synthesized through functionalization of the membrane pores offer enhanced reactivity due to increased surface area at the polymer-solution interface and low diffusion limitations. Oxidative techniques utilizing free radicals have proven effective for both the destruction of toxic organics and non-environmental applications. Most previous work focuses on reactions in the homogeneous phase; however, the immobilization of reactants in membrane pores offers several advantages. The use of polyanions immobilized in a membrane or chelates in solution prevents ferric hydroxide precipitation at near-neutral pH, a common limitation of iron(Fe(II/III))-catalyzed hydrogen peroxide (H_2O_2) decomposition. The objectives of this research are to develop a membrane-based platform for the generation of free radicals, degrade toxic organic compounds using this and similar solution-based reactions, degrade toxic organic compounds in droplet form, quantify hydroxyl radical production in these reactions, and develop kinetic models for both processes.

In this study, a functionalized membrane containing poly(acrylic acid) (PAA) was used to immobilize iron ions and conduct free radical reactions by permeating H_2O_2 through the membrane. The membrane's responsive behavior to pH and divalent cations was investigated and modeled. The conversion of Fe(II) to Fe(III) in the membrane and its effect on the decomposition of hydrogen peroxide were monitored and used to develop kinetic models for predicting H_2O_2 decomposition in these systems. The rate of hydroxyl radical production, and hence contaminant degradation can be varied by changing the residence time, H_2O_2 concentration, and/or iron loading. Using these membrane-immobilized systems, successful removal of toxic organic compounds, such as pentachlorophenol (PCP), from water was demonstrated.

Another toxic organic compound of interest for water treatment applications is trichloroethylene (TCE). Due to its limited solubility in water, a majority of the TCE is often present in the form of droplets. In this study, effective TCE droplet degradation

using chelate-modified, iron-catalyzed free radical reactions at near-neutral pH was demonstrated. In order to predict the degradation of aqueous and non-aqueous phase TCE for these reactions, a mathematical model was constructed through the use of droplet mass transfer correlations and free radical reaction kinetics.

KEYWORDS: Functionalized membrane, free radical, hydrogen peroxide, chelate-modified, membrane reactor

SCOTT ROMAK LEWIS

4/29/2011

SOLUTION PHASE AND MEMBRANE IMMOBILIZED IRON-BASED FREE RADICAL REACTIONS: FUNDAMENTALS AND APPLICATIONS FOR WATER TREATMENT

By

Scott Romak Lewis

DR. D. BHATTACHARYYA

Director of Dissertation

DR. S. RANKIN

Director of Graduate Studies

4/29/2011

Date

RULES FOR THE USE OF DISSERTATIONS

Unpublished dissertations submitted for the Doctor's degree and deposited in the University of Kentucky Library are as a rule open for inspection, but are to be used only with due regard to the rights of the authors. Bibliographical references may be noted, but quotations or summaries of parts may be published only with the permission of the author, and with the usual scholarly acknowledgements.

Extensive copying or publication of the dissertation in whole or in part also requires the consent of the Dean of the Graduate School of the University of Kentucky.

A library that borrows this dissertation for use by its patrons is expected to secure the signature of each user.

Name	Date

DISSERTATION

Scott Romak Lewis

The Graduate School

University of Kentucky

2011

SOLUTION PHASE AND MEMBRANE IMMOBILIZED IRON-BASED FREE RADICAL REACTIONS: FUNDAMENTALS AND APPLICATIONS FOR WATER TREATMENT

DISSERTATION

A dissertation submitted in partial fulfillment of the
requirements for the degree of Doctor of Philosophy in the
College of Engineering
at the University of Kentucky

By
Scott Romak Lewis

Lexington, Kentucky

Director: Dr. Dibakar Bhattacharyya, Alumni Professor of Chemical Engineering

Lexington, Kentucky

2011

ACKNOWLEDGEMENTS

First and foremost, I would like to thank Prof. Dibakar Bhattacharyya for his support and guidance through the past few years. His thoughtfulness and encouragement have been very important to me throughout my time at UK. I would also like him for encouraging me to get my M.S. degree and then convincing me to get my Ph.D. instead. I would like to thank Prof. Sylvia Daunert for guidance ever since I began the IGERT program. I would also like to thank the members of my doctoral committee: Prof. J. Zach Hilt and Prof. Bruce J. Hinds for providing technical input and helping me improve the finished product. I would also like to thank Dr. Marc Knecht for being on my committee. I would like to thank Prof. Lindell Ormsbee, director of the Kentucky Water Resources Research Institute, and Mr. Steve Hampson, associate director of the Kentucky Research Consortium for Energy and Environment, for insight regarding research and practical aspects of this project. Thank you as well to those who took the time to teach and familiarize me a wide variety of analytical techniques including Mr. John May, Ms. Tricia Coakley, and Dr. Frank Huggins.

I would like to thank the National Science Foundation – Integrative Graduate Education and Research Traineeship (NSF-IGERT), the National Institute of Environmental Health Sciences Superfund Research Program (NIEHS-SRP), NIEHS Supplement grant, and the Department of Energy (DOE) for the funding of this research.

I am very fortunate to have many fond memories of my experience as a graduate student. Despite the never-ending list of things to do, I thank my classmates and friends within the department for keeping things fun and interesting and leaving me with

memories I will never forget, especially Mr. Vence Easterling, Dr. Harry Hunter, Mr. Chris Laine, Dr. John Medley, Mr. Paritosh Wattamwar, and Mr. Vinod Kanniah.

To my labmates past and present: Mr. Morgan Campbell, Dr. David Meyer, Mr. Noah Meeks, Mr. Peter Frailie, Dr. Vasile Smuleac, Dr. Abhay Ladhe, Dr. Saurav Datta, Dr. Yongchao Li, Mrs. Li Xiao, Mr. Minghui Gui, Dr. Yit Hong Tee and previous undergraduate students: Mr. Andrew Lynch, Mr. Alex Montague, Mr. Joel Vice, Mr. Eric Coker, Mr. Joe Amundson, Mr. Andrew Boyer, and Mr. Zach Zimmerman, thank you for making lab a good place to work. I'd like to extend a special thanks to Morgan and Dave for their excellent advice on anything from lab to everyday life and to Peter and Andrew L. for challenging me scientifically (and strategically). I would also like to thank my roommate of five years who has made me laugh harder than anyone else. Tyler, thanks buddy.

I owe a special thanks to Miss Ashley Hawkins for all of the emotional and technical support she has provided me. It has been a long journey and she was always willing to lend a helping hand. I thoroughly enjoyed the innumerable lunchtime conversations and ideas we were able to develop.

Most importantly, this journey would not have been possible without my parents, sister, and other family members who have supported me every step of the way. I cannot express how thankful I am to have them as such an integral part of my life. Mom and Dad, not only did you pass the ChemE gene on to me, but the lessons you taught me helped me get to where I am today.

Table of Contents

List of Tables

List of Figures

Chapter 1 Introduction

Free radical reactions are of great importance to biological and chemical systems ranging from medical applications to biotechnology to environmental remediation. For the latter, conventional iron-catalyzed H_2O_2 decomposition (standard Fenton reaction) has been used extensively for the generation of free radicals for the destruction of toxic organic compounds at low pH. Through the addition of a chelating agent or immobilization within a functionalized synthetic membrane, these reactions can be conducted efficiently at near-neutral pH. They can also be used to control the rate of H_2O_2 decomposition and membranes functionalized with negatively-charged polyelectrolytes provide the additional benefits of preventing iron loss and those associated with responsive behavior. The purpose of this work is to better understand these free radical reactions at near-neutral pH in the presence of such complexing agents, how they can be used to conduct interfacial reactions in membrane and solution-based systems for the degradation of toxic organic compounds, and to develop quantitative models for the prediction of reactant behavior in both systems.

This chapter summarizes and outlines the relevance and objectives of the work contained in this dissertation. Background information and the materials and methods used are given in Chapters 2 and 3, respectively. The first section of this dissertation outlines the importance of free radical reactions and how their highly-emphasized detrimental effects to biological systems can be used to effectively degrade contaminants present in water (Chapter 4). The second section describes the importance of synthetic membranes to water purification and how, through functionalization, they can be used for catalytic, oxidation-based contaminant degradation (Chapter 5). Modeling of the reactivity of the membrane-immobilize iron-catalyzed H_2O_2 decomposition reactions and pH-responsive behavior of this system as well as the use of such platforms for the destruction of model cells are also discussed (Chapters 6 and 7). Finally, the plan for the implementation of these oxidative, as well as iron-based reductive, technologies at a Superfund site is discussed (Chapter 8).

1.1 Solution phase, iron-based free radical reactions

Providing access to safe drinking water has been identified as one, and possibly the most important, of the grand challenges facing scientists in the 21st century (Omenn 2006). The contamination of groundwater aquifers by toxic organic compounds is a widespread problem that prevents these potentially potable sources from being used for drinking water. Many chemical processes have been developed for the remediation of such waters and include the use of oxidative and reductive pathways. Some of these oxidative methods utilize highly reactive free radicals to degrade and potentially mineralize these harmful compounds. Although there has been much research done on how to prevent the formation of free radicals in biological systems to prevent oxidative damage, the focus of this research is to enhance free radical production near neutral pH conditions. The fundamental reactions used to generate the free radicals were based on the well-established iron-catalyzed decomposition of H_2O_2, which takes place most efficiently at low pH.

In the United States, approximately two-thirds of the over 1,200 most serious hazardous waste sites in the nation are contaminated with trichloroethylene (TCE), a potentially carcinogenic compound. TCE and similar species represent the large class of chlorinated organics responsible for the contamination of many potential drinking water sources around the world. Various studies have investigated the use of free radical reactions to degrade TCE (Pignatello et al. 2006). Due to its limited solubility in water, TCE readily forms droplets, providing a unique opportunity to study the free radical reactions taking place at the well-defined droplet-water interface. The specific objectives were:

- Investigate the fundamental Fe(II) to Fe(III) conversion and hydroxyl radical generation in iron-catalyzed H_2O_2 decomposition
- Demonstrate degradation of TCE droplets using iron-catalyzed H_2O_2 decomposition at low pH
- Control free radical production at near-neutral pH via addition of a chelating agent

- Investigate effects of complexation of iron ions by a chelating agent on iron speciation and H_2O_2 decomposition
- Utilize these modified reactions to degrade target contaminant in actual groundwater
- Demonstrate degradation of TCE present as droplets and dissolved in the aqueous phase using interfacial iron-catalyzed free radical reactions at near-neutral pH
- Develop a kinetic model to predict the solution and interfacial reactions for the degradation of TCE in both aqueous and droplet phases at near-neutral pH
- Apply modified free radical reactions to degrade TCE in a simulated groundwater aquifer

1.2 Membrane immobilized, iron-based free radical reactions

Functionalized membrane materials can be used to complex iron ions in a similar manner to the chelating compounds described in the previous section. Recent advances in membrane technology have led to an increased use of synthetic membranes for water treatment including the removal of viruses and unwanted chemicals from contaminated sources of water (Shannon et al. 2008). Traditionally, synthetic membranes have been used as permeable barriers for the physical separation of two bulk phases, permitting the transport of solutes based on size or differences in diffusion/sorption rates. By functionalizing these membranes with a stimuli-responsive polymer present as either grafted chains or a crosslinked network, the dimensions of the pores can be controlled by simple modulation of the stimulus (light, pH, ionic strength, etc.) resulting in the formation of a controllable nanoporous structure (Wandera et al. 2010). Functionalization of a poly(vinylidene fluoride) (PVDF) support membrane with poly(acrylic acid) (PAA) creates a pH-responsive membrane capable of capturing cations via ion exchange. When operated under pressure-driven convective flow, these membranes provide reactants rapid access to active sites, thereby minimizing the mass transfer limitations associated with other high surface area-to-volume materials. By immobilizing the iron species required for free radical generation from H_2O_2 within such platforms, no separation of the iron species from the treated effluent is required. The specific objectives were:

- Characterize the PVDF-PAA membrane's composition, structure, and permeability
- Investigate and model the pH-responsive behavior of these membranes
- Determine the effect of multivalent cations on membrane performance as well as the stability of iron ions post-capture
- Determine reactivity of membranes containing immobilized iron ions (PVDF-PAA-Fe(II)/Fe(III)) with H_2O_2
- Develop kinetic models for H_2O_2 decomposition by iron ions immobilized in PVDF-PAA membranes
- Develop a kinetic model for the degradation of target organic compounds via membrane-immobilized iron-catalyzed free radical reactions
- Investigate applicability of membrane-immobilized iron-catalyzed H_2O_2 decomposition reactions for the destruction of model cells
- Utilize PVDF-PAA platform for the facile synthesis of iron oxide/ferrihydrite nanoparticles

Chapter 2 Background

This chapter provides an overview of the literature studies on free radical reactions and functionalized membranes. It begins with a discussion on the formation and importance of free radicals to biological systems. This is followed by a discussion on how free radical generating systems have been used to remove toxic organic compounds from water. Next, the basis for a different type of water treatment technology, filtration via the use of synthetic membranes, is outlined and continues into how these materials can be functionalized to extend their use to a multitude of other applications.

2.1 Free radical reactions

Free radicals are atoms or molecules that contain one or more unpaired electrons. As such, they are highly reactive in nature, with few exceptions, and can be found throughout biological and a variety of chemical systems. Since the reactions associated with the formation of free radicals may not be sufficiently controlled by normal biological mechanisms, excessive free radical formation can have deleterious effects on biomolecules (Valko et al. 2005). Because of this, there a tremendous amount of research has been devoted to investigating and trying to limit the formation of free radicals in biological systems (Beckman et al. 1990; Djuric et al. 2001). Nonetheless, these reactions are still necessary for normal biological function. For instance, in the body's response to infection, free radicals, specifically reactive oxygen species (ROS) and reactive nitrogen species (RNS), play important roles in signaling and tissue injury mediation and are some of the species generated by antimicrobial systems of phagocytes (Fang 2004).

One of the most reactive ROS is the hydroxyl radical (OH•), which is an electrophile and strong oxidizing agent (E^0=2.73 V). The reaction of hydroxyl radicals in aqueous solution can be classified into four categories: addition, hydrogen abstraction, electron transfer, and radical interaction (Dorfman et al. 1973). Addition occurs when the hydroxyl radical reacts with an unsaturated compound, forming a free radical. Hydrogen abstraction occurs when the hydroxyl radical abstracts a hydrogen atom from another compound, forming water and a free radical. Electron transfer generally occurs with

multivalent ions and results in the oxidation of the ion and the formation of a hydroxide ion. Radical interaction, or termination, occurs when the hydroxyl radical reacts with another radical to form a stable product.

Although there are various mechanisms by which ROS are formed, metal-based reactions are responsible for many of the undesirable effects that take place in biological systems including enhanced lipid peroxidation and DNA base modification (Welch et al. 2002). Additionally, the "autoxidation" of various biomolecules may actually be dependent upon their coordination with metallic ions, which can act as a mediator between the biomolecule and molecular oxygen (Miller et al. 1990). One example is ascorbic acid, which binds to Fe(III), reduces it to Fe(II), which is oxidized by molecular oxygen to form Fe(III) and superoxide (Miller et al. 1990). One of the main mechanisms for hydroxyl radical generation is from the reaction of a transition metal ion with hydrogen peroxide (H_2O_2):

$$M^{n+} + H_2O_2 \rightarrow M^{(n+1)+} + OH^- + OH\bullet$$

For biological systems, these can include metal ions of copper, cobalt, chromium, vanadium, cadmium, and arsenic; however, one of the most reactive and well-studied is iron (Valko et al. 2005). Iron's most common oxidation states are Fe(II) and Fe(III), but other species have been isolated, including the ferryl ion, Fe(IV). The mechanism for the formation of free radicals from Fe^{2+} and H_2O_2 was first proposed by Haber and Weiss in 1934 and is referred to as the standard Fenton reaction (Fenton's reagent) (Barb et al. 1949; De Laat and Gallard 1999):

$$Fe^{2+} + H_2O_2 \rightarrow Fe^{3+} + OH^- + OH\bullet \qquad k_1 = 63\ M^{-1}s^{-1} \qquad (2.1)$$

The rate constant of this reaction is widely reported as 63 $M^{-1}s^{-1}$, but varies with pH due to Fe(II) speciation (Kwan and Voelker 2003). Through a series of propagation reactions (Reactions 2.2 - 2.16), ferric iron is reduced to ferrous iron then reacts to form more hydroxyl radicals via Reaction 2.1 (Ravikumar and Gurol 1994; Lin and Gurol 1998; De Laat and Gallard 1999; Wang and Lemley 2001; Pignatello et al. 2006). Iron is said to be catalytic in this respect. It should also be noted that the rate constant for Reaction 2.2 is four orders of magnitude lower than that of Reaction 2.1, and therefore can be considered the rate-limiting step in this catalytic cycle.

$Fe^{3+} + H_2O_2 \rightarrow Fe^{2+} + HO_2\bullet + H^+$ $k_2 = 2 \times 10^{-3}\ M^{-1}\ s^{-1}$ (2.2)

$Fe^{2+} + OH\bullet \rightarrow Fe^{3+} + OH^-$ $k_3 = 3.2 \times 10^{8}\ M^{-1}\ s^{-1}$ (2.3)

$Fe^{2+} + HO_2\bullet \rightarrow Fe^{3+} + HO_2^-$ $k_4 = 1.2 \times 10^{6}\ M^{-1}\ s^{-1}$ (2.4)

$Fe^{2+} + O_2^-\bullet + 2H^+ \rightarrow Fe^{3+} + H_2O_2$ $k_5 = 1 \times 10^{7}\ M^{-1}\ s^{-1}$ (2.5)

$Fe^{3+} + HO_2\bullet \rightarrow Fe^{2+} + O_2 + H^+$ $k_6 = 2 \times 10^{3}\ M^{-1}\ s^{-1}$ (2.6)

$Fe^{3+} + O_2^-\bullet \rightarrow Fe^{2+} + O_2$ $k_7 = 5 \times 10^{7}\ M^{-1}\ s^{-1}$ (2.7)

$H_2O_2 + OH\bullet \rightarrow H_2O + HO_2\bullet$ $k_8 = 3.3 \times 10^{7}\ M^{-1}\ s^{-1}$ (2.8)

$H_2O_2 + HO_2\bullet \rightarrow H_2O + O_2 + OH\bullet$ $k_9 = 3.1\ M^{-1}\ s^{-1}$ (2.9)

$OH\bullet + OH\bullet \rightarrow H_2O_2$ $k_{10} = 6 \times 10^{9}\ M^{-1}\ s^{-1}$ (2.10)

$OH\bullet + HO_2\bullet \rightarrow H_2O + O_2$ $k_{11} = 7.1 \times 10^{9}\ M^{-1}\ s^{-1}$ (2.11)

$OH\bullet + O_2^-\bullet \rightarrow OH^- + O_2$ $k_{12} = 1.01 \times 10^{10}\ M^{-1}\ s^{-1}$ (2.12)

$HO_2\bullet + HO_2\bullet \rightarrow H_2O_2 + O_2$ $k_{13} = 8.3 \times 10^{5}\ M^{-1}\ s^{-1}$ (2.13)

$HO_2\bullet + O_2^-\bullet + H_2O \rightarrow H_2O_2 + O_2 + OH^-$ $k_{14} = 9.7 \times 10^{7}\ M^{-1}\ s^{-1}$ (2.14)

$HO_2\bullet \rightarrow H^+ + O_2^-\bullet$ $k_{15} = 1.58 \times 10^{5}\ s^{-1}$ (2.15)

$H^+ + O_2^-\bullet \rightarrow HO_2\bullet$ $k_{16} = 1 \times 10^{10}\ M^{-1}\ s^{-1}$ (2.16)

Where $O_2\bullet^-$ is superoxide radical anion, $HO_2\bullet$ is perhydroxyl radical, and HO_2^- is hydroperoxide anion, all of which have been associated with oxidative damage to biomolecules. Due to the destructive nature of excessive quantities of free radicals to biological systems, a myriad of studies have been conducted on using these reactions to degrade unwanted compounds present in surface and groundwaters.

2.2 Chemical processes for the degradation of toxic organic compounds

Various chemical-based treatment technologies exist for the detoxification of contaminated water sources. These include oxidative and reductive technologies which can be used for the treatment of toxic organic compounds above or below ground. Most advanced oxidative processes (AOPs) involve the generation of free radicals, which can be utilized for the degradation of various pollutants (Pignatello et al. 2006) and

disinfection (Kohanski et al. 2010). Photolytic degradation involves the use of a light source (usually UV) either by itself, with a photocatalyst (such as TiO_2 nanoparticles or Fe(II/III)), or with a photocatlyst and an oxidant (such as H_2O_2) (Pandiyan et al. 2002). Ozone (O_3) is an oxidant that must be produced on-site and can react with pollutants either directly or via free radical formation (Watts and Teel 2006). The use of peroxides, such as H_2O_2, and a catalyst, such as iron, is also very effective for the rapid generation of free radicals and subsequent oxidation of pollutants.

The reactants used for the standard Fenton reaction are environmentally friendly and inexpensive, especially when compared to other oxidative techniques. Hydrogen peroxide has a wide variety of industrial applications, especially as a bleaching agent, but is also used as a household antiseptic and even rocket propellant (Patnaik 2003). The main method of commercial production is via the autooxidation of ethyl anthraquinol in an organic solvent (Patnaik 2003). As shown in Reaction 2.1, when Fe(II) and H_2O_2 react, the hydroxyl radical is produced, which reacts with most organic contaminants (Haber and Weiss 1934). Although other radical species are present during this process (Pignatello et al. 2006), hydroxyl radicals are responsible for the majority of contaminant degradation which proceeds as follows for a chlorinated organic compound, A (Benitez et al. 1999):

$$A + OH\bullet \longrightarrow I \xrightarrow{OH\bullet} P + Cl^- \qquad (2.17)$$

Where *I* represents the intermediate compounds formed and P represents the oxidized products of the chlorinated organics. The hydroxyl radical's reaction rate with most organic contaminants is on the order of 10^8 – 10^{10} M^{-1} s^{-1} and is therefore diffusion limited (~10^{10} M^{-1} s^{-1} in water) (Watts and Teel 2005). Although these free radical reactions are highly effective for degrading organic contaminants, they may require the addition of other reagents and downstream processing for the removal of iron precipitates from water.

Several problems arise when applying this process to contaminated groundwater and/or wastewater effluent. The high buffering capacity of these systems maintains a near-neutral pH, resulting in the precipitation of Fe(III) as $Fe(OH)_3$ (Watts and Teel 2005). Lowering the solution pH may be a feasible solution for small treatment areas; however, this is not the case for larger areas. $Fe(OH)_3$ precipitation not only prevents

Fe(III) from reducing to Fe(II), but can also cause injection-well plugging in the case of *in situ* treatment. Other problems include rapid heat generation, limited mobility of the reactants, and the hazards of transporting highly concentrated hydrogen peroxide. This raises the following question: if it is difficult to maintain free radical generation in groundwater at near-neutral pH due to iron precipitation, why are free radical reactions so prevalent in biological systems which are maintained at physiological pH? The answer lies in the fact that biological systems have various biomolecules and ligands that are capable of complexing with the iron ions, thereby preventing their precipitation from solution. These include high-capacity, low-affinity proteins such as ferritin (~4500 atoms of iron per molecule) and low-capacity, high affinity proteins such as transferrin (2 atoms of iron per molecule) (Valko et al. 2005). Similarly, the standard Fenton reaction can be modified with a chelating agent to prevent the precipitation of iron out of solution for water treatment applications.

2.3 Chelate-modified Fenton reaction

Various modified Fenton or "Fenton-like" processes are popular AOPs that have adjusted the standard Fenton reaction by adding thermal, chemical, electrochemical, or photolytic enhancements to eliminate some of the problems mentioned earlier (Laine and Cheng 2007). The problems related to the application of the standard Fenton reaction for water treatment can also be alleviated through the use of the chelate-modified Fenton reaction. This involves the addition of a nontoxic chelate (L) such as citrate or gluconic acid. The chelate is capable of binding ferrous and ferric iron, reducing concentrations of Fe(II) and Fe(III) in solution. This limits the amounts of Fe(II) and Fe(III) available for reaction with H_2O_2 thus controlling the rate of hydroxyl radical generation. The use of a chelate for remediation in aerobic environments also minimizes Fe(II) oxidation by O_2. Li et al. (2007) demonstrated that dissolved oxygen has no effect on the degradation of trichlorophenol (TCP) by the chelate-modified Fenton reaction using poly(acrylic acid) (PAA) as the complexing agent. Sun and Pignatello (1992) documented the interactions of dozens of chelating agents, such as EDTA and catechol, with Fe(III) as well as their effect on the reactivity of the Fe(III)-chelate complexes with H_2O_2 for 2,4-D oxidation. A

modified Fenton reaction using crosslinked chitosan as the chelating agent has also been used for the oxidative degradation of trichloroethylene (TCE) (Lee and Lee 2010). TCE is a common pollutant found in many groundwater aquifers that has proven to be very difficult to remove (see Section 2.6). Additionally, gluconic acid and hydrogen peroxide can be generated on-site, eliminating the need for transportation of highly concentrated hydrogen peroxide (Ahuja et al. 2007).

A chelating agent can also be incorporated onto various surfaces, creating a platform for iron immobilization. High-capacity ion exchange materials can also be used to immobilize iron ions. Despite the high capacity of ion exchange beads, mass transport is dependent on diffusion, which can make for slow rates of degradation if H_2O_2 and the target organic compound must diffuse in and out of the beads' micro and mesopores. However, by making this ion exchange material, and hence the iron ions immobilized within it, highly accessible to the reactants, the overall rate of reaction can be increased. Synthetic membranes containing these ion exchange groups provide the opportunity to permeate the reactants through the membrane pores via pressure-driven flow, thereby providing the reactants greater access to the immobilized iron ions.

2.4 Synthetic membranes and membrane functionalization

In many industries, the separation step of a given process may be the most important and costly. Industries ranging from biomedical and pharmaceutical to water treatment and food and beverage processing rely on synthetic membranes for the manufacture of products including chemicals and electronics (Ho and Sirkar 1992; Charcosset 2006; Fritzmann et al. 2007; Stamatialis et al. 2008). However, these processes can be energy-intensive when used for the removal of toxic organic compounds from water and the resulting concentrated waste stream must undergo further processing. Conventional membrane processes can be based on size (microfiltration, MF; ultrafiltration, UF), charge and/or size (nanofiltration, NF), or solubility (reverse osmosis, RO; pervaporation, PV) of species (Noble and Stern 1995; Bhattacharyya and Butterfield 2003; Ng and Kim 2007). With the intent of imitating the multiple functionalities characteristic of naturally occurring membranes, various polymers, biological

compounds, nanostructures, and functional groups have been incorporated onto the surfaces of synthetic membranes, extending their applicability to more advanced separation processes (Jirage et al. 1997; Lee et al. 2002; Merkel et al. 2002; Letant et al. 2003; Hinds et al. 2004; Kumar et al. 2007; Park et al. 2007; Stuart et al. 2010) and catalysis (Lu et al. 2006).

A wide variety of ligands have been used for membrane functionalization, the most common being polymers, aminoacids/polyaminoacids, metal affinity, ion exchange, etc. (Klein 2000; Shi et al. 2008). Among these, membrane modification with ion exchange ligands has received extensive attention in a variety of processes and applications including nanofiltration (Hollman and Bhattacharyya 2004; Hu and Dickson 2007), enzyme immobilization and biocatalysis (Smuleac et al. 2006; Datta et al. 2008), catalysis (Kidambi and Bruening 2005; Shah et al. 2005), and heavy metal capture (Ritchie et al. 1999; Hestekin et al. 2001; Sgarlata et al. 2008; Ladhe et al. 2009; Vasudevan et al. 2009). Layer-by-layer (LbL) assemblies have gained considerable attention as a facile method for the functionalization of a variety of surfaces including the selective functionalization of membrane pores and/or exterior surfaces (Bruening et al. 2008). Figure 2.1 illustrates two ways by which membrane pores can be functionalized with polyelectroyltes for enzyme immobilization. Previous work has demonstrated that the immobilization of glucose oxidase (GOx) in membrane-based LbL assemblies increases enzyme stability and maintains reactivity (Smuleac et al. 2006; Datta et al. 2008). These functionalized membranes have been used for the enzymatic generation of H_2O_2 from glucose and oxygen and can be operated under convective flow (Duke et al. 1969).

2.5 Stimuli-repsonsive membrane behavior

By functionalizing synthetic membranes with a stimuli-responsive polymer present as either grafted chains or a crosslinked network, the dimensions of the pores can be controlled by simple modulation of the stimulus resulting in the formation of a controllable nanoporous structure. Many of the same techniques used for the functionalization of other surfaces can be used to modify membrane surfaces and pores as

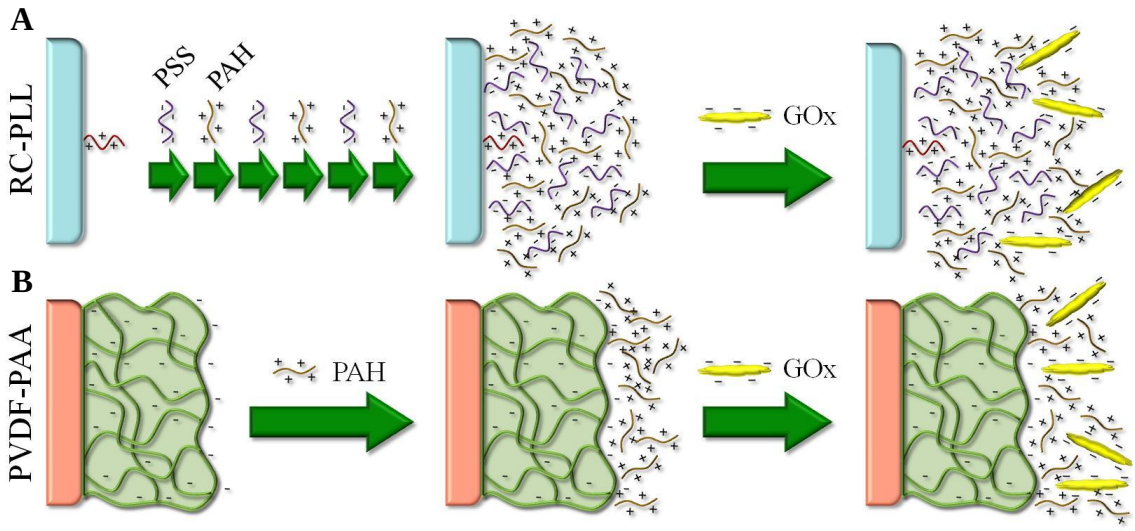

Figure 2.1. Schematic of electrostatic enzyme immobilization in layered polyelectrolyte membrane platforms. (A) Epoxide-activated regenerated cellulose (RC) membrane with covalently-attached poly(L-lysine-hydrochloride) (PLL). The (+)-charged PLL serves as the base for alternating layers of (-)-charged poly(styrene sulfonate) (PSS) and (+)-charged poly(allylamine hydrochloride) (PAH). The enzyme of interest, glucose oxidase, GOx, is negatively charged at neutral pH and therefore is immobilized in the outer PAH layer. (B) Similar to (A) except that the base membrane of poly(vinylidene fluoride) (PVDF) has been functionalized with (-)-charged poly(acrylic acid) (PAA) gel. This is followed by the addition of a layer of PAH and subsequent GOx.

well. Temperature-responsive membranes can be synthesized through the incorporation of poly(N-isopropylacrylamide) (PNIPAAm) which exists in a swollen state at temperatures below its lower critical solution temperature (LCST) and collapses at temperatures above its LCST (Schild 1992). Several investigators have used PNIPAAm-functionalized membranes to control the rejection of various solutes by varying the temperature of the system (Spohr et al. 1998; Liang et al. 1999; Reber et al. 2001). Photo-responsive membranes require the incorporation of photo-chromic monomers within the polymer being used to functionalize the membrane (Wandera et al. 2010). Upon photo-irradation, these units change conformation and have been used for controlling membrane permeability (Ishihara et al. 1984), selectivity (Anzai et al. 1983), cross-membrane conductance (Kinoshita et al. 1986), and even enantioselective adsorption (Yashima et al. 1995). Membranes exhibiting responsive behavior towards electric or magnetic fields have not been studied as extensively, but have been shown to effectively modulate pore diameter (Yamauchi et al. 1993; Yang et al. 2008). A large class of functionalized membranes has been developed to exhibit controlled responses to changes in pH and/or ionic strength. This is accomplished via the incorporation of ionizable molecules within the functionalized membrane including acrylic acids, acrylamides, and various moieties containing these functional groups (polypeptides, methacrylates, etc.). These membranes have been used for a variety of applications ranging from controlling permeability and selectivity to drug delivery (Hu and Dickson 2009; Wandera et al. 2010). Aside from their pH-responsive behavior, membranes functionalized with poly(acrylic acid) have been proven suitable for heavy metal capture and nanoparticle synthesis (Xu et al. 2005; Lewis et al. 2009).

There are several methods of PAA functionalization on membranes, as shown in Figure 2.2. Various membranes can be used as platforms (supports) for PAA functionalization, but should have suitable thermal and chemical stability for the desired application. One method of PAA immobilization on membrane supports is by forming polyelectrolyte layer-by layer (LbL) assemblies via alternating adsorption of polycations and polyanions. Thus, thin films containing oppositely charged polyelectrolytes are formed on the external membrane surface (Dai and Bruening 2002; Kidambi and Bruening 2005; Dotzauer et al. 2006).

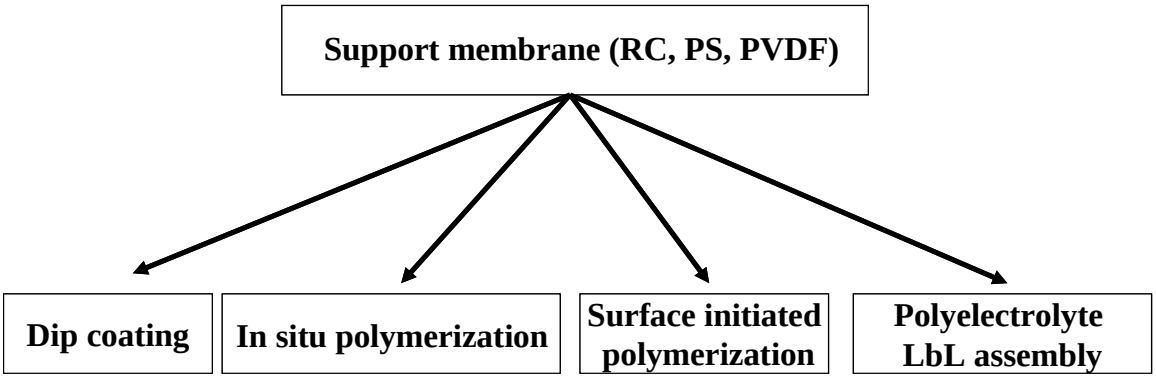

RC – Regenerated cellulose
PS – Polysulfone
PVDF – Polyvinylidene fluoride

LbL – Layer-by-Layer

Figure 2.2. Various approaches for PAA-functionalization of membrane supports.

The simplest method involves dipping the membrane in a PAA solution. The PAA diffuses inside the membrane pores and the chains are cross-linked by ethylene glycol (EG) to prevent leaching from the membrane. However, it was shown that PAA is coated primarily on the external membrane surface and at the pore mouth, thus blocking the PAA diffusion inside (Xu et al. 2005). This method does not take advantage of the internal membrane surface, and dramatically reduces the membrane pore size.

Another approach is to polymerize the monomer, acrylic acid, inside the membrane pores. This can be obtained by either surface-initiated or *in situ* polymerization. In the former, initiator groups are immobilized on the membrane and the polymerization occurs via a radical transfer mechanism after addition of the monomer (Singh et al. 2008). In the latter, the membrane is soaked in polymerization solution containing the initiator, monomer, and cross-linking agent. This solution diffuses inside the membrane pores and random polymerization occurs by heating the membrane (Xu et al. 2005; Xu and Bhattacharyya 2007).

These functionalized membranes can then be used to capture Fe(II) and subsequently used to conduct free radical reactions in the presence of H_2O_2. When operated under pressure-driven convective flow, these membranes provide reactants rapid access to active sites, thereby minimizing the mass transfer limitations associated with other high surface area-to-volume materials. The generated free radicals can then be used to degrade toxic organic compounds. Thus, by integrating the oxidative reactions into a membrane-based process, we are able to minimize the disadvantages associated with the separate processes of filtration and AOPs.

2.6 Groundwater Remediation of TCE

Trichloroethylene (TCE) is a volatile, halogenated organic compound that was once a widely used degreasing agent. Two decades ago, over 200 million pounds of TCE were produced in the United States each year (Vogel et al. 1987). Although the majority of TCE lost to the environment is via volatization, large plumes of TCE have been reported in various groundwater systems (Rivett et al. 2001). Since concentrations of TCE can be above the solubility limit in water (1000 - 1100 ppm), a majority of the TCE

is often present in the form of a dense, non-aqueous phase liquid (DNAPL), particularly at high depth (Russell et al. 1992). Several current remediation techniques successfully treat the dissolved TCE, but are unable to treat the DNAPL itself, resulting in an eventual rebound of TCE in the groundwater. Over the years, much effort has been put into the cleanup of TCE and other contaminants using various remediation technologies. An efficient and cost effective procedure is required for removing toxic organic compounds from groundwater.

Many different strategies have been used for the removal of TCE and other toxic organic compounds from the subsurface. Pump-and-treat methods have long been used for groundwater remediation, but are very expensive for the amount of contaminant removed and require long periods of time to treat the affected area. In air-stripping operations, TCE is transferred from groundwater to air, but not destroyed. Biological remediation can be performed under both aerobic and anaerobic conditions and is capable of completely mineralizing TCE (Russell et al. 1992; Laine and Cheng 2007), but these methods have limited applicability. Degrading TCE through the use of chemicals via oxidative and reductive pathways has been proven to be an effective groundwater remediation technology (Laine and Cheng 2007).

It was once thought that since TCE is already in an oxidized state, attempting to further oxidize the compound would not be an effective remediation strategy (Russell et al. 1992). However, several powerful oxidants are able to effectively degrade TCE and many other organic contaminants. Various advanced oxidative processes (AOPs) have been used for *in situ* chemical oxidation (ISCO). Currently, the three main oxidants in use for ISCO are permanganate ($KMnO_4$ $NaMnO_4$), ozone (O_3), and Fenton's reagent.
Permanganate, usually in the form of $KMnO_4$, has the slowest reaction rate of the three oxidants, but also has the highest stability. It has been proven effective from a pH of 3.5 to 12 and, depending on the pH, degrades pollutants by either direct oxidation or hydroxyl radical (OH•) generation (Struse et al. 2002). Although it can treat a wide variety of pollutants, it has proven ineffective on BTEX, diesel fuel, and gasoline (Amarante 2000). Ozone (O_3) is also capable of oxidizing pollutants by either direct oxidation or hydroxyl radical generation, but mainly under acidic conditions (Brunet et

al. 1984; Masten and Hoigne 1992; Yasunaga and Hirotsuji 2008). It is also very unstable in the subsurface and requires expensive on-site generation (Amarante 2000).

2.7 TCE Degradation

Hydroxyl radical degradation of TCE is second order in nature ($k_{TCE} = 4 \times 10^9$ $M^{-1}s^{-1}$) and generally forms intermediates such as di- and trichloroacetic acids, which are more easily degraded by microbes (Pignatello et al. 1999; Watts and Teel 2005; Li et al. 2007). These are then oxidized further by hydroxyl radicals and, if run to completion, the final products are expected to be organic acids and carbon dioxide. On the fringes of the reactive zone in groundwater systems, the intermediates and some TCE may not be fully oxidized. In the subsurface, most hydrophobic organic contaminants present in concentrations higher than their solubility limits are in droplet form (Roy-Perreault et al. 2005; Yaron-Marcovich et al. 2007). These droplets are generally trapped within the soil, making them very difficult to treat and impeding their dissolution into the aqueous phase (Kennedy and Lennox 1997). Figure 2.3 illustrates a possible distribution of TCE in the subsurface.

Sorption of contaminants to soil surfaces could also affect *in situ* degradation by limiting their availability to free radical attack. Watts et al. (1994) showed that hexachlorobenzene sorbed to silica sand surfaces exhibits greater rates of degradation using a Fenton-like system than was lost by desorption. In addition to direct contaminant destruction, Morgan and Watkinson (1992) showed the addition of hydrogen peroxide aids in the bioremediation of groundwater.

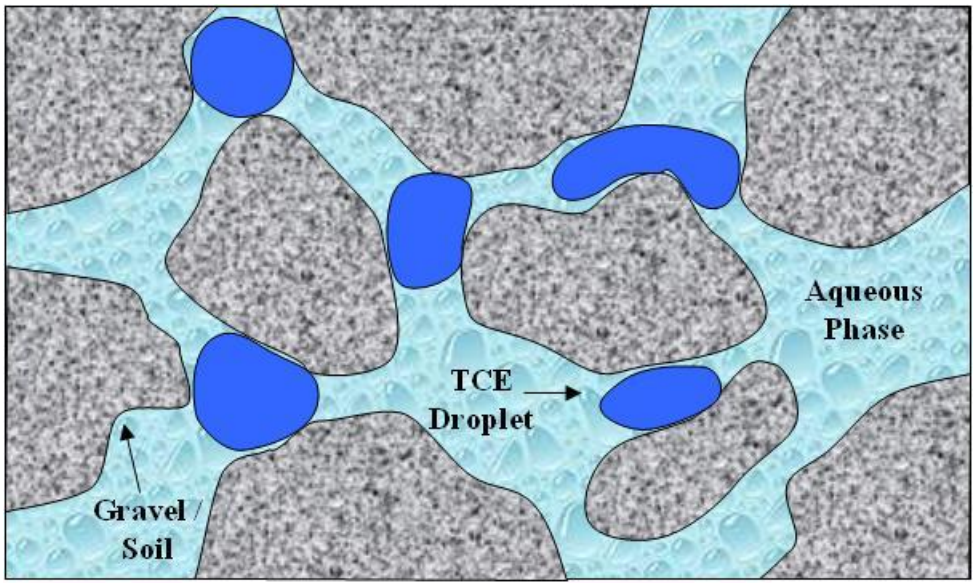

Figure 2.3. Illustrative example of DNAPL distribution in aquifer (adapted from Kennedy and Lennox, 1997).

Chapter 3 Experimental and Analytical Methods

This chapter discusses the materials, membrane functionalization, experimental procedures, equipment, and analytical methods used.

3.1 Materials

All chemicals used were of reagent grade unless otherwise noted. Acetonitrile (HPLC-grade), deionized ultrafiltered (DIUF) water, ethanol, ferrous sulfate, ferrous chloride, ferric chloride, hydrogen peroxide, iron reference standard (1000 ppm) , pentane, sodium chloride, sodium citrate, sodium hydroxide, sodium phosphate, sulfuric acid, and trichloroethylene (TCE) were purchased from Fisher Scientific. Acrylic acid, benzoic acid (BA), benzoyl peroxide, 2,9-dimethyl-1,10-phenanthroline (DMP), 4-hydroxybenzoic acid (p-hBA), pentachlorophenol (PCP), 3-(2-pyridyl)-5,6-diphenyl-1,2,4,-triazine-4′,4′′-disulfonic acid sodium salt (ferrozine), sodium phosphate, thionine acetate, titanium(IV) oxysulfate (15 wt % in dilute sulfuric acid), toluene, and trimethylolpropane triacrylate (TMPTA) were purchased from Sigma-Aldrich. Copper(II) sulfate and potassium persulfate were purchased from EM Science. Chloride reference solution (1000 ppm) was purchased from Thermo Electron Corporation. Sodium nitrate was purchased from LabChem Inc. 2,4,6-Trichlorophenol (TCP) and 2-(N-morpholino)ethanesulfonic acid (MES) were purchased from Acros Organics. Calcium reference standard (1000 ppm) was purchased from Ricca Chemical Company.

Hydrophobic poly(vinylidene fluoride) (PVDF) microfiltration membranes with a thickness of 125 μm, nominal pore size of 450 nm, and porosity of 75 % were obtained from Millipore Corporation.

3.2. Methods

3.2.1. Membrane functionalization

A method reported by Gabriel and Gilberg (1993) was followed to functionalize the pores of hydrophobic PVDF membrane with PAA by *in situ* polymerization of acrylic acid. Although various membrane materials can be used for this application, PVDF was chosen for its high chemical and thermal stabilities. The polymerization reaction was carried out in organic solvent with hydrophobic PVDF membranes to ensure proper wetting. The polymerization solution, which generally contained 70 wt % toluene (solvent), 30 wt % acrylic acid (monomer), 1.2 wt % TMPTA (cross-linker), and 0.5 wt % benzoyl peroxide (initiator), was mixed thoroughly in a closed vessel. In order to synthesize membranes with different PAA loading and crosslinking, the reactant concentrations were varied and were in the ranges of 70 to 95.5 wt % toluene, 0.14 to 0.5 wt % benzoyl peroxide, 4 to 15 wt % acrylic acid, and 0.16 to 0.6 wt % TMPTA. This procedure and mechanism for the polymerization reaction have been described previously (Gabriel and Gillberg 1993; Xu and Bhattacharyya 2007).

A PVDF membrane was dipped in the polymerization solution for 2 min, sandwiched between 2 teflon or glass plates and placed in an oven at 90 °C for 4 h. Nitrogen gas was continuously supplied to remove oxygen, which acts as an inhibitor for the polymerization reaction. After removal from the oven, the plates and membrane were allowed to cool before immersion in a DIUF water bath to loosen the membrane from the plates. In order to remove non-polymerized compounds and excess solvent, the membranes were soaked in a DIUF/EtOH mixture overnight and then dried before use.

Reactive membrane preparation

After polymerization, PAA was converted to Na-form by either soaking the PVDF-PAA membrane in a solution of 0.0001 - 0.1 M NaOH or permeating the solution through the membrane. To immobilize Fe^{2+}, the membrane was either soaked in 100 mL of a 3.8 mmol/L solution of $FeCl_2.4H_2O$ in deoxygenated water (pH of 5-6) or the solution was permeated through the membrane. Prior to and after the ion exchange step,

the membrane matrix was washed with copious amount of deoxygenated water. Since Fe^{2+} is prone to oxidation by O_2, these membranes were used immediately.

Direct ferrihydrite/iron oxide nanoparticle synthesis in membrane pores.

A PVDF-PAA-Fe^{2+} membrane with sub-maximal iron loading was added to a stirred buffered solution at pH 5.5-6.5 with 0.2 M H_2O_2 for 1 h (Cornell and Schwertmann 2003). The membrane was washed with deionized (DI) water and immersed in a solution at pH 13.5 for 2-3 h. After rinsing the membrane, it was dried at 80 °C for 1 h before SEM and Mössbauer spectroscopy analysis. It should be noted that the drying step had no effect on the iron oxide structure, as confirmed by Mössbauer analysis of similar samples prepared without drying at elevated temperature. All pH adjustments were performed using NaOH.

3.2.2. Membrane and nanoparticle characterization

Scanning Electron Microscopy (SEM)

Surface morphology of the bare, PAA-coated, and nanoparticle-modified membranes were examined by a Scanning Electron Microscopy instrument, Hitachi S-3600.

Confocal Laser Scanning Microscopy (CLSM)

CLSM images were acquired using a Leica SP1 Inverted Confocal Microscope with a 63 × 1.32 objective lens. All images were stored as 8-bit images with resolution of 1024 × 1024 over an area of 158.7 μm × 158.7 μm. All membranes were stained via the ion exchange of positively-charged thionine (as thionine acetate) in 100 mmol/L sodium phosphate buffer solution at pH 7 in the negatively-charged PAA domain. This was followed by multiple washings with 100 mmol/L sodium phosphate buffer solution at pH 7. An excitation wavelength of 488 nm was used image the thionine on the surface of the membranes. The images in Figure 5.2 were obtained by taking the average fluorescence at 594 nm of 10 images taken 0.6 μm apart through a depth of 6 μm within the membranes.

Fourier Transform InfraRed (FTIR) Spectroscopy

The Fourier Transform Infrared spectra of the bare and PAA-coated PVDF membranes were recorded on a Varian 7000e FTIR with attenuated total reflectance (ATR). Membranes were dried at 90 °C for four hours before testing. Data was collected using 128 scans at a resolution of 4 cm^{-1}.

Thermogravimetric Analysis (TGA)

Dried PVDF-PAA membrane samples were cut into small pieces for TGA analysis with a PerkinElmer STA 6000 Simultaneous Thermal Analyzer. The heating sequence was conducted in an inert atmosphere at a helium flowrate of 20 mL/min. Sample temperature was raise to 35 °C and held for 10 min, then increased to 750 °C at a rate of 10 °C/min, where it was then held for 10 min. Sample size used was 22.5 mg.

Mössbauer spectroscopy

^{57}Fe Mössbauer spectra were obtained with the assistance of Dr. Frank Huggins. A conventional Mössbauer spectrometer with a ^{57}Co-based γ-ray source was used to collect data over 1024 channels at 292 ± 2 K. The spectrum was calibrated using metallic iron. Membrane samples were cut-up so as to fit in 1.2 cm diameter plastic compression holders for analysis. After data collection, the percentage of each iron species was determined by the peak area under the each species in relation to the peak area for all species. More details can be found in Karr 1978.

3.2.3. Analytical methods

Metal ions (Fe, Ca, Na)

Fe, Ca, and Na ions were quantified using either Atomic Absorption (AA) or Inductively Coupled Plasma – Atomic Emission Spectroscopy (ICP-AES). The AA was a Varian SpectrAA 220 Fast Sequential atomic absorption spectrometer equipped with a Fisher Scientific Fe data-coded, hollow cathode lamp. The lamp was operated at a wavelength of 386.0 nm. For Fe, the calibration curve was created using 7 different

concentrations ranging from 90 to 900 μmol/L with R^2 = 0.9993 and average analytical error of 1.3%. The ICP-AES used was a Varian model. The internal standard used was yttrium chloride (1 mg/L). The standards and experimental samples were acidified with concentrated nitric acid (1-5 % of total volume) before analysis to keep all metals dissolved and minimize variations in the background matrix.

Fe^{2+}/Fe^{3+} concentration

The concentration of Fe^{2+} was measured using the ferrozine method (Stookey 1970; Voelker and Sulzberger 1996). The calibration curve was created using five different concentrations of Fe^{2+} ranging from 9 to 180 μmol/L with R^2 = 0.992 and average analytical error of 3.6%.

Hydrogen peroxide (H_2O_2)

Hydrogen peroxide concentrations were measured using one of two methods. In the method described by Kosaka et al. (1998), 1 mL each of 0.01 M copper(II) sulfate, 2,9-dimethyl-1,10-phenanthroline (DMP) solution, and 0.1 M phosphate buffer (pH 7) were added to 3 mL of sample. DMP solution was prepared by dissolving 1 g DMP in 100 mL ethanol. The absorbance of the solution was measured at 454 nm using a Varian Cary 300 spectrophotometer. The calibration curve was created using 12 concentrations ranging from 10 to 300 μM with R^2 = 0.9997 and average analytical error of 2.0 %. The second method was based on the work of Clapp et al. (1989). Ten μL of 15 wt % titanium(IV) oxysulfate solution was added to 1 mL of sample and analyzed at 407 nm. The calibration curve was created using 10 concentrations ranging from 25 to 3200 μM with R^2 = 0.9999 and average analytical error of 1.7 %.

Gas Chromatography / Mass Spectroscopy (GC/MS) for TCE

After a sample from the reaction vessel was taken, TCE was extracted with pentane previously spiked with an internal standard of 100 ppm EDB. TCE concentrations were measured by manually injecting a 1 μL liquid sample in a 60 m × 0.25 mm × 1.4 μm film thickness Supelco SPB-624 fused silica capillary column installed in a Hewlett Packard 5890 Series II Gas Chromatography and Mass

Spectrometer, model number 5971. The column was operated at 35 °C for 2 min, raised to a final temperature of 190 °C at a rate of 10 °C /min, and held for 2 min. The carrier gas used was ultra high purity helium. The calibration curve was created using 7 concentrations ranging from 0.035 to 2.77 mmol/L TCE with R^2 = 0.9982 and average analytical error of 5.3%.

High Performance Liquid Chromatography (HPLC) for aromatics

The concentration of PCP, benzoic acid, and 4-hydroxybenzoic acid was measured using a Shimadzu HPLC with photodiode array detector and a Premier C18, 5 μm, 250 mm × 4.6 mm column. For PCP, the column was operated under isocratic flow conditions of 0.6 mL/min acetonitrile and 0.2 mL/min water. The calibration curve was created using the absorbance of 9 different quantities of PCP ranging from 0.05 to 2.5 nmol at 220 nm with R^2 = 0.9998 and average analytical error of 2.5%. For TCP, the column was operated under isocratic flow conditions of 0.8 mL/min pH 2.5 water (0.01 M phosphate) and 0.2 mL/min acetonitrile. The calibration curve was created using the absorbance of 16 different quantities of TCP ranging from 0.02 to 10 nmol at 292 nm with R^2 = 0.999 and average analytical error of 1.2 %. For the analysis of benzoic acid and p-hydroxybenoic acid, the column was operated under gradient flow conditions with solvent A as acetonitrile and solvent B as pH 2.5 water (0.01 M phosphate). The solvent phase was varied as follows: 0-5 min, 70 vol % B; 5-11 min, linearly decreased to 30 vol % B; 11-23 min, linearly decreased to 10 vol % B; 23-25 min, held at 10 vol % B. This gradient was required to separate para-hydroxybenzoic acid from its ortho- and meta-substituted isomers. The calibration curves for BA and 4-hBA were created using the absorbance of 6 different quantities of BA ranging from 0.05 to 2.5 nmol at 228 nm with R^2 = 0.9998 and average analytical error of 2.4 % and 6 different quantities of p-hBA ranging from 0.05 to 2.5 nmol at 254 nm with R^2 = 0.9999 and average analytical error of 2.1 %

Cl^- analysis

Either a Thermo Orion ion-selective electrode or an Accumet Chloride Combination Electrode was used for measuring Cl^- concentrations. The calibration curve

was created using 6 concentrations ranging from 0.14 to 5.6 mmol/L Cl^-. In agreement with previous Cl^- analysis by our group, multiple calibrations were produced with different concentrations of citrate to account for citrate interference (Li et al. 2005). R^2 values ranged from 0.9933 to 0.9987 with average analytical error from 3.8% to 8.6%. Calibration curves were checked with standards before measuring samples.

3.2.4 Experimental procedures

TCE degradation in solution and droplet phases

For standard Fenton reactions, ferrous sulfate was added to deoxygenated DIUF water and the pH was adjusted to ~3. For chelate-modified Fenton reactions, sodium citrate was added to deoxygenated DIUF water, the pH was adjusted to ~3, followed by the addition of ferrous salt and adjustment of the pH to neutral. TCE was added to these solutions, which were then sealed and allowed to mix for certain reaction times. For experiments with TCE present in both aqueous and organic (droplet) phases, saturated solutions of TCE were prepared overnight and excess TCE constituting the organic phase was added before initiating the reaction. For batch experimentation, reactions were conducted in 500 mL flasks with continuous mixing at 600 rpm and N_2 in the headspace (~ 75 mL) at room temperature (22-25 °C). The spherical flasks had three ports in the top of the vessel which were sealed with glass fittings: one contained an inlet for a pH probe, one contained a septum for sampling, and the final port contained either an inlet for a thermometer or a glass plug. Samples (4.5 – 5.0 mL) were taken using a syringe inserted through the septum. H_2O_2 was injected through a septum to initiate the reaction in either one dose for lower concentrations or six doses over 10 minutes for higher concentrations. The temperature of the reaction solution was found to increase a maximum of 3 °C for experiments with the highest concentrations of reactants used (8 mmol/L Fe^{2+} and 32 mmol/L H_2O_2). In control experiments, some loss of TCE occurred due to volatization over the reaction time. Adjustments to pH were made using 4 N H_2SO_4 and 6.25 N NaOH. Experiments used for kinetic modeling were conducted in triplicate.

As part of this study, site-specific RGA aquifer materials were collected from a location identified by Sexton (2006) as an outcrop of the Regional Gravel Aquifer

(RGA). Groundwater samples for experiments using natural water were collected from a local residential well outside of the TCE contaminant plumes from areas surrounding the Paducah Gaseous Diffusion Plant (PGDP) and supplied by the Kentucky Research Consortium for Energy and Environment (KRCEE) in cooperation with the Kentucky Water Resources Research Institute (KWRRI). When received, this water contained no TCE. The groundwater properties are shown in Table 3.1.

Standard Fenton reaction for Fe conversion and benzoic acid oxidation

For the oxidation of benzoic acid using the standard Fenton reaction, reactions were conducted in 500 mL flasks with 400 mL of solution and N_2 in the headspace (~ 175 mL) with continuous mixing at 600 rpm at a temperature of 20-22 °C. The spherical flasks had three ports in the top of the vessel which were sealed with glass fittings: one contained an inlet for a pH probe and sampling, one contained the N_2 diffuser, and the final port contained a thermometer. Deoxygenated DIUF water was spiked with benzoic acid (if included) followed by the iron salt. Reactions were initiated by adding H_2O_2. During experimentation, the pH was not adjusted, but was within the range of 2.95 to 3.07. Samples of 4 mL were taken at selected times: 1.5 mL for H_2O_2 analysis, 1 mL for Fe(II)/Fe(III) analysis, and 1.5 mL for HPLC analysis of benzoic acid and its oxidized products. The sample for benzoic acid analysis was spiked with 75 μL 1-propanol (5 vol %) to quench any subsequent free radical reactions. All experiments were conducted in duplicate.

Convective flow experiments

All convective flow experiments except those for Ca^{2+}/Fe^{2+} capture were conducted in a stirred, dead-end membrane cell from Millipore Corporation with external surface area of 33.2 cm^2 (Product number XFUF07601). The stirred cell was placed on a Styrofoam base to insulate it from any heat that may have been generated by the stir plate. The convective flow experiments for Ca^{2+}/Fe^{2+} capture were conducted in a dead-end stainless steel cell from Osmonics with external surface area of 13.2 cm^2. Experiments with buffer utilized 1 mmol/L MES adjusted to pH 6 with NaOH.

Table 3.1. DOE Site Average Water Quality Based on 10 Monitoring Wells

Alkalinity	82	mg L^{-1}
Ca^{2+}	24	mg L^{-1}
Cl^{-}	55	mg L^{-1}
Dissolved Oxygen (DO)	3	mg L^{-1}
Fe(II) / Fe(III)	0.3	mg L^{-1}
NO_3^{-}	3	mg L^{-1}
PO_4^{3-}	2	mg L^{-1}
SO_4^{2-}	13	mg L^{-1}
Total Dissolved Solids (TDS)	293	mg L^{-1}
Total Organic Carbon (TOC)	1.2	mg L^{-1}

Chapter 4 Solution-Based Free Radical Reactions in Aqueous and Interfacial Systems

This chapter focuses on the understanding of the generation of free radicals in aqueous systems using the standard and modified Fenton (H_2O_2 decomposition) reactions. The conversion of Fe(II) to Fe(III) in the presence of H_2O_2 and the quantification of hydroxyl radical generation via the use of a well established probe compound is studied in order to better understand the standard Fenton reaction. This reaction is then used generate free radicals at the well-defined interface of TCE droplets and water. Then, the effect of a chelating agent on Fe(II) and Fe(III) concentration in solution is quantified using equilibrium values of Fe-hydroxide species and Fe-citrate complexes reported in the literature. The effects of these Fe-chelate equilibria and of iron speciation on hydrogen peroxide degradation are then discussed. The applicability of the chelate-modified Fenton reaction to groundwater systems is tested using natural water and, separately, a packed column for simulated groundwater flow. Finally, a kinetic model for the degradation of TCE via dissolved-phase and interfacial free radical reactions for both the aqueous and non-aqueous phases (droplet) is developed. Sections 4.2 – 4.9 are **published** in **Lewis, Lynch et al. (2009)**.

4.1 Fe(II) to Fe(III) conversion and hydroxyl radical quantification with standard Fenton reaction

In the standard Fenton reaction, the conversion of Fe(II) to Fe(III) takes place quickly and is accompanied by the rapid consumption of H_2O_2 and generation of free radicals. In order to better understand how this reaction proceeds, it is necessary to understand at what rate this iron oxidation takes place. Figure 4.1 shows the conversion of Fe(II) to Fe(III) in the presence of equimolar (100 μM) concentrations of Fe(II) and H_2O_2 (conditions are given in the first column of Table 4.1). For the first 5 min of reaction, only 0.5 mol H_2O_2 is consumed per mol of Fe(II) converted to Fe(III); however, this ratio increases to ~ 2 or greater for the next 40 min, before almost all of the Fe(II) has been converted to Fe(III). Since the rate of reaction between Fe(III) and H_2O_2 is

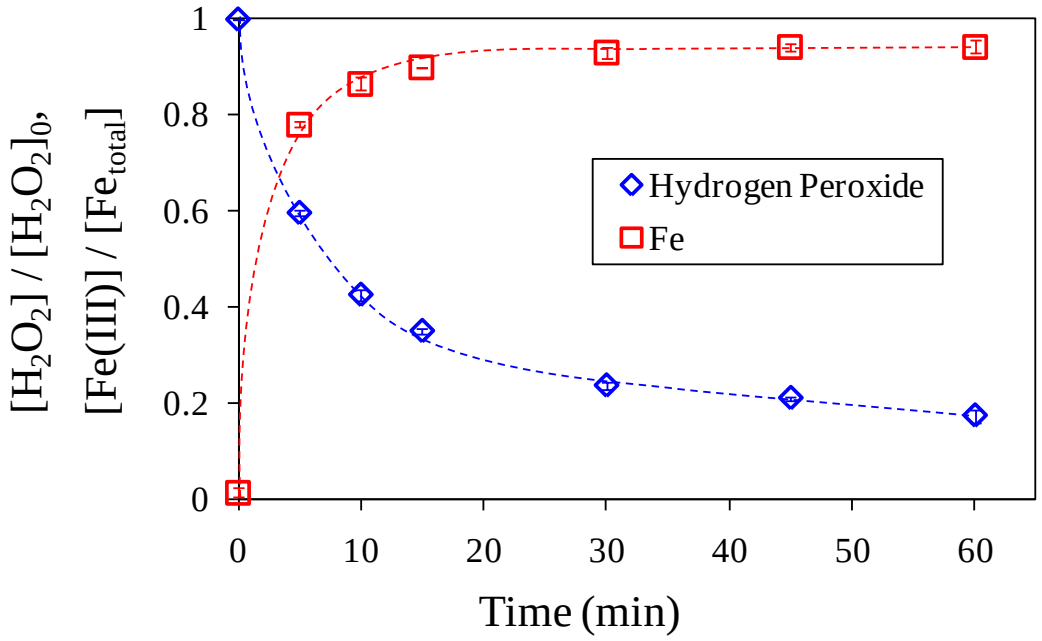

Figure 4.1. Fe(II) to Fe(III) conversion and H_2O_2 decomposition for the standard Fenton reaction (Fe(II)-H_2O_2) as a function of time at pH 3. Initial conditions given in Table 4.1. Volume = 0.4 L. Error bars represent one standard deviation.

Table 4.1. Initial conditions and efficiency of hydroxyl radical generation for experiments involving Fe(II) to Fe(III) conversion and hydroxyl radical capture through the use of benzoic acid as a hydroxyl radical scavenger. Volume = 0.4 L. Error represents one standard deviation.

Initial Fe Species	Fe(II)	Fe(III)	Fe(II)
Fe (μmol L^{-1})	99 ± 0	103 ± 1	108 ± 2
Initial H_2O_2 (μmol L^{-1})	100	100	118 ± 3
Initial Benzoic Acid (μmol L^{-1})	N/A	70.3 ± 0.7	93.6 ± 1.8
Reaction Time (h)	1	9	2
Total OH• Generated / Total H_2O_2 Consumed	N/A	1.01 ± 0.11	0.19 ± 0.00

considerably slower than that of Fe(II) and H_2O_2, the non-stoichiometric conversion of Fe(II) at the outset of the reaction is most likely caused by the large quantities of hydroxyl radical being generated which will also react with Fe(II). After this initial high rate of reaction, the trend reverses, requiring more H_2O_2 to convert one mol of Fe(II) to Fe(III).

Various methods have been used to quantify free radical production including electron spin resonance (ESR) which detects the presence of unpaired electrons. Since free radicals generally have short lifetimes, investigators have used free radical "trapping" compounds (generally nitroxyl probes) that will react with the free radicals, forming longer-lived species that can be detected by ESR (Halliwell and Whiteman 2004). ESR is capable of detecting these radicals at the time of formation, but other methods have been developed to "trap" hydroxyl radicals in compounds that can be quantified through the use of HPLC/UV-Vis. In order to quantify the production of hydroxyl radicals in Fenton systems containing either Fe(II) or Fe(III) initially, a probe compound, benzoic acid (BA), was utilized. After undergoing hydroxylation by hydroxyl radicals, *o*-, *m*-, and *p*-hydroxybenzoic acids account for 90 ± 5 % of all products formed (Keenan and Sedlak 2008). These isomers have been reported to form in a molar ratio of 1.7, 2.3, and 1.2, respectively, and with phenol (formed via decarboxylation), account for almost all hydroxyl radicals produced (Klein et al. 1975). Previous work has determined the yield of *p*-hydroxybenzoic acid (*p*-hBA) to be one mol per 5.87 mol of hydroxyl radicals generated (Mopper and Zhou 1990; Joo et al. 2005). This value was used to calculate the theoretical quantity of hydroxyl radicals generated from the quantity of *p*-hBA formed. These experiments were conducted at a low pH (~ 3.0) in order to prevent Fe(III) precipitation. The conditions for the testing of hydroxyl radical production via reaction of H_2O_2 and either Fe(II) or Fe(III) are shown in the second and third columns of Table 4.1. For experiments starting with Fe(II), the concentration of Fe(II) was verified at the beginning of the experiment to ensure no oxidation to Fe(III) had occurred (98 ± 2 mol % Fe(II)). The variation in H_2O_2 decomposition, benzoic acid oxidation, total quantity of hydroxyl radicals generated, and the mols of hydroxyl radicals formed per mol of H_2O_2 decomposed for the Fe(III) and Fe(II) systems are shown as a function of time in Figures 4.2 and 4.3, respectively.

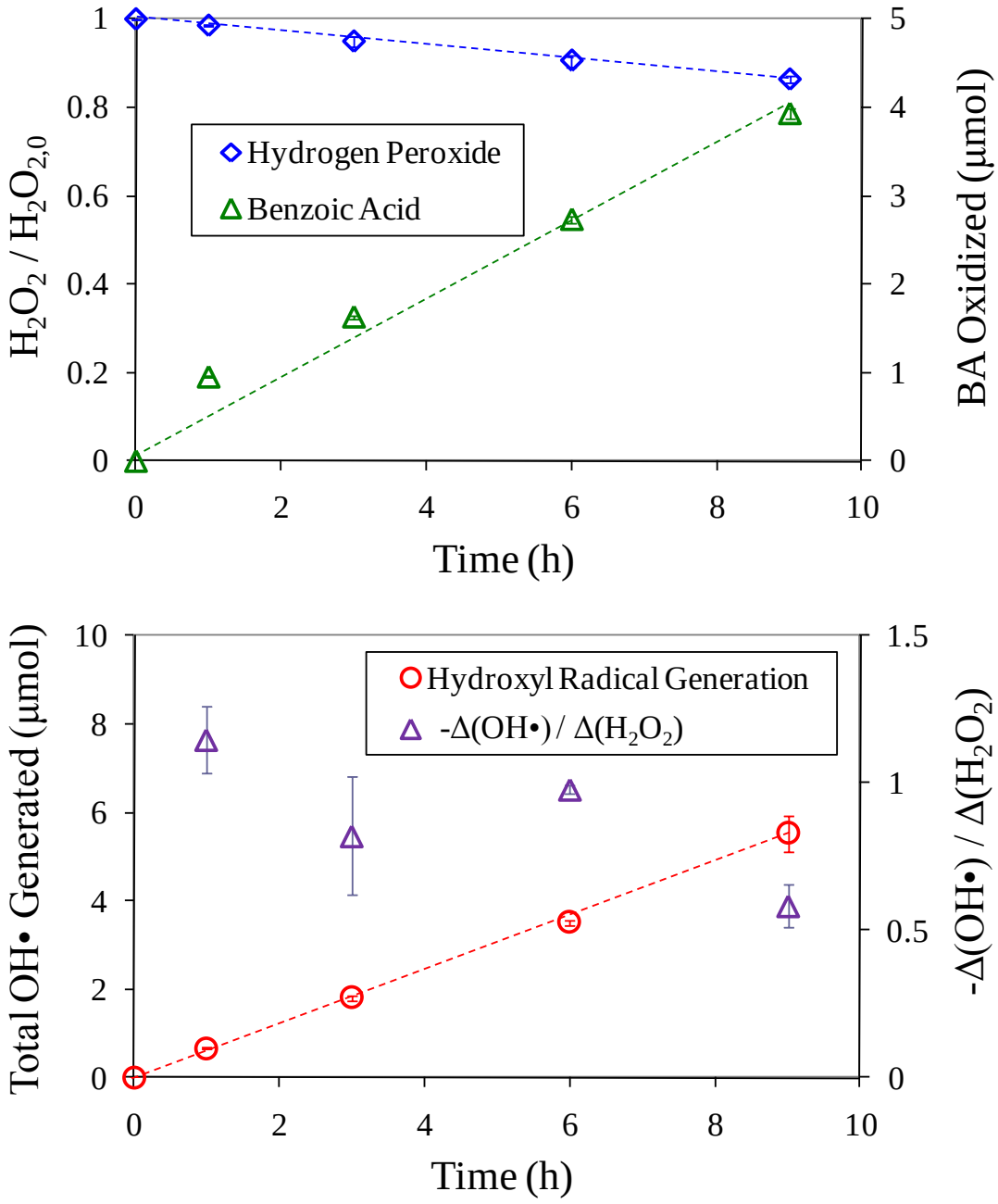

Figure 4.2. Variation in H_2O_2 decomposition, benzoic acid (BA) oxidation, total quantity of hydroxyl radicals generated, and the mol of hydroxyl radicals formed per mol of H_2O_2 decomposed for an Fe(III)-H_2O_2-BA system as a function of time at pH 3. Initial conditions given in Table 4.1. Volume = 0.4 L. Error bars represent one standard deviation.

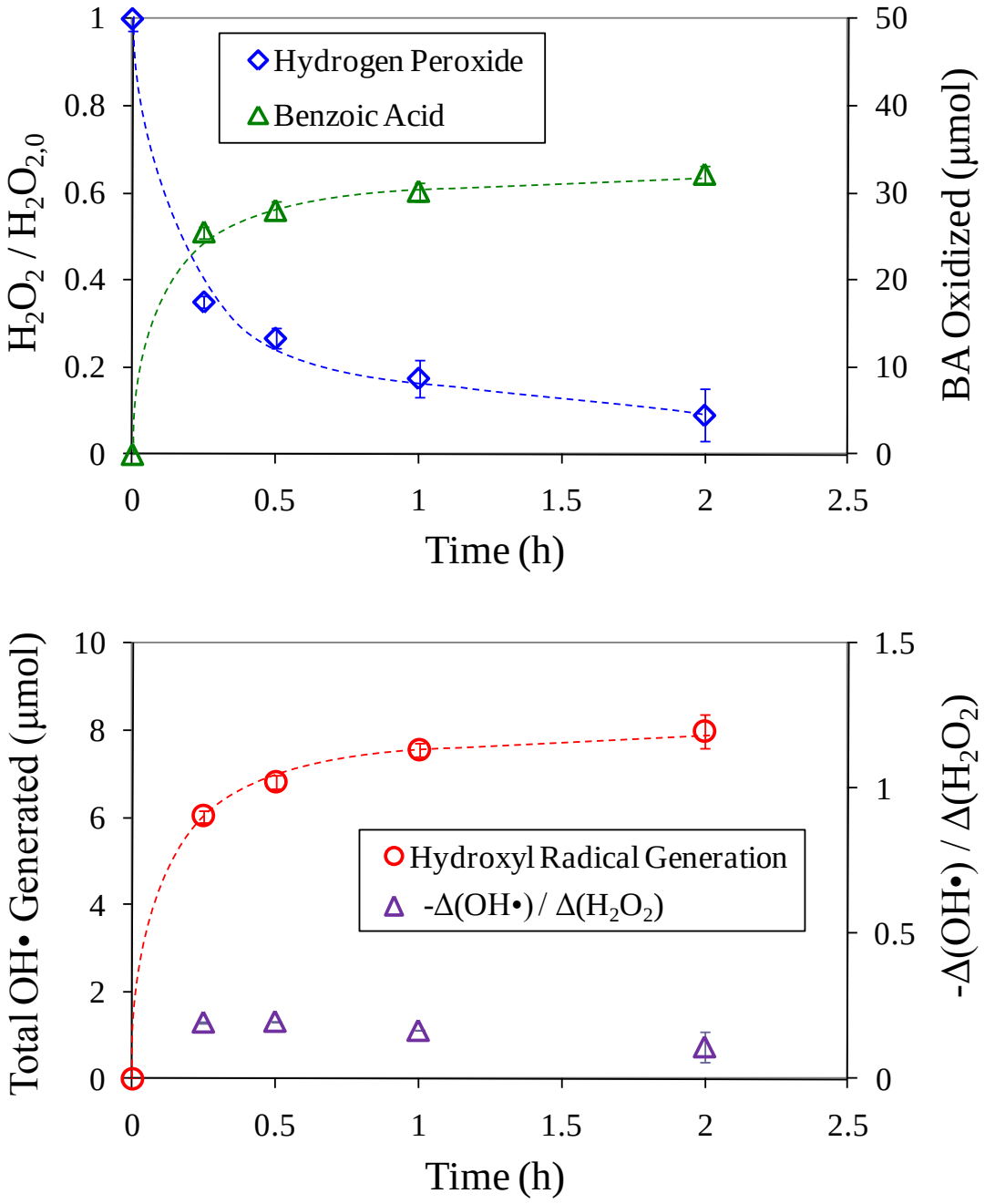

Figure 4.3. Variation in H_2O_2 decomposition, benzoic acid oxidation, total quantity of hydroxyl radicals generated, and the mol of hydroxyl radicals formed per mol of H_2O_2 decomposed for an Fe(II)-H_2O_2-BA system as a function of time at pH 3. Initial conditions given in Table 4.1. Volume = 0.4 L. Error bars represent one standard deviation.

The oxidation of benzoic acid, the rate of H_2O_2 decomposition, and the rate of hydroxyl radical generation in the Fe(III)-H_2O_2-BA are linear with respect to time. This is because the rate of reaction of Fe(III) with H_2O_2 is much slower than Fe(II) with H_2O_2 (see Equations 2.1 and 2.2), resulting in relatively constant concentrations of both Fe(II) and Fe(III). This leads to a constant rate of OH• generation, as seen in Figure 4.2. On the other hand, the oxidation of benzoic acid and decomposition of H_2O_2 occur rapidly in the Fe(II)-H_2O_2-BA system due to the fast rate of reaction of Fe(II) with H_2O_2. This system generated over 6 μmol of OH• in the first 0.25 h of reaction, which is more than the Fe(III)-H_2O_2-BA did in 9 h. However, upon inspection of the mol of OH• generated per mol of H_2O_2 decomposed, this measure of efficiency is 1.01 ± 0.11 for the Fe(III) system whereas it is only 0.19 ± 0.00 for the Fe(II) system. One caveat to these calculations is that they use the concentration of *p*-hBA to determine the concentration of OH•. For systems with rapid OH• generation and a limited quantity of the main OH• "trapping" compound (BA) available, there are most likely more reactions taking place than what has been accounted for. This could include the oxidation of *p*-hBA by OH•, which would lead to the incorrect assumption that the rate of OH• generation is very low. By the end of the reaction for the Fe(II) system, the concentration of benzoic acid is only 13 % of the initial concentration whereas 86 % is remaining in the Fe(III) system. Even though these factors should be taken into consideration, this large difference in efficiency of OH• generation is something to be considered when the controlled generation of OH• is desired.

4.2 TCE droplet degradation with standard Fenton reaction

The standard Fenton reaction operates most efficiently at pH below 3 (Pignatello et al. 2006). However, as discussed earlier, application of Fenton processes at low pH in large groundwater systems is highly impractical. A series of experiments using a 1:1 TCE:Fe(II) molar ratio were conducted in order to determine the optimum amount of hydrogen peroxide for complete dechlorination of both TCE droplets and TCE in the aqueous phase. These experiments were conducted at a low initial pH of approximately 2.5 and allowed to continue without pH adjustment as the pH did not vary significantly as

the reaction proceeded. Twenty hours after adding the hydrogen peroxide, the quantities of TCE and Cl^- were analyzed, as shown in Figure 4.4. The 1:1 H_2O_2:Fe(II) molar ratio resulted in the formation of 47% of the maximum possible Cl^- concentration and an 81% reduction in the amount of TCE present. The higher H_2O_2:Fe(II) ratios degraded almost 100% of the available TCE and formed approximately 82% of the maximum possible Cl^-. In the control, in which no H_2O_2 was added, a 29% loss of TCE was observed. In order to analyze the amount of TCE present in the droplet phase via extraction, the reactor vessel was opened, therefore contributing to TCE loss due to volatility. Since no droplets were present when the analysis of TCE was performed on the vessels containing H_2O_2, this problem was only encountered in the control run. This loss is the largest contributor to the deviations between the actual and theoretical chloride formation. Another contributing factor is the presence of chlorinated organic intermediates. This data indicates the optimum H_2O_2:Fe(II) molar ratio for dechlorination of TCE in both droplet and dissolved form at pH 2.5 is between 1:1 and 2:1. Teel et al. (2001) found the optimum H_2O_2:Fe(II) molar ratio to be 1:1 for TCE degradation in the aqueous phase. H_2O_2 in excess of this 1:1 ratio is required to degrade the TCE present in droplet form.

When similar reactions are performed (without chelate) at near-neutral or high pH, the amount of TCE degraded drops dramatically. Thus, this process must be modified to perform efficiently at near-neutral pH.

4.3 Iron-chelate equilibria

The use of a chelate reduces the amount of free Fe(II) and Fe(III) in solution, but is pH dependent. The equilibrium reactions associated with citrate as well as the complexation of Fe species with citrate are given in Equations 4.1-4.10, where L = L^{4-} (Inczedy 1976; Brady and Humiston 1982; Li et al. 2005).

$$Fe^{2+} + L \Leftrightarrow Fe(II)L \qquad K_1 = 10^{15.5} \qquad (4.1)$$

$$Fe^{2+} + H^+ + L \Leftrightarrow Fe(II)HL \qquad K_2 = 10^{19.1} \qquad (4.2)$$

$$Fe^{2+} + 2H^+ + L \Leftrightarrow Fe(II)H_2L \qquad K_3 = 10^{24.2} \qquad (4.3)$$

$$Fe^{3+} + L \Leftrightarrow Fe(III)L \qquad K_4 = 10^{25} \qquad (4.4)$$

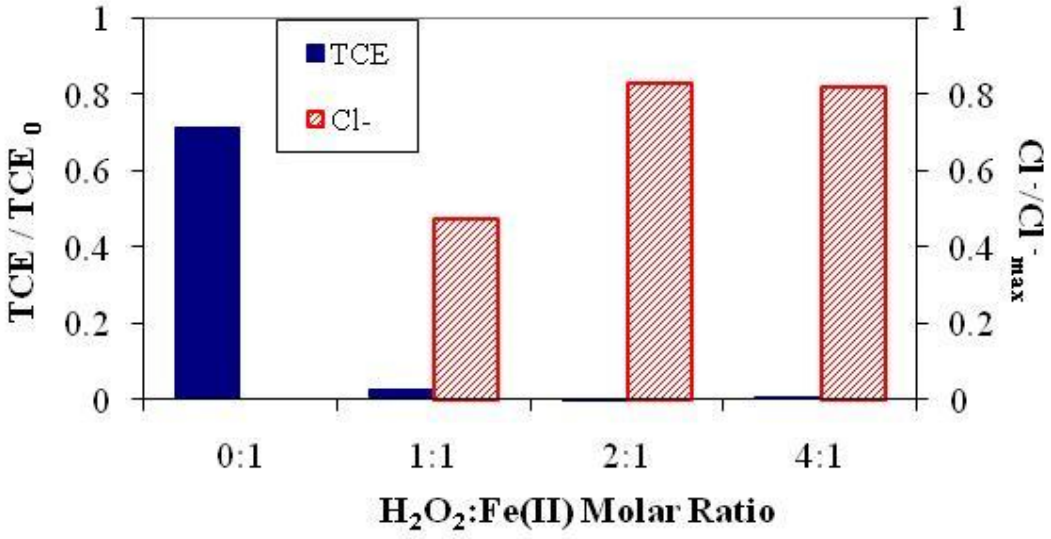

Figure 4.4. TCE reacted and Cl^- formed at 20 h for varying Fe(II):H_2O_2 molar ratios with equivalent initial TCE concentration of 15.2 mmol/L and TCE:Fe(II) molar ratio of 1:1. TCE present in both aqueous and organic phases. Control experiment conducted with no addition of H_2O_2. pH ~ 2.5.

$$Fe^{3+} + H^{+} + L \Leftrightarrow Fe(III)HL \qquad K_5 = 10^{27.8} \qquad (4.5)$$

$$Fe^{3+} + 2H^{+} + L \Leftrightarrow Fe(III)H_2L \qquad K_6 = 10^{28.4} \qquad (4.6)$$

$$H^{+} + L \Leftrightarrow HL \qquad K_7 = 10^{16} \qquad (4.7)$$

$$H^{+} + HL \Leftrightarrow H_2L \qquad K_8 = 10^{5.1} \qquad (4.8)$$

$$H^{+} + H_2L \Leftrightarrow H_3L \qquad K_9 = 10^{5.4} \qquad (4.9)$$

$$H^{+} + H_3L \Leftrightarrow H_4L \qquad K_{10} = 10^{3.0} \qquad (4.10)$$

Using Equations 4.1-4.10 and those associated with the hydrolysis of Fe^{2+} and Fe^{3+} (Equations 4.11-4.17), the speciation of virtually any Fe-citrate solution can be computed for a given pH (Baes and Mesmer 1976). The speciation of ferrous iron is shown in Figure 4.5. As pH approaches neutral, only a small amount of Fe is in an uncomplexed form. As pH decreases, more iron is released from this complex, which results in an increase in the overall rate of reaction. Similar calculations for ferric iron have been made, as shown in Figures 4.6 and 4.7, demonstrating how the presence of a chelating agent alters the speciation of Fe(III).

$$Fe^{2+} + H_2O \Leftrightarrow Fe(II)(OH)^{+} + H^{+} \qquad K_{11} = 10^{-9.5} \qquad (4.11)$$

$$Fe^{2+} + 2H_2O \Leftrightarrow Fe(II)(OH)_2(aq) + 2H^{+} \qquad K_{12} = 10^{-20.5} \qquad (4.12)$$

$$Fe^{2+} + 2OH^{-} \Leftrightarrow Fe(II)(OH)_2(s) \qquad K_{sp1} = 10^{-14.7} \qquad (4.13)$$

$$Fe^{3+} + H_2O \Leftrightarrow Fe(III)(OH)^{2+} + H^{+} \qquad K_{14} = 10^{-3.05} \qquad (4.14)$$

$$Fe^{3+} + 2H_2O \Leftrightarrow Fe(III)(OH)_2^{+} + 2H^{+} \qquad K_{15} = 10^{-6.31} \qquad (4.15)$$

$$Fe^{3+} + 3H_2O \Leftrightarrow Fe(III)(OH)_3(aq) + 3H^{+} \qquad K_{16} = 10^{-12} \qquad (4.16)$$

$$Fe^{3+} + 3OH^{-} \Leftrightarrow Fe(III)(OH)_3(s) \qquad K_{sp2} = 10^{-36} \qquad (4.17)$$

Adjusting the [L]:[Fe] ratio allows one to control the amount of Fe(II) and Fe(III) in solution and alter the generation of hydroxyl radicals as desired. In order to correctly determine the rates of free radical generation, quantification of the equilibrium distribution of iron is necessary.

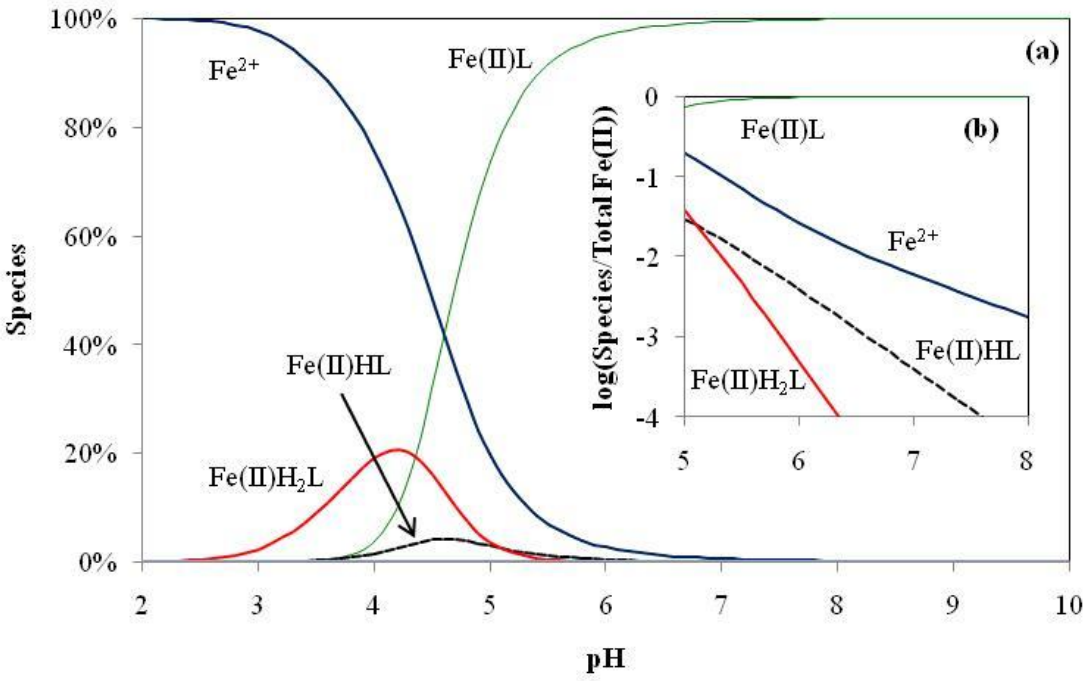

Figure 4.5. (a) Fe(II) species distribution as a function of pH. Total [Fe(II)] = 10 mmol/L, L/[Fe(II)]= 1, L = citrate. **(b)** Fe(II) species distribution for pH = 5 to 8.

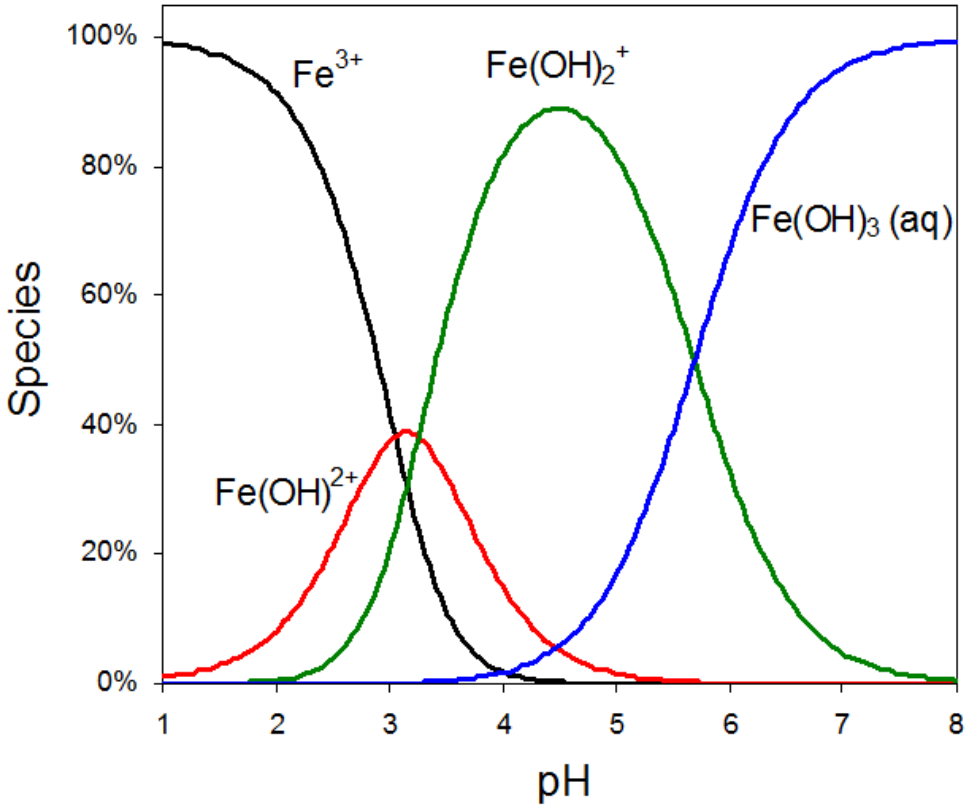

Figure 4.6. Fe(III) species distribution (no chelate) as a function of pH. Total [Fe(III)] = 10 mmol/L.

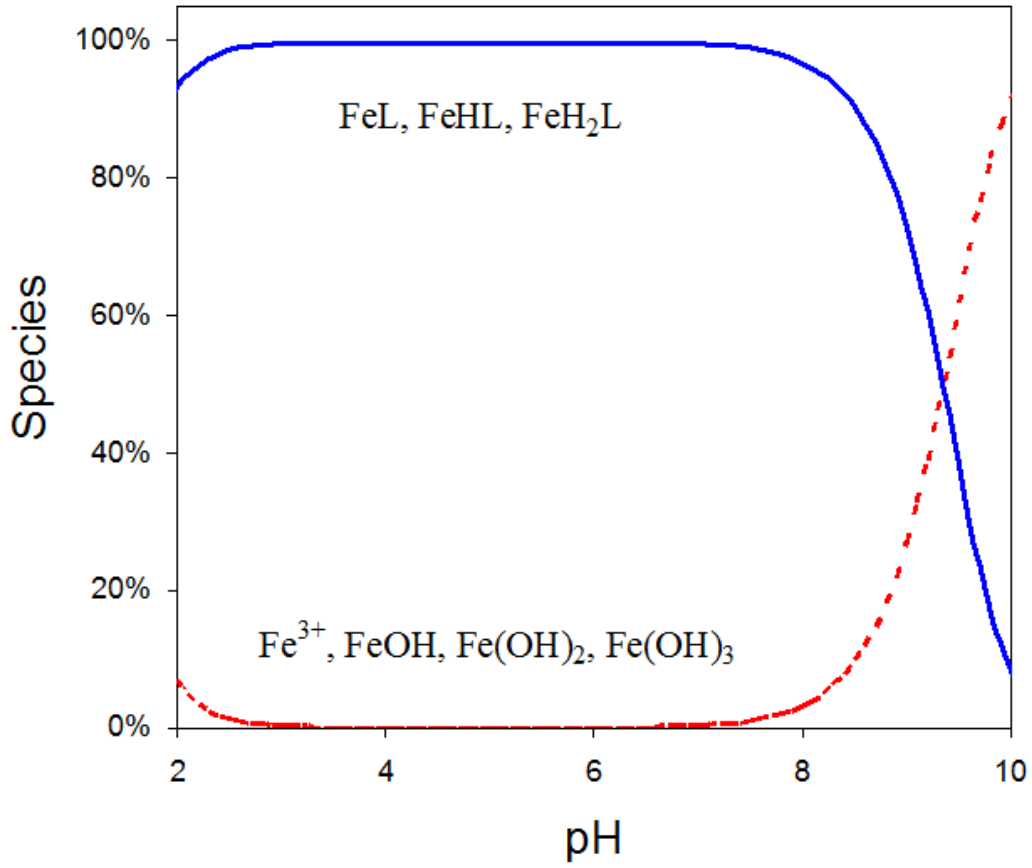

Figure 4.7. Fe(III) species distribution as a function of pH. Total [Fe(III)] = 10 mmol/L, L/[Fe(III)]= 1, L = citrate.

4.4 Effect of L:Fe ratio and Fe speciation on H_2O_2 decomposition

The initial reaction rate of Fe(II) with H_2O_2 is very rapid, but as more Fe(II) is oxidized to Fe(III), the decomposition of H_2O_2 slows significantly due to the higher reaction rate of H_2O_2 with Fe(II) compared to Fe(III) (Reactions 2.1 and 2.2, respectively). Figures 4.8 and 4.9 illustrate the decomposition of H_2O_2 in the presence of ferrous and ferric iron, respectively, with varying [L]:[Fe] molar ratios (L = citrate). When ferrous iron is used, the initial rate of H_2O_2 decomposition is very rapid. However, when ferric iron is used, the decomposition is much slower and almost linear, indicating a zero-order reaction. As expected, the rate limiting step in the reactions between ferrous/ferric iron and H_2O_2 is Reaction 2.2 and thus confirms the rate of the reaction depends mostly on the concentration of Fe(II). In addition to the speciation of iron, the [L]:[Fe] ratio plays an important role in determining the rate of H_2O_2 degradation. This rate decreases as this molar ratio is increased from 1:1 to 4:1 and, in conjunction with other findings, indicates Fe-citrate complexes are nonreactive with H_2O_2 when compared to uncomplexed iron (Li et al. 2007). Increasing the L:Fe ratio increases the efficiency of H_2O_2 consumption by reducing the rate of hydroxyl radical production. Lowering the concentration of uncomplexed Fe species should reduce the quantities of H_2O_2 and hydroxyl radicals consumed in Reactions 2.8-12, leaving more hydroxyl radicals available for reaction with TCE. Depending on the conditions present at a given groundwater site, the [L]:[Fe] and [Fe(II)]:[Fe(III)] ratios can be adjusted to allow for the optimization of H_2O_2 consumption and TCE degradation.

4.5 TCE degradation with chelate-modified Fenton reaction in natural water

At near-neutral pH, both Fe(II) and Fe(III) are almost entirely complexed with citrate as Fe(II)L and Fe(III)L, respectively. Due to this chelation, H_2O_2 decomposition and TCE degradation take place at much lower rates than without a chelate. Regardless, these chelate-modified Fenton reactions are still capable of degrading greater than 80% of TCE in natural water using a Fe(II):L:H_2O_2 molar ratio of 1:1:8 with initial Fe(II) concentration of 1.5 mmol/L and initial TCE concentration of 1.1 mmol/L, as shown in

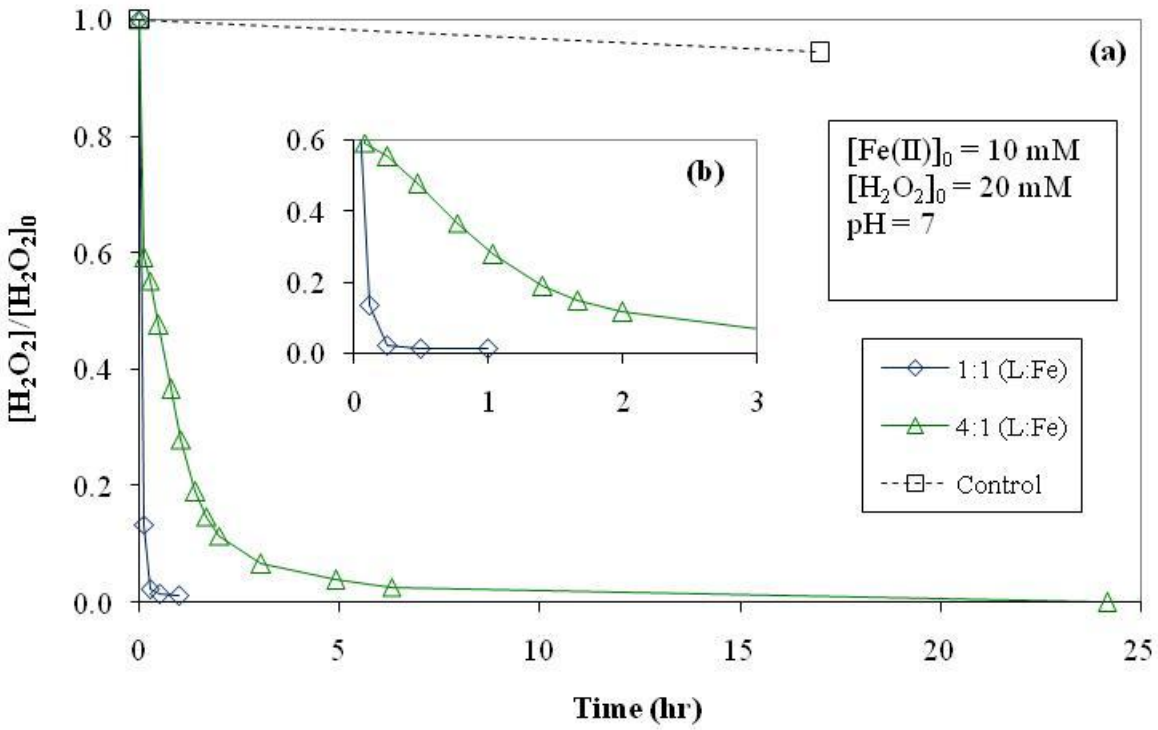

Figure 4.8. (a) Role of ferrous iron (Fe(II)) on H_2O_2 decomposition with varying [L]:[Fe] molar ratio. L = citrate. **(b)** H_2O_2 decomposition for t = 0 to 3 h.

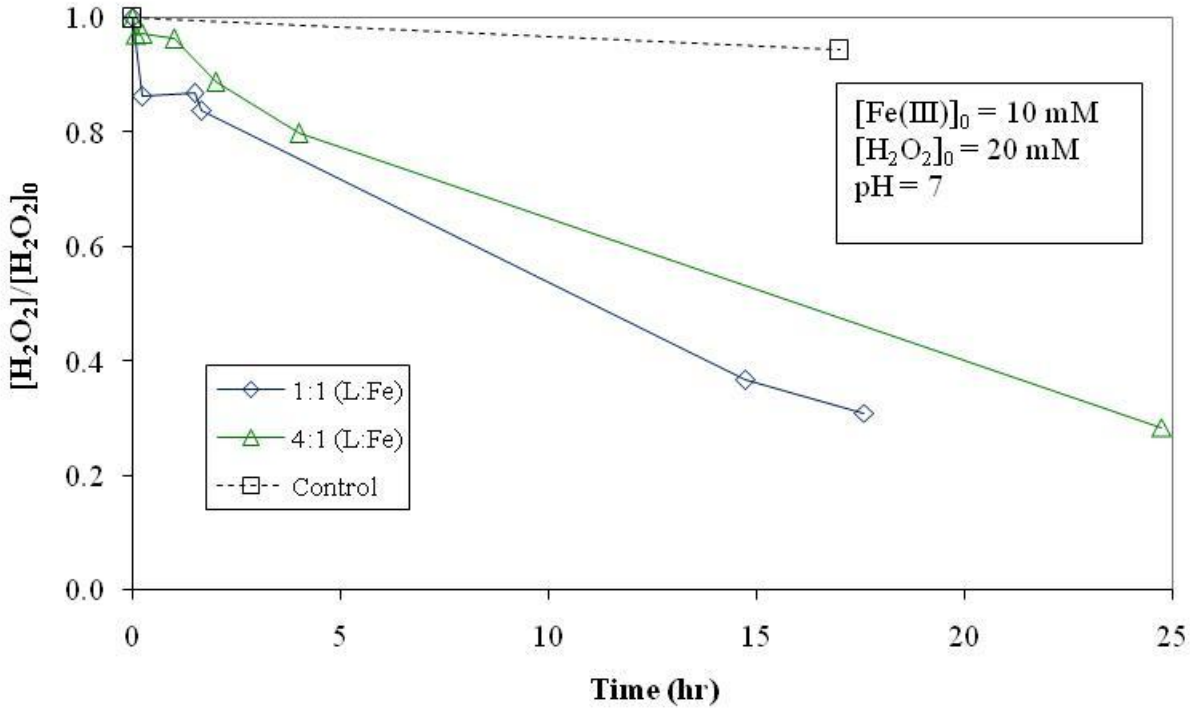

Figure 4.9. Role of ferric iron (Fe(III)) on H_2O_2 decomposition with varying [L]:[Fe] molar ratio. L = citrate.

Figure 4.10. These experiments were conducted in order to quantify the degradation of TCE in the water containing a representative chemical background for the contaminated area. These chelate-modified Fenton reaction experiments ([L]:[Fe] = 1:1) were spiked with 1.1 mmol/L TCE and conducted at an initial pH of 7 and allowed to continue without pH adjustment, reaching a final pH of approximately 5. The 4:1 H_2O_2:Fe(II) molar ratio resulted in the formation of 33% of the maximum possible Cl^- concentration and a 52% reduction in the amount of TCE present. Doubling the quantity of H_2O_2 resulted in the degradation of 87% of the available TCE and formed 59% of the maximum possible Cl^-. A 13% loss of TCE was observed in the control. Although doubling the amount of H_2O_2 increased the amount of TCE degraded, it did not do so proportionately. Thus, the same amount of H_2O_2 applied periodically over a longer time should increase the efficiency of this process. Seol and Javandel (2008) found that high H_2O_2:Fe^{2+} ratios (greater than 330:1) may reduce the efficiency of contaminant degradation in solutions acidified with citric acid (pH ~ 3).

4.6 Aqueous phase (no droplets) kinetic modeling of TCE degradation

The governing rate law for the second-order reaction of TCE with OH• is shown in Equation 4.18, where $[TCE]_{aq}$ is the concentration of TCE in the aqueous phase (mmol/L) and [OH•] is the concentration of hydroxyl radicals (mmol/L).

$$\frac{d[TCE]_{aq}}{dt} = -k_{TCE}[TCE]_{aq}[OH\bullet] \tag{4.18}$$

If [OH•] is assumed to be constant and small, this reaction becomes first order. Substituting the observed rate constant, $k'_{TCE} = k_{TCE} \times [OH\bullet]$ into Equation 4.18 and solving for [TCE] yields Equation 4.19.

$$[TCE]_{aq} = [TCE]_{aq,0} \times \exp(-k'_{TCE} \times t) \tag{4.19}$$

For the kinetic data in Figure 4.11 ([L]:[Fe] = 1:1, pH = 6), $k'_{TCE} = 0.614\ h^{-1}$ ($R^2 = 0.916$, SSE = 0.18 $mmol^2$). The steady-state value of [OH•] = 4.26×10^{-11} mmol/L was obtained by dividing the observed rate constant by the intrinsic rate constant reported in literature. Li et al. (2005) calculated a steady-state [OH•] = $(1.68 \pm 0.10) \times 10^{-10}$ mmol/L for pH = 6 in the presence of trichlorophenol (TCP) ($k_{TCP} = 5.48 \times 10^9\ M^{-1}s^{-1}$). Although the reaction

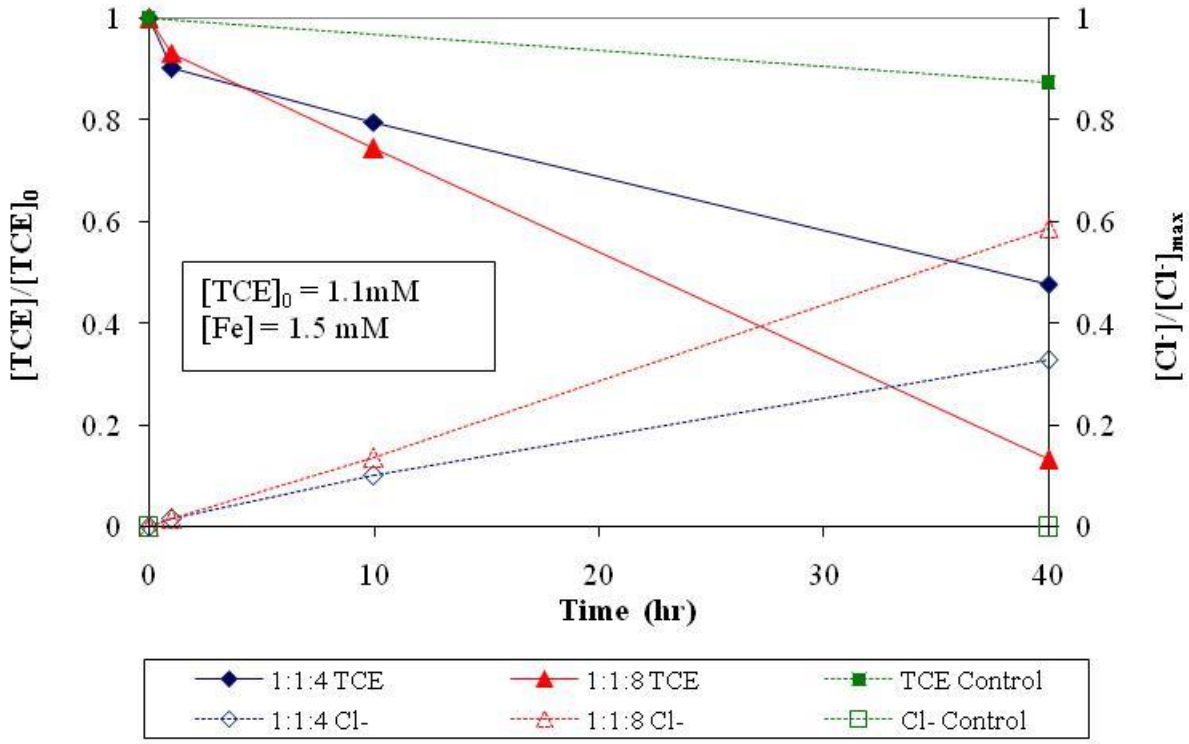

Figure 4.10. TCE reacted and Cl^- formed for varying Fe(II):L:H_2O_2 molar ratio with initial TCE concentration of 1.1 mM, where L is citrate. Conducted in natural water obtained from the DOE site. Control experiment conducted without H_2O_2. Initial pH = 7.

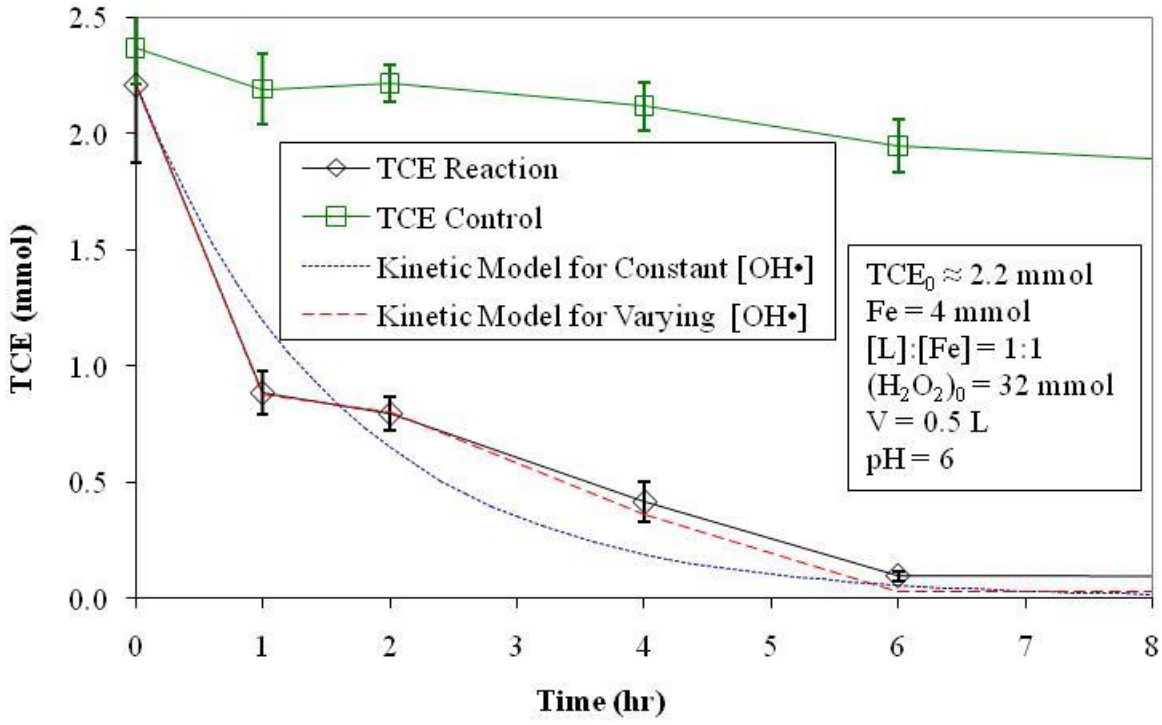

Figure 4.11. TCE degradation and proposed kinetic models using constant [OH•] (Equation 29) and varying [OH•] (Equation 32). Control experiment conducted with no addition of H_2O_2.

conditions for these studies are not identical, similar concentrations of reactants were used, yielding comparable results. Li et al. (2005) noted that their reported value of [OH•] is greater than the actual value due to intermediate compounds competing for hydroxyl radicals.

Although this assumption is effective, it fails to consider the dependence of [OH•] on hydrogen peroxide concentration. For instance, after the addition of hydrogen peroxide to a system containing mostly Fe(II), there will be a large drop in $[H_2O_2]$ due to its rapid reaction with Fe^{2+} to form Fe^{3+}. The result is a large increase in [OH•] and a corresponding drop in pollutant concentration followed by a reduction in the rate of reaction, given the appropriate conditions. Improvements to the constant [OH•] model can be made by assuming the quantity of OH• formed is proportional to the rate of hydrogen peroxide decomposition. Substituting Equations 4.20 and 4.21 into Equation 4.18 and solving for [TCE] yields Equation 4.22.

$$[OH\bullet] = \alpha \times \left(-\frac{d[H_2O_2]}{dt} \right) \tag{4.20}$$

$$k''_{TCE} = k_{TCE} \times \alpha \times [H_2O_2]_0 \tag{4.21}$$

$$[TCE]_{aq} = [TCE]_{aq,0} \times \exp(-k''_{TCE} \times (1 - [H_2O_2]/[H_2O_2]_0)) \tag{4.22}$$

This model, shown in Figure 4.11, yields k''_{TCE} = 4.30 (R^2 = 0.965, SSE = 0.012 $mmol^2$). The quantity of TCE lost due to volatization was considered to be small (about 12%) in relation to the quantity of TCE degraded via reaction with hydroxyl radicals and therefore not included in the calculation for the rate constant of TCE. The experimental H_2O_2 values and calculated [OH•] for this model are shown in Figure 4.12.

TCE degradation is accompanied by Cl^- formation, with a possible maximum (mmol Cl^- formed) / (mmol of TCE degraded) = 3. However, due to the formation of chlorinated intermediates which compete with TCE for hydroxyl radicals, complete TCE dechlorination was not necessarily observed. Figure 4.13 shows the kinetic data for Cl^- formation as well as the theoretical quantities of Cl^- produced for the model based on Equation 4.22 with (mmol Cl^- formed) / (mmol TCE reacted) = 2 and 3. Analysis of the kinetic data indicates the actual (mmol Cl^- formed) / (mmol TCE reacted) = 2.8 ± 0.3, signifying almost complete degradation of TCE.

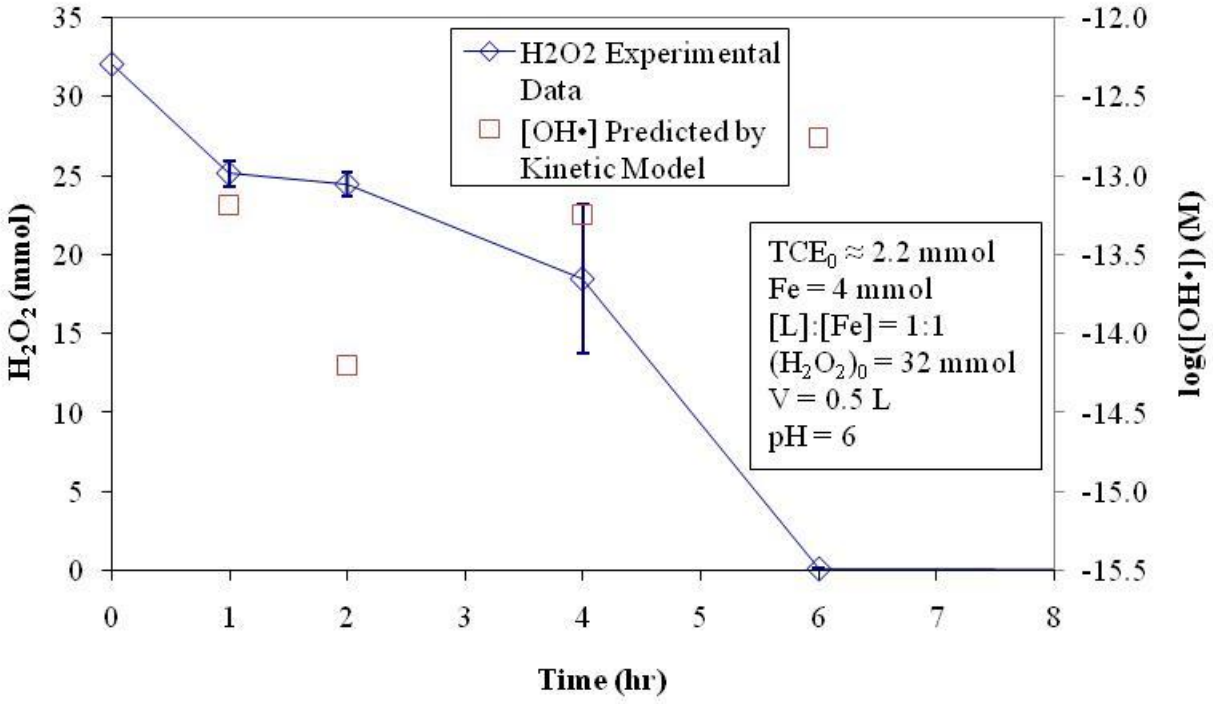

Figure 4.12. H_2O_2 consumption and [OH•] for proposed kinetic model using varying [OH•] (Equation 32).

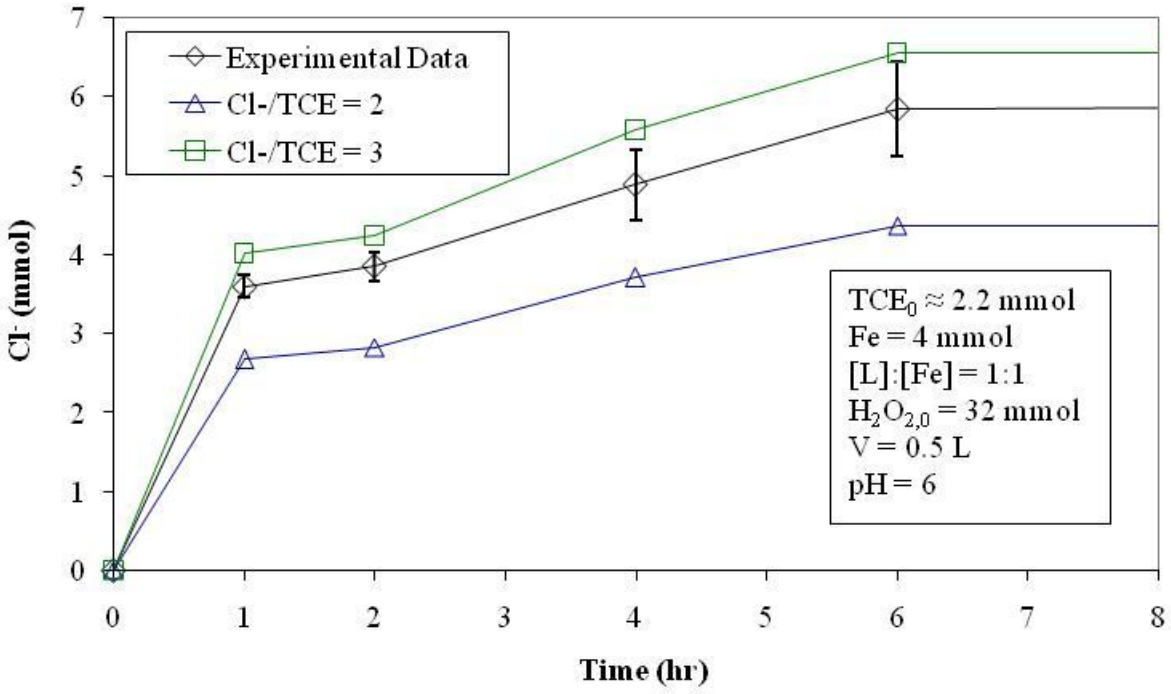

Figure 4.13. Cl^- formation for proposed kinetic model using varying [OH•] (Equation 32) for (mmol Cl^- formed) / (mmol TCE reacted) = 2 and 3.

4.7 Two-phase (TCE droplet-water) kinetic modeling of TCE degradation

In this section, a model for the degradation of TCE in two-phase systems, as seen in Figure 4.14, is presented. In this system, n droplets of radius R (m) are present in a sealed reactor vessel of volume V (L). The vessel is stirred in order to maintain the organic-phase TCE in the form of droplets, which maintain a velocity of U (m/s) relative to the surrounding fluid. A mass-transfer boundary layer of thickness δ (m) is formed around the droplet, creating a TCE concentration gradient.

The governing equations for this model consist of balances on the TCE droplets (Equation 4.23) and the concentration of TCE in the bulk phase, $[TCE]_{aq}$, (Equation 4.24) both varying with respect to time. In these equations, W_r (mmol s^{-1} m^{-2}) is the mass flux of TCE from the droplet surface to the bulk phase, S is the surface area of one droplet (initial S = 2.4×10^{-5} m^2) (n = 100 was used for calculations), ρ_{TCE} is the density of TCE (g/cm^3), and M_{TCE} is the molecular weight of TCE (g/mol). Because $[H_2O_2] > 0$ for the majority of the experiments, the proposed constant [OH•] model is used to calculate the degradation of TCE in the aqueous phase. These equations (along with the noted assumptions) can be solved simultaneously to yield a dynamic profile for $[TCE]_{aq}$ and R.

$$V\frac{d[TCE]_{aq}}{dt} = -k'_{TCE}\times V\times[TCE]_{aq} + W_r\times S\times n \tag{4.23}$$

$$\frac{4\pi R^2\rho_{TCE}}{M_{TCE}}\frac{dR}{dt} = -W_r\times S \tag{4.24}$$

In order to calculate W_r (mol s^{-1} m^{-2}), Equation 4.25 is used, where k_c is the mass transfer coefficient (m/s) and $[TCE]_{sat}$ is the maximum dissolved concentration of TCE in the aqueous phase (8 mmol/L is used for calculations).

$$W_r = k_c([TCE]_{sat} - [TCE]_{aq}) \tag{4.25}$$

The boundary layer thickness can be calculated from k_c, a function of the Sherwood number (Sh). To calculate this coefficient, Equations 4.26-4.28 are used, where Re is the Reynolds number, Sc is the Schmidt number, ν is the dynamic viscosity of water, and $D_{TCE\text{-}water}$ is the binary diffusion coefficient of TCE in water (9.4×10^{-10} m^2/s) (Montgomery 1996; Fogler 1999; Reichert et al. 2004).

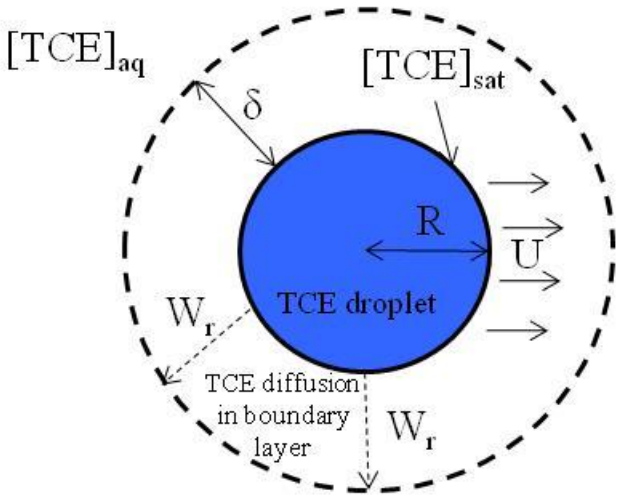

Figure 4.14. Schematic of TCE droplet dissolution into aqueous solution.

$$\mathrm{Re} = \frac{U \times (2R)}{\nu} \tag{4.26}$$

$$Sc = \frac{\nu}{D_{TCE-water}} \tag{4.27}$$

$$Sh = \frac{2R \times k_c}{D_{TCE-water}} = 2 + 0.6 \times \mathrm{Re}^{1/2} \times Sc^{1/3} \tag{4.28}$$

Because U is the velocity of the particle relative to the surrounding fluid, it is very difficult to measure. However, using the theory of stationary slip velocity, the minimum relative velocity can be estimated by calculating the settling velocity of the droplet in a stationary media (Harriott 1962; Reichert et al. 2004). Since R changes with time, the drag coefficient, C_D, is a function of time. Because in-depth fluid dynamics calculations are beyond the scope of this research, a simple correlation between U and R is required. Using Equation 4.29 is to estimate C_D from Re and the equations for calculating settling velocity, a linear relationship between U and R was formulated for values of R ranging from 0 to 0.0015 m, as seen in Equation 4.30 (R^2 = 0.995 with 12 points) (Munson et al. 1998; Brown and Lawler 2003).

$$C_D = \frac{24}{\mathrm{Re}}(1 + 0.150\,\mathrm{Re}^{0.681}) + \frac{0.407}{1 + \frac{8710}{\mathrm{Re}}} \tag{4.29}$$

$$U = 126.4 s^{-1} \times R \tag{4.30}$$

For the chelate-modified Fenton reaction, it can be safely assumed that no Fe or citrate species are present in the TCE droplets since these will be ionized at near-neutral pH. Additional model assumptions include:

- Reactions only occur in the bulk aqueous phase
- OH• is the only species that reacts with TCE
- Liquid phase is uniformly mixed and isothermal
- Uniform droplet size, distribution, and relative velocity of droplets
- Droplets are spherical and have smooth surfaces
- Negligible TCE loss due to volatility (TCE is present in excess such that the quantity of TCE lost due to volatization is not important compared to the quantity of TCE degraded via reaction with OH•)

Parametric variations were performed on k_c to determine its effect on $[TCE]_{aq}$ and R. As expected, the rate of dissolution of the droplets is directly proportional to the value of k_c. The minimum and maximum calculated values for k_c are 4.6×10^{-5} m/s and 9.9×10^{-4} m/s, respectively.

The predicted model values indicate no droplets should be present after 18 h and that TCE degradation should be complete after 22 h. According to visual observation, the droplets did not disappear until approximately 28 h. Thus, the value of k' and/or k_c is likely overestimated.

The H_2O_2 degradation profile for a chelate-modified Fenton reaction system in the presence of excess TCE in droplet form is shown in Figure 4.15. Because the dechlorination of TCE is the main focus of this study, it was measured solely by Cl^- production in the aqueous phase. After complete consumption of the initial amount of H_2O_2 (12 h), a second spike of equal quantity was made. The second addition leads to an increase in Cl^- formation, proving that multiple injections of H_2O_2 can be used repeatedly in these systems to further degrade contaminants. The initial spike of H_2O_2 resulted in the production of 10.9 mmol Cl^-, whereas the second spike produced only 5.9 mmol. This significant difference and occurs for two reasons: 1) More Fe^{2+} is available in the initial stages of the reaction and 2) when TCE concentrations are lower, less hydroxyl radicals are consumed from reaction with TCE, increasing the rates of Reactions 2.8-12 and 7. The result is a higher rate of H_2O_2 degradation, which explains why H_2O_2 is consumed faster after the second injection than the first (Figure 4.15). Figure 4.16 shows the actual and model-predicted amounts of Cl^- formed.

After the first hour of the reaction, Cl^- production is relatively constant and correspond closely to the model-predicted values (Equations 4.23 and 4.24) for (mmol Cl^- formed) / (mmol TCE reacted) = 1. This is significantly less Cl^- formation than in the aqueous-phase TCE experiments despite the larger (mmol Cl^- formed) / (mmol H_2O_2 consumed) for the system with droplets. Even though the initial $[H_2O_2]$:[Fe] ratios are the same, some of this disparity can be explained by the different $[TCE]_{aq}$:[Fe] ratios, which are ~1:1 for the system with no droplets and ~2:1 for the for the system containing droplets.

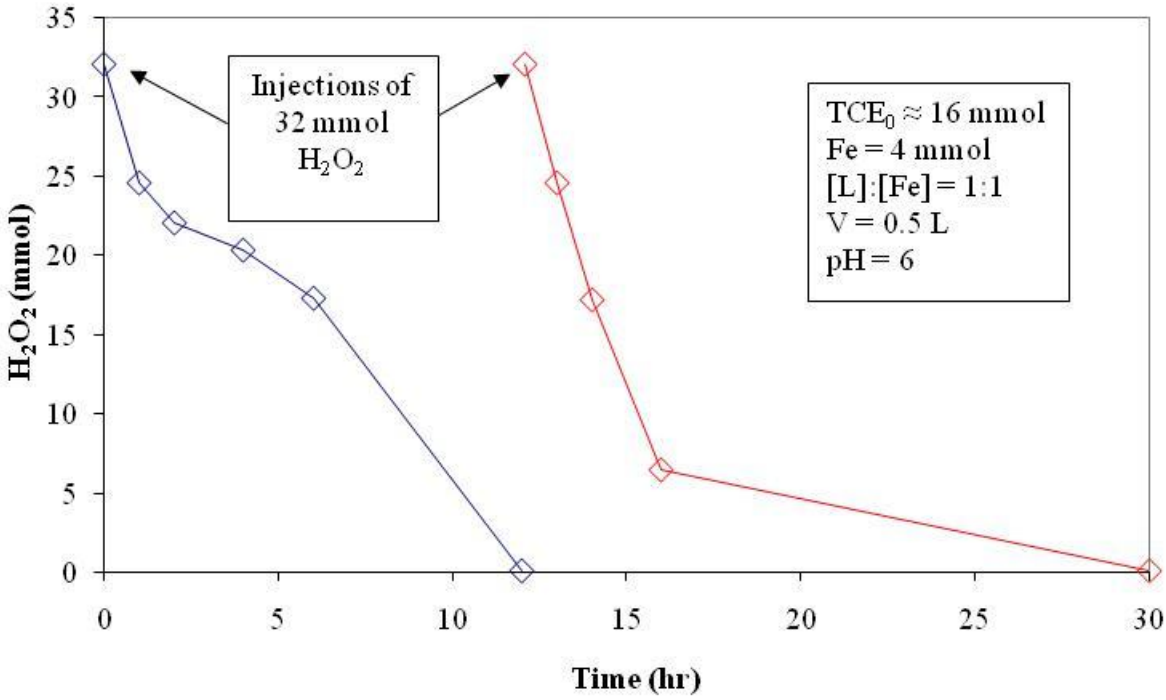

Figure 4.15. H_2O_2 degradation profile for chelate-modified Fenton reaction in two-phase TCE system. H_2O_2 injected at time = 0 h and 12 h.

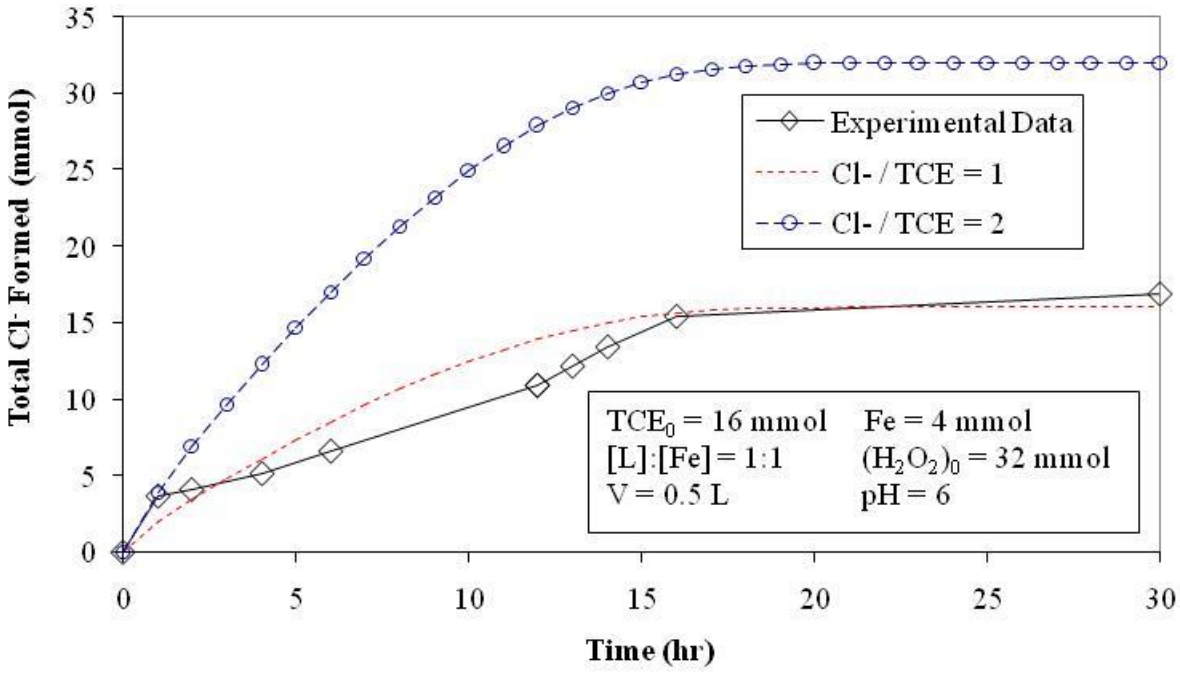

Figure 4.16. Cl^- formation profile for chelate-modified Fenton reaction in two-phase TCE system. Experimental results for H_2O_2 injected at time = 0 h and 12 h. Model-predicted results for (mmol Cl^- formed) / (mmol TCE reacted) = 1 and 2 using Equations 33 and 34.

Although most TCE degradation is thought to occur via oxidation by hydroxyl radicals, it has been proven that other radical species formed during Fenton reaction propagations are capable of degrading toxic organics. Watts et al. (2005) used an Fe(III)-catalyzed modified Fenton reaction with chelate at pH 3 with a high H_2O_2:Fe(III) ratio to destroy DNAPLs of carbon tetrachloride and chloroform**.** These contaminants were chosen because of their resistance to oxidation via hydroxyl radicals (k_{OH}**.** on the order of 10^6 $M^{-1}s^{-1}$) (Haag and Yao 1992). The main species responsible for this is superoxide radical anion ($O_2\bullet^-$) (Watts and Teel 2006). Other oxidants include perhydroxy radical ($HO_2\bullet$), hydroperoxide anion (HO_2^-), which are present in many of the free radical reactions (Ravikumar and Gurol 1994; Lin and Gurol 1998; De Laat and Gallard 1999; Wang and Lemley 2001; Pignatello et al. 2006). Superoxide radical anion, the conjugate base of perhydroxy radical (Equation 4.31), could also play a role in the destruction of TCE DNAPLs.

$$HO_2\bullet \Leftrightarrow O_2^-\bullet + H^+ \qquad K_{31} = 1.58 \times 10^{-5}\ M \qquad (4.31)$$

Li et al. (2007) showed that superoxide radical anion concentrations were two orders of magnitude higher for a chelate-modified Fenton reaction system ([L]:[Fe] = 1:1) than for a standard Fenton reaction system (no chelate), both containing [Fe] = 0.2mM and [H_2O_2] = 0.5 mM.

4.8 Efficiency of chelate-modified Fenton reaction

One way to determine the efficiency of H_2O_2 use for TCE degradation is to compare the quantity of Cl^- formed to the quantity of H_2O_2 reacted. For the chelate-modified Fenton reaction data in Figures 4.13 (no TCE droplet) and 4.16 (with TCE droplets), the time-averaged (mmol Cl^- formed) / (mmol H_2O_2 reacted) values are given in Figure 4.17. Overall, this ratio is larger in the presence of TCE droplets since there is more TCE available to be degraded, but for these reaction conditions, between 0.2 and 0.5 mmol of Cl^- are formed per mmol H_2O_2 reacted. In order to completely degrade 1 mmol TCE, approximately 6 to 15 mmol H_2O_2 are required. This is in contrast to the efficiency of the standard Fenton reaction (Figure 4.4), which yields (mmol Cl^- formed) / (mmol H_2O_2 reacted) = 1.2 to 1.5, meaning 2 to 2.5 mmol H_2O_2 are needed to completely

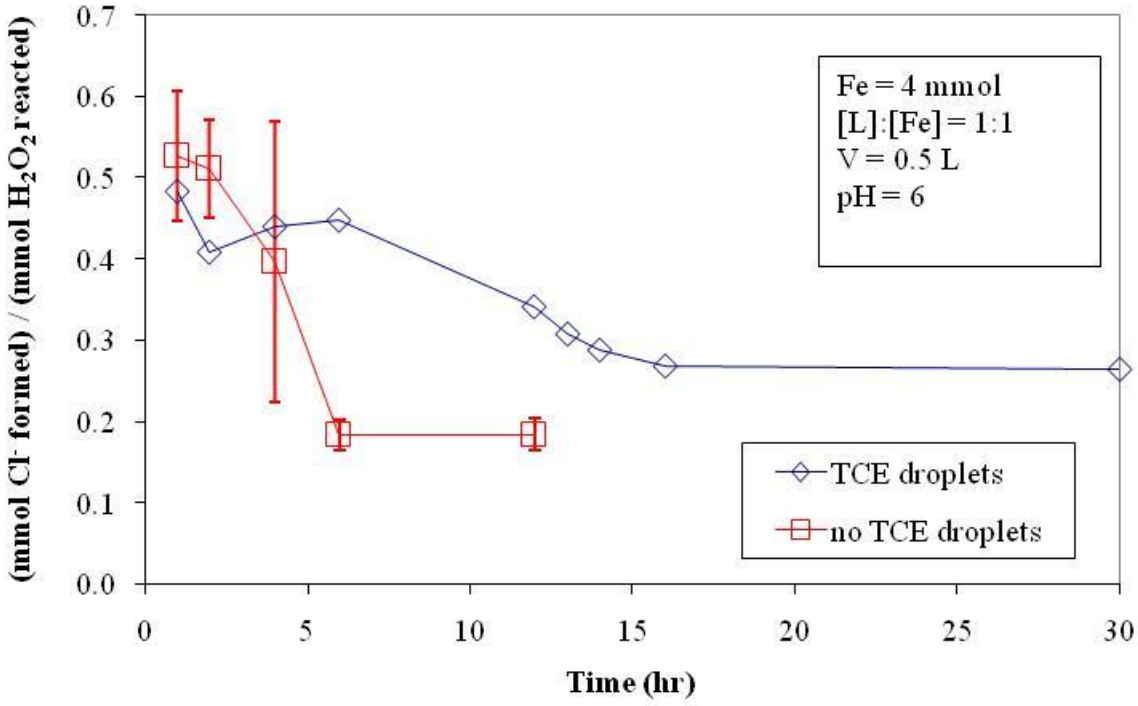

Figure 4.17. (mmol Cl^- formed) / (mmol H_2O_2 reacted) for one system containing no TCE droplets ($TCE_0 \approx 4$ mmol) and one with TCE droplets ($TCE_0 \approx 16$ mmol).

degrade 1 mmol TCE. Considering the standard Fenton reaction takes place at optimum operating conditions, the results for the chelate-modified Fenton reaction are very reasonable and can be increased by injecting H_2O_2 in small doses over a longer period of time, increasing the L:Fe ratio, and/or other methods.

4.9 Packed column studies for simulated groundwater injection

Natural sub-surface matter may negatively affect H_2O_2 propagation reactions via H_2O_2 degradation by inorganic reductants and H_2O_2 decomposition to H_2O and O_2 (Pignatello et al. 2006). The possibility exists to use the naturally occurring iron found in the subsurface to catalyze a Fenton-like reaction; however, this would only be applicable to a limited number of remediation sites due to the high concentrations of naturally occurring iron required for significant contaminant destruction. The rate of hydroxyl radical generation must also be great enough to overcome hydroxyl radical scavenging that takes place in the subsurface. Ravikumar and Gurol (1994) found that the addition of a small amount of soluble iron to sand containing bound iron results in a dramatic increase in hydrogen peroxide decomposition. For practical applications, the chelate-modified Fenton reaction was used to degrade TCE in a simulated gravel aquifer. A column packed with RGA gravel was filled with 2.25 L of DIUF water containing 0.41 mM TCE, 1.5 mM Fe(II), and 1.5 mM citrate at near-neutral pH, as seen in Figure 4.18. The circulation rate was adjusted to give an equivalent groundwater velocity of 2.5 ft/day. At 0 h and 24 h, H_2O_2 was injected into the top of the column so as to yield a 2:1 [H_2O_2]:[Fe] molar ratio. TCE dechlorination results are shown in Figure 4.19 with (mmol Cl^- formed) / (mmol TCE degraded) ≈ 3.

After a period of 24 h, approximately 40% of the TCE had been degraded up to a depth of at least 2 ft. Insignificant degradation was observed at a depth of 3 ft given the reactants had not had sufficient time to traverse that distance. After 48 h, TCE degradation at a depth of 3 ft had reached approximately 40%. The chelate-modified Fenton reaction is capable of degrading significant quantities of TCE in the presence of RGA gravel under simulated groundwater flow.

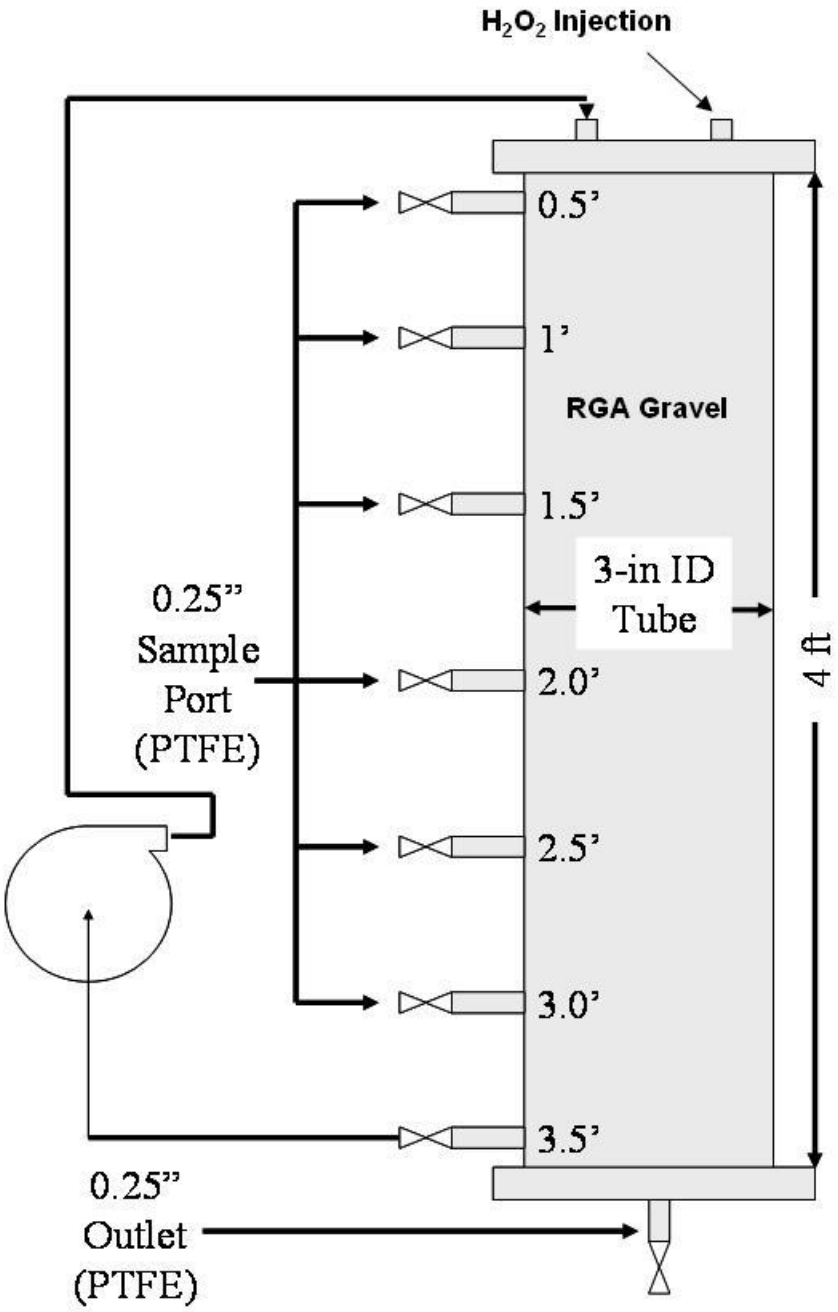

Figure 4.18. Column packed with RGA gravel for simulation of TCE degradation in groundwater systems using chelate-modified Fenton reaction. Void volume = 2.25 L.

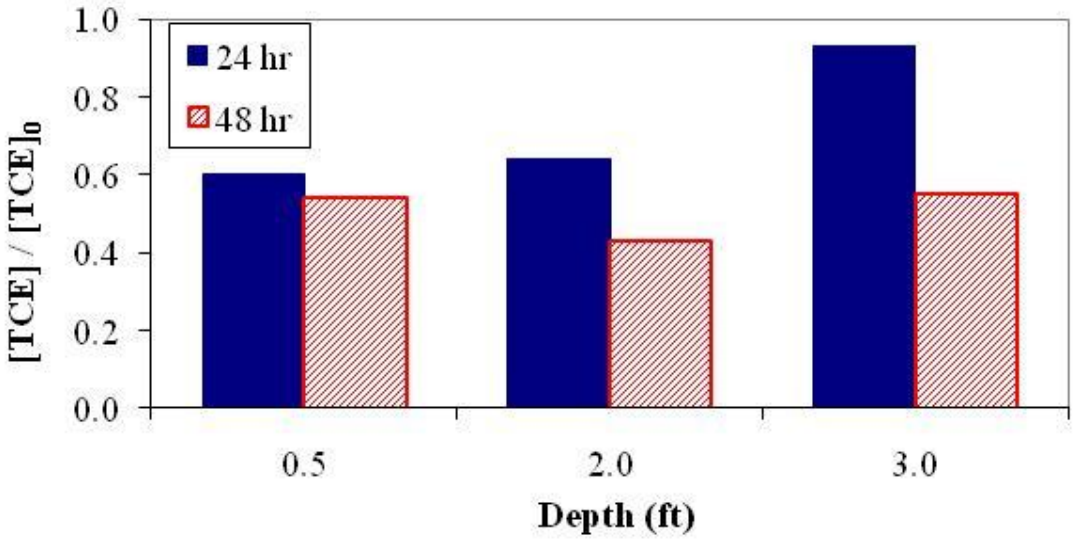

Figure 4.19. TCE dechlorination results for RGA packed column. $[TCE]_0$ = 0.41 mM, [Fe] = 1.5 mM, [L]:[Fe] = 1:1. H_2O_2 injections at 0 and 24 h for 2:1 $[H_2O_2]$:[Fe] molar ratio. Column flowrate = 2.5 ft/day. (mol Cl^- formed) / (mol TCE reacted) ≈ 3 (not shown in figure).

Chapter 5 Stimuli-Responsive Membranes for Free Radical Reactions

The stimuli-responsive behavior of the PVDF-PAA membrane is the main focus of the first part of this chapter. The composition and structure of the membranes are examined before discussing their stimuli-responsive behavior to pH and cations. Next, the selectivity and stability of various immobilized cations are examined. Finally, the stimuli-responsive behavior of these membranes for the removal of adsorbed organic contaminants is discussed. The second part of this chapter includes the results and discussion regarding the use of PVDF-PAA membranes for free radical production and subsequent degradation of organic compounds. The importance of the effect that iron species distribution within the membrane domain has on the decomposition of H_2O_2 is outlined first. This is followed by the quantification and modeling of steady-state H_2O_2 decomposition as a function of residence time for a PVDF-PAA-Fe(III) membrane. This same membrane system is then used for the degradation of PCP from water at circumneutral pH. Sections 5.4 – 5.6 and parts of Section 5.1 are **published** in **Lewis, Smuleac, et al. (2009)**.

5.1 Composition and structure

Functionalizing the pores of a support membrane with PAA creates a nanostructred material ideal for iron ion immobilization (for reaction with H_2O_2) due to its high ion exchange capacity (Lewis et al. 2009) and the stability of immobilized iron ions in the presence of other cations. To synthesize this membrane, a network of PAA was created within the pores of a poly(vinylidene fluoride) (PVDF) membrane using a simple *in situ* polymerization technique.

The functionalization of the PVDF membranes with PAA was characterized by FTIR spectroscopy. The chemical structures for the hydrophobic PVDF and PAA-coated PVDF membranes were studied by FTIR-ATR spectroscopy (Figure 5.1). The PAA-coated PVDF membrane shows a strong absorption band at 1710 cm^{-1} and a broad absorption band from 2500 – 3300 cm^{-1}, whereas the blank hydrophobic PVDF membrane does not. These bands are due to the presence of C=O and O-H bond

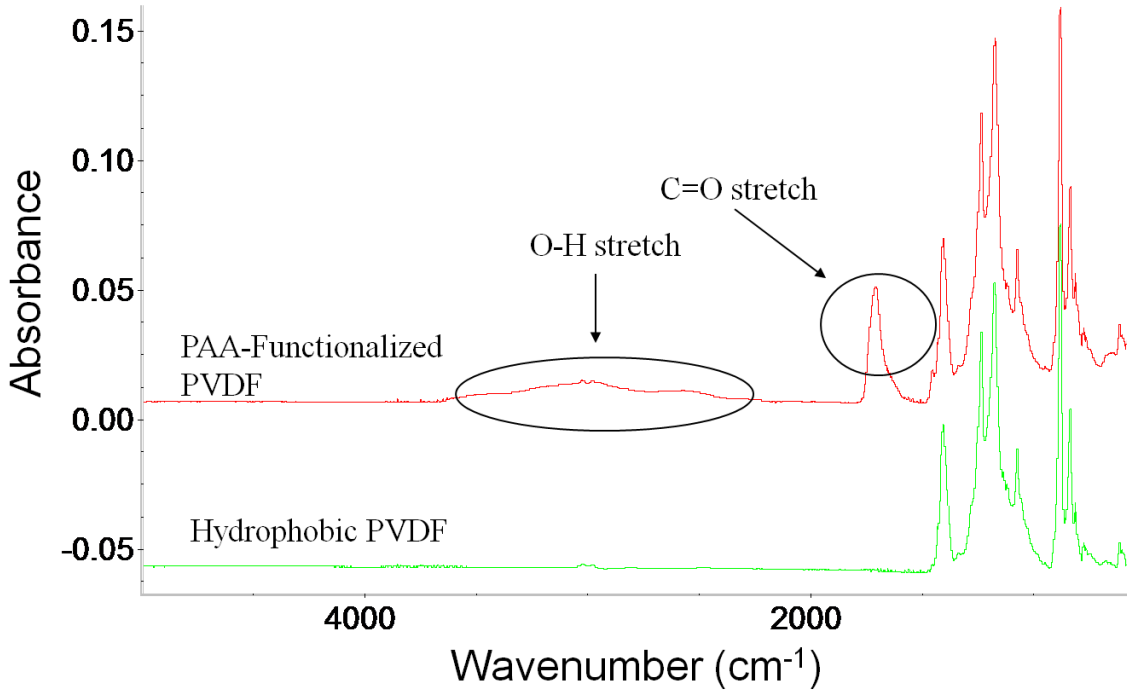

Figure 5.1. FTIR-ATR spectra for hydrophobic PVDF and PAA-functionalized PVDF membranes.

stretching, respectively, in carboxylic acid groups, indicating successful PAA formation within the functionalized membrane. The strong absorption band at 1140-1280 cm^{-1} is characteristic of CF_2 found in PVDF. Xu and Bhattacharyya (2008) performed both FTIR analysis and STEM-EDS mapping on hydrophobic PVDF membranes functionalized with PAA. FTIR data showed C=O bond stretching was present in the modified hydrophobic PVDF membranes, but not in the unfunctionalized PVDF membrane, indicating successful PAA functionalization. STEM-EDS mapping indicated the presence of oxygen atoms, also confirming the formation of PAA. Additionally, The presence of PAA in the membrane pores has been verified through the detection of oxygen via Energy Dispersive X-Ray (EDX) analysis.

Given the variability associated with this polymerization process, it is important to ascertain the uniformity of the PAA coating within the PVDF membrane. A cationic fluorescent dye, thionine, was bound to the carboxylate groups of PAA via ion exchange for subsequent analysis with Confocal Laser Scanning Microscopy (CLSM). Through the use of CLSM, we were able to observe thionine binding through the depth of the membrane while in a hydrated state and without altering the membrane structure. The CLSM images in Figure 5.2 constitute the average fluorescence of multiple images taken at different depths throughout the PVDF-PAA and unmodified PVDF membranes. The fluorescence of the blank PVDF membrane was much lower in intensity than the PVDF-PAA membrane and was due to the background fluorescence of the membrane itself and/or physically adsorbed thionine, indicating the presence of PAA throughout the PVDF-PAA membrane pores.

TGA was used to ascertain the thermal stability of the PVDF-PAA membranes. There appear to be four different temperature regions in which weight loss takes place, as seen in Figure 5.3. The mass loss from 35 to 140 °C is due to free and bound water within the PAA domain (1.5 wt %) (Shao and Lutkenhaus 2010). Next, loss from 140 to 335 °C is most likely due to the release of water from anhydride formation as well as loss of methane, acrylic acid monomer, and carbon dioxide (10 wt %) (Dubinsky et al. 2004). From 335 to 438 °C, PAA chain scission and subsequent loss of these fragments leads to a reduction of 10.4 wt % (Dubinsky et al. 2004). This chain scission continues at higher temperature, but 438 °C is the onset temperature of PVDF, initiating its degradation (Li

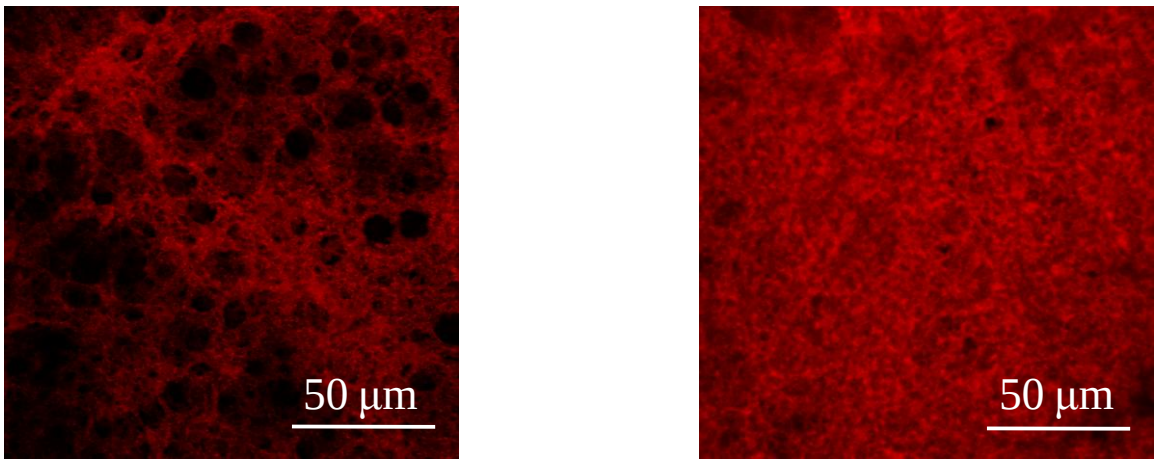

Figure 5.2. CLSM imaging of a PAA-functionalized PVDF membrane. CLSM fluorescent images of PVDF and PVDF-PAA membranes stained with thionine (488 nm excitation). Brighter areas indicate higher concentrations of thionine.

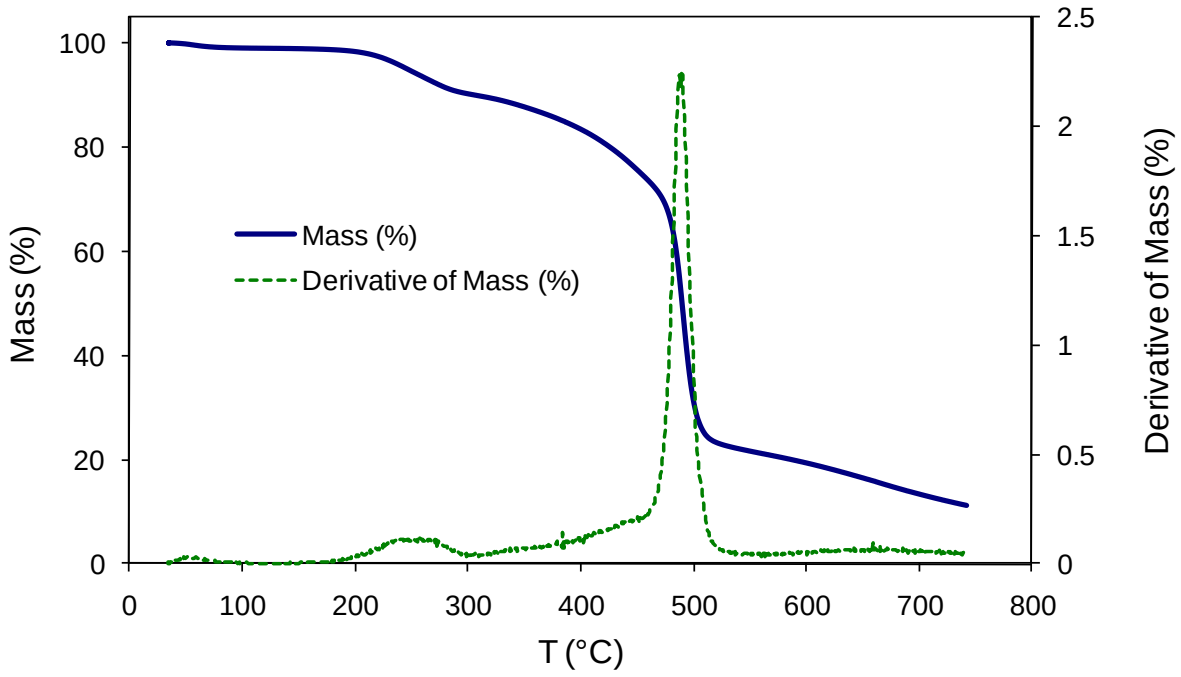

Figure 5.3. TGA thermogram of a PVDF-PAA membrane. Solid line: mass % versus temperature. Dashed line: derivative of mass % loss versus temperature.

et al. 2009). Mass loss from 438 to 750 °C was 67.2 wt % and the 11.3 wt % residual is most likely PVDF char (Li et al. 2009).

5.2 Stimuli-responsive behavior

The pH-responsive behavior of the PAA network permits controlled opening and closing of the PAA-coated membrane pores (Hu and Dickson 2009). The effect of varying pH on water flux through the PVDF-PAA functionalized membrane is shown in Figure 5.4. It can be seen that as the permeate pH is increased, the flux decreases, with a significant drop of approximately one order of magnitude occurring between pH 3 and pH 6. This is in agreement with the findings of Hu and Dickson (2007), who conducted similar tests on PVDF membrane pores filled with PAA. Upon closer inspection of the flux modulation at a pH closer to the pK_a in a different membrane containing less PAA, the flux decreases by almost a factor of two when increasing the pH from 4.8 to 5.4 (Figure 5.5). Since the pK_a of PAA can be 4.25, the pK_a of acrylic acid, and higher (Ito et al. 1990), the PAA network will maintain a relatively neutral charge at a low pH, leaving it in a retracted state. As the pH is increased, more -COOH groups will become ionized, resulting in an elongation of the PAA network due to charge repulsion. While in the elongated state, there is significantly less core leakage and thus lower permeate flux than in the retracted state. Previous work has demonstrated how variations in crosslinking and PAA loading affect the pH-responsive behavior, and therefore water flux and solute rejection, of similar membranes (Hu and Dickson 2007; Hu and Dickson 2009)

In addition to tuning pore size via pH alterations, divalent cation (Fe(II) and Ca^{2+}) capture for the modulation of water flux through the membrane was investigated. Figure 5.6 shows the cumulative quantities of Ca^{2+} and Fe(II) captured in the membrane during operation under convective flow as well as the effect this had on the water flux through the membrane. Within the first 5 min, a slight drop in pH was observed, accounting for the initial increase in flux. However, once the pH of the permeate had stabilized at approximately 4.4, the flux continued to increase with time. Because of the increased shielding of the negatively charged carboxylate groups by divalent cations in comparison to the displaced monovalent cations (Na^+ and H^+) (Karppi et al. 2010), their capture

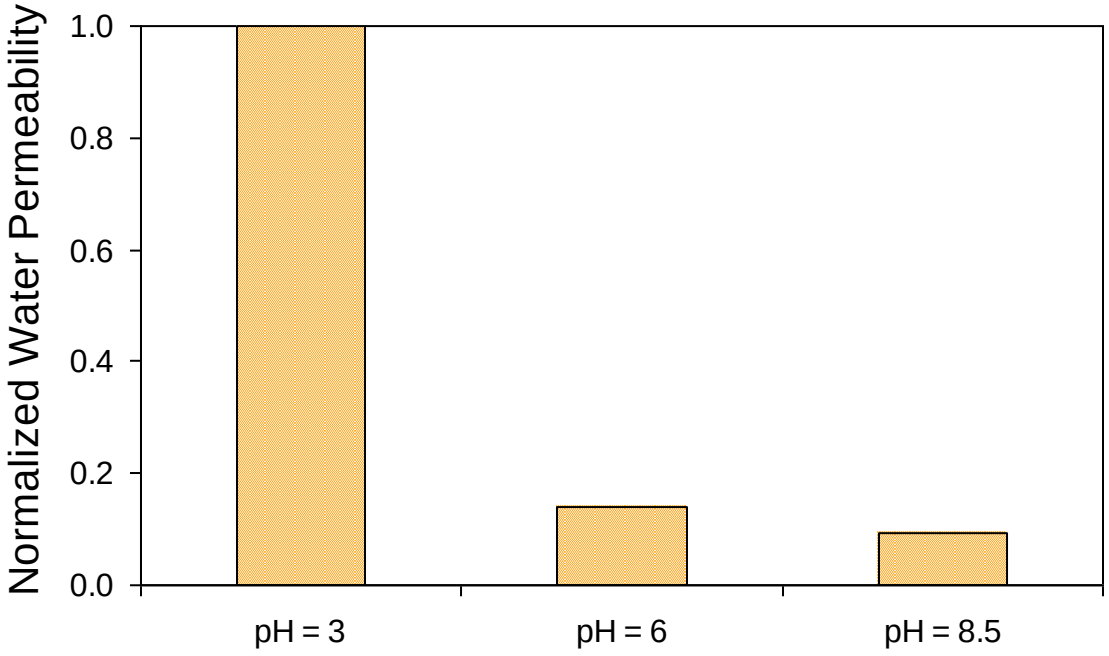

Figure 5.4. Water permeability dependence on pH for PAA-functionalized PVDF membrane. All flux values are normalized with respect to the permeability at pH = 3 (2.5×10^{-4} cm^3 cm^{-2} bar^{-1} s^{-1}). Pressure ranged between 0.7 and 2.8 bar.

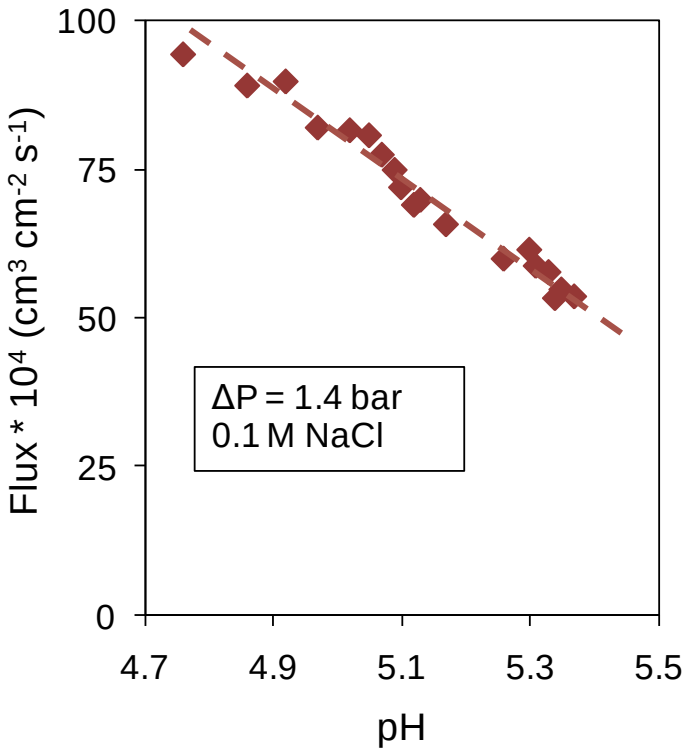

Figure 5.5. Water permeability dependence on pH for PAA-functionalized PVDF membrane for pH ranging from 4.8 to 5.4.

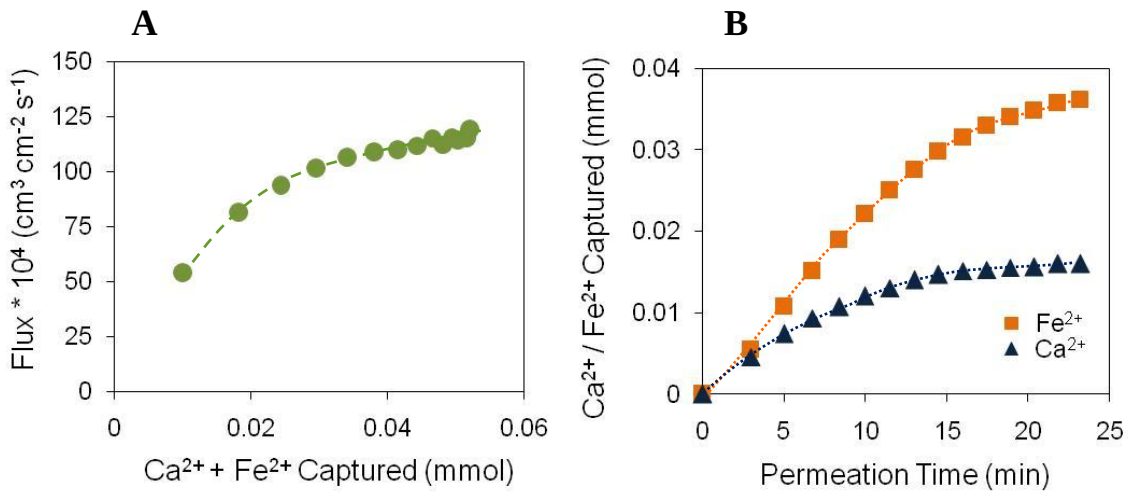

Figure 5.6. Divalent cation-responsive water flux through PVDF-PAA membrane. (A) Water flux as a function of cumulative divalent cation (Fe(II) and Ca^{2+}) loading. (B) Cumulative divalent cation capture with time. Feed contains 0.50 mmol/L Fe(II) and 0.50 mmol/L Ca^{2+}; permeated at 1.4 bar; feed pH 5.0; permeate pH 4.4; external membrane area = 13.2 cm^2; (mol Na^+ + H^+ released) / (mol Fe(II) + Ca^{2+} captured) = 2.1 ± 0.5.

resulted in increased water flux through the membrane, indicating a collapse of the PAA gel.

5.3 Cation exchange and stability

By immobilizing iron ions in the PVDF-PAA domain, the iron-functionalized membrane provides the platform needed for the generation of free radicals from H_2O_2. In order to ensure that Fe(II) was being captured by the PAA network and not precipitating in the membrane pores, it was necessary to monitor the release of the cation displaced by Fe(II) during ion exchange. For this reason, and to prevent pH drop during Fe(II) capture, the PVDF-PAA membranes were pre-loaded with Na^+ (PVDF-PAA-Na^+). It was observed that for every mol of Fe(II) captured, approximately 2 mol of Na^+ were released, indicating successful capture in the PAA domain. It is important to note that there was no evidence of iron precipitation during loading and leaching of iron from the membrane during experimentation was either insignificant or undetectable.

While Fe(II) was preferentially captured over Ca^{2+} during loading, it is important to establish the stability of the previously immobilized iron in the presence of other multivalent ions commonly found in natural water. For this, two PVDF-PAA membranes, one containing 0.90 mmol Fe(II) and the other containing 0.82 mmol Fe(III) were immersed in separate deoxygenated solutions, each with 2 mmol/L Ca^{2+} (as $CaCl_2$) at near-neutral pH. After equilibration for 1 h, the Ca^{2+} had displaced a small quantity of the Fe(II) in the first membrane; however, none of the Fe(III) was displaced in the other membrane. The increased stability of Fe(III) over Fe(II) indicates that although it may generate free radicals at a slower rate, Fe(III) may be the more desirable species for specific applications and/or long-term use. Nonetheless, the increased rate of OH• production from H_2O_2 in the presence of Fe(II) compared to Fe(III) in the solution phase could make it more suitable for contaminant degradation in the membrane domain.

While the possibility exists to reduce Fe(III) to Fe(II) via addition of a reducing agent, the unloading and reloading of iron can be easily achieved due in part to the pH-responsiveness of the gel. To demonstrate the ease with which the iron ions can be unloaded from these membranes, two membranes, one containing Fe(II) and the other

containing Fe(III), were added to separate solutions under acidic conditions, resulting in the release of the iron ions from both membranes. Fe(II) was subsequently recaptured within the PAA gel with no detectable loss of ion exchange capacity (see Table 5.1).

5.4 pH responsive behavior for removal of adsorbed organic contaminants

In addition to the inorganic ions, it is important to understand how organic compounds present in solution will interact with these membranes, especially at near-neutral pH. To determine this interaction, two PVDF-PAA membranes were immersed in 20 mL of a pH 6.0 buffered solution containing 1 mmol/L MES and 100 μmol/L TCP, the model organic compound, and shaken for 20 h to ensure equilibration. TCP is an ideal compound to use for studying adsorption to these membranes because it will be present in its ionized and nonionized forms at pH levels found in natural waters (pK_a of 6.1) (Mackay 2006). After equilibration, 5.7 ± 0.4 % of the TCP had adsorbed to the membranes (15 ± 1 nmol TCP / mol PAA) and the pH had dropped to 5.61 ± 0.01 due to the ion exchange of Na^+ for H^+. At this pH, approximately 3/4 of the TCP molecules are nonionized and not all of the carboxylic acid groups of PAA will be ionized, allowing for the adsorption of non-ionized TCP. Since contamination of the membranes is undesirable, it is important to be able to remove these and similar pollutants from the membrane. By adding the membranes with adsorbed TCP to solutions containing 1 mM NaOH and allowing them to equilibrate (final pH of 7.48 ± 0.04) for 18 h, 95 ± 9 % of the TCP was desorbed from the PVDF-PAA membranes. At this pH, approximately 95 % of the TCP molecules and 100 % of the carboxylic acid groups of PAA are ionized. This demonstrates how the pH-responsiveness of the PAA gel can be utilized for self-cleaning applications.

5.5 Reactivity of H_2O_2 and conversion of immobilized Fe(II) to Fe(III)

Ion exchange groups immobilized within membrane pores have been used for a variety of applications involving metal capture. Several investigators have utilized Nafion membranes for the immobilization of Fe(II)/Fe(III) and subsequent reaction with H_2O_2

Table 5.1. Fe(II) / Fe(III) loading and unloading from PVDF-PAA membrane. Immobilized Fe(III) in PVDF-PAA-Fe(III) obtained by oxidizing previously captured Fe(II) with H_2O_2 solution. Analytical error as standard deviation is given with experimental values.

Fe Ion Capture / Release (mmol)	Membrane	
	PVDF-PAA-Fe^{2+}	PVDF-PAA-Fe^{3+}
First Capture	0.094 ± 0.009	0.072 ± 0.007
First Release	0.109 ± 0.011	0.070 ± 0.007
Second Capture	0.099 ± 0.010	
Second Release	0.103 ± 0.010	

(Espro et al. 2000; Espro et al. 2001; Fernandez et al. 2003; Parra et al. 2004). Espro et al. (2000, 2001) applied an Fe(II)-H_2O_2 Fenton system at elevated temperature and pressure for the oxidation of light alkanes. Fernandez et al. (2003) used a photoassisted Fe(III)-H_2O_2 system for the oxidation of target organics. Parra et al. (2004) utilized a similar photoassisted Fenton reaction for the oxidation of 4-chlorophenol.

The relative amounts of Fe(II) and Fe(III) present within the membrane domain determine the rate at which H_2O_2 is decomposed. In order to better understand how iron speciation affects H_2O_2 decomposition and therefore OH• formation within the membrane domain, a PVDF-PAA membrane containing only Fe(II) was used for decomposition of H_2O_2. A reaction mixture containing 0.07 mmol/L H_2O_2 and 1 mmol/L MES buffer at pH 6.0 was permeated through the membrane in a convective flow cell under N_2 atmosphere. Because of the high reactivity of Fe(II), initial H_2O_2 conversion was near 100%, but decreased with time, reaching a steady-state of approximately 40% (Figure 5.7). At this point, most of the iron ions immobilized in the membrane should be present as Fe(III). To confirm this, the conversion of Fe(II) to Fe(III) within the PAA-filled pores was investigated by passing a solution containing 150 μmol/L H_2O_2 through another membrane via convection. As the H_2O_2 permeated, Fe(II) was gradually converted to Fe(III), until only Fe(III) remained, as seen in Figure 5.8. It should be noted that for Figures 5.8 through 5.10, residence time, τ, was calculated by dividing the volume of water uptake by the dry PVDF-PAA membrane by the total flowrate through the membrane. This is not the same method used to calculate residence time for Figure 5.7, which is described in Chapter 6.

No iron was released during H_2O_2 permeation. It is important to note that in solutions at pH = 6, soluble Fe(III) is not present as Fe^{3+}, but mainly as $Fe(OH)_2^+$ and $Fe(OH)_{3,aq}$. Because of this, COO-Fe(III) complexes may also be hydroxylated within the PAA domain. Until all iron is present as Fe(III), the rate of H_2O_2 decomposition will not reach a steady state since the apparent concentrations of the iron species are constantly changing. This is because the reaction of Fe(III) with H_2O_2 and/or radical species becomes the rate-limiting step.

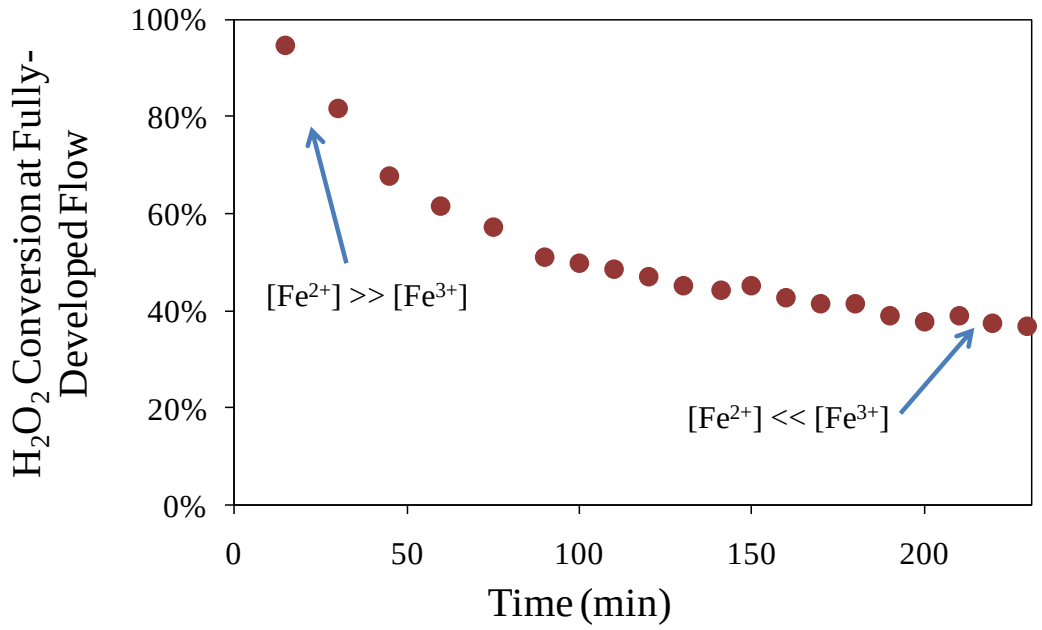

Figure 5.7. H_2O_2 conversion in PVDF-PAA-Fe(II) membrane. H_2O_2 conversion profile as a function of pore volumes permeated (time) for a membrane containing 0.13 mmol Fe(II) at time = 0. Operated under pressure-driven convective flow. Permeated at 0.68 bar; pH 6; residence time = 2 s; H_2O_2 feed side concentration of 0.07 mmol/L.

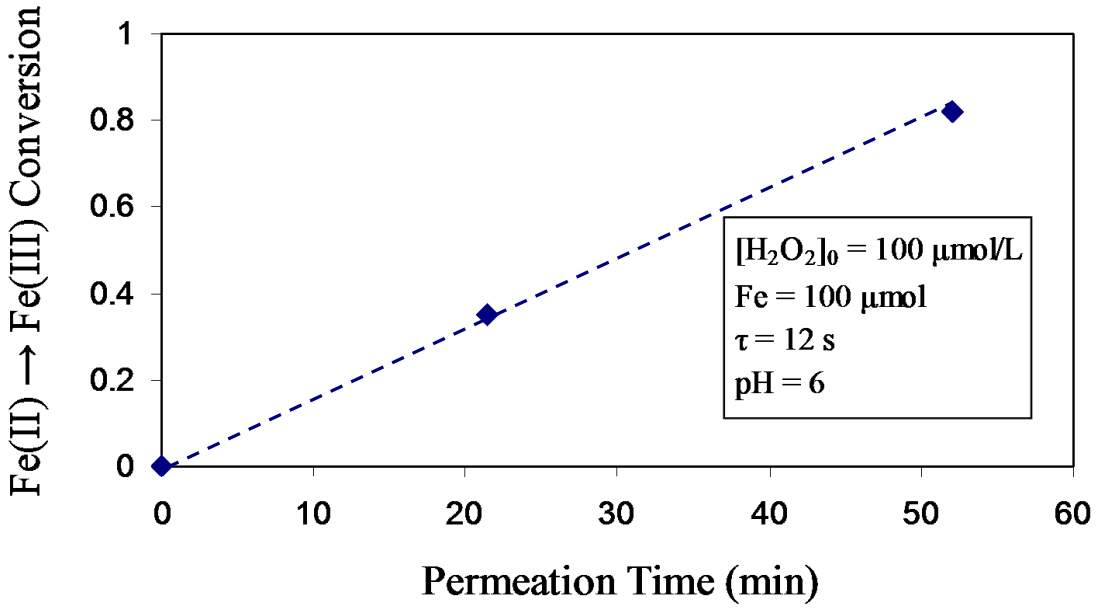

Figure 5.8. Fe(II) → Fe(III) conversion for membrane-immobilized Fenton reaction as a function of permeation time for feed containing 100 µmol/L H_2O_2. ΔP = 0.68 bar. External membrane area = 33.2 cm^2, thickness = 125 µm.

5.6 Modeling of H_2O_2 decomposition using membrane-immobilized Fe(III)

For steady state experimentation, Fe(III) was not directly loaded into the membrane since it would precipitate at the pH required to obtain significant loading (above the pK_a of PAA). Therefore, 22 μmol of Fe(II) were loaded into the membrane (external area = 33.2 cm^2, thickness = 125 μm) and oxidized with a solution containing H_2O_2 until complete conversion to Fe(III) was achieved. Hydrogen peroxide solutions at varying concentrations and residence times were then permeated through the membrane. Figure 5.9 shows the conversion of H_2O_2 as a function of residence time at pH = 6. Residence time was varied by changing ΔP. Assuming the membrane behaved as a continuous stirred-tank reactor and the decomposition of H_2O_2 was first-order, the first-order rate constant, k_{CSTR}, was calculated to be $(7.8 \pm 0.8) \times 10^{-3}$ s^{-1} (shown in Figure 5.9) using Equation 5.1, where $[H_2O_2]_0$ is the feed concentration of H_2O_2, $[H_2O_2]$ is the permeate concentration of H_2O_2, τ is the residence time, and r_{H2O2} is the rate of H_2O_2 decomposition. Assuming [Fe(III)] is constant, the second-order rate constant, k'_{CSTR} was found to be $(8.1 \pm 0.7) \times 10^{-2}$ $M^{-1}s^{-1}$ (Equation 5.2).

$$-r_{H_2O_2} = \frac{[H_2O_2]_0 - [H_2O_2]}{\tau} = k_{CSTR} \times [H_2O_2] \quad (5.1)$$

$$k_{CSTR} = k'_{CSTR} \times [Fe(III)] \quad (5.2)$$

The calculated value is approximately 40 times greater than k_3. This is in agreement with the investigations of Fernandez et al. (1998), who found the rate of azo-dye degradation in a photo-assisted Fenton reaction immobilized in a Nafion membrane was similar to that of a homogeneous reaction with approximately 100 times more Fe(III). It has been reported that Fe-carboxylate complexes on the surface of the membrane could be responsible for this reactivity (Fernandez et al. 2003). These complexes may also be responsible for the stability of PAA in the presence of free radicals (Fernandez et al. 2003).

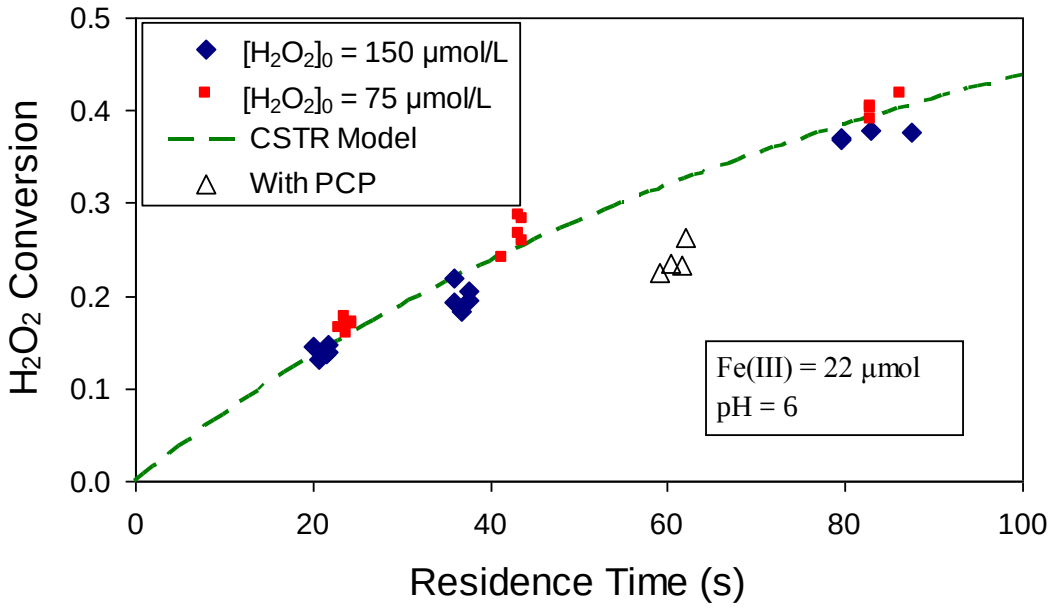

Figure 5.9. H_2O_2 conversion as a function of residence time for membrane-immobilized Fenton reaction with 22 µmol of captured Fe(III) at pH = 6. $[H_2O_2]_0$ = 150 µmol/L for feed with 20 µmol/L PCP. Residence time was varied by changing ΔP. External membrane area = 33.2 cm^2, thickness = 125 µm.

5.7 Toxic organic degradation using membrane-immobilized free radical reactions

Pentachlorophenol (PCP) was once a widely used fungicide for wood preservation that was banned from use in 1987. It is a toxic compound that can still be found in soils at several sites of wood preserving industries. PCP degradation via reaction with free radicals has been conducted, but most studies have been performed either with the assistance of UV light (photo-Fenton) (Engwall et al. 1999; Fukushima and Tatsumi 2001) or at high temperature (Liou et al. 2004). Liou et al. (2004) used a Fe(III)-resin system to oxidize PCP in solution at elevated temperatures, achieving over 90% degradation. Fukushima and Tatsumi (2001) achieved greater than 90% removal of PCP after 300 min of UV-irradiation in a H_2O_2/Fe(III)/humic acid system.

By permeating a solution containing 150 μmol/L H_2O_2 and 20 μmol/L PCP through a PAA/PVDF membrane containing immobilized Fe(III), PCP was degraded at initial pH = 6 and 25^{o}C temperature (Figure 5.10). The conversions of H_2O_2 and PCP were 24% ± 2% and 27% ± 2% (5.4 μmol/L), respectively, for a residence time of 60 ± 2 s. This corresponded to 7.1 mol H_2O_2 consumed / mol PCP degraded. These conversions can be adjusted by varying the amount of iron loading, residence time, and/or the pH. This degradation of PCP is greater than the ~ 5% (~ 2.5 μmol/L) results previously reported by Fukushima and Tatsumi (2001) using solution-phase Fe(III)-H_2O_2 reactions (with higher H_2O_2 concentration) at pH = 5.

H_2O_2 conversion for the solutions containing PCP was lower than those containing no PCP, as seen in Figure 5.9. This is to be expected since PCP acts as a scavenger of hydroxyl radicals, lowering the rate of reaction between the radicals and H_2O_2, therefore the rate of H_2O_2 decomposition.

5.8 Membrane-immobilized ferrihydrite/iron oxide nanoparticles

While the membranes previously used for free radical reactions contained iron ions, various forms of ferrihydrite/iron oxide nanoparticles can be synthesized in the membrane domain for similar oxidative reactions. These nanoparticles provide greater reaction rates than their bulk counterparts (Hermanek et al. 2007), and with the addition

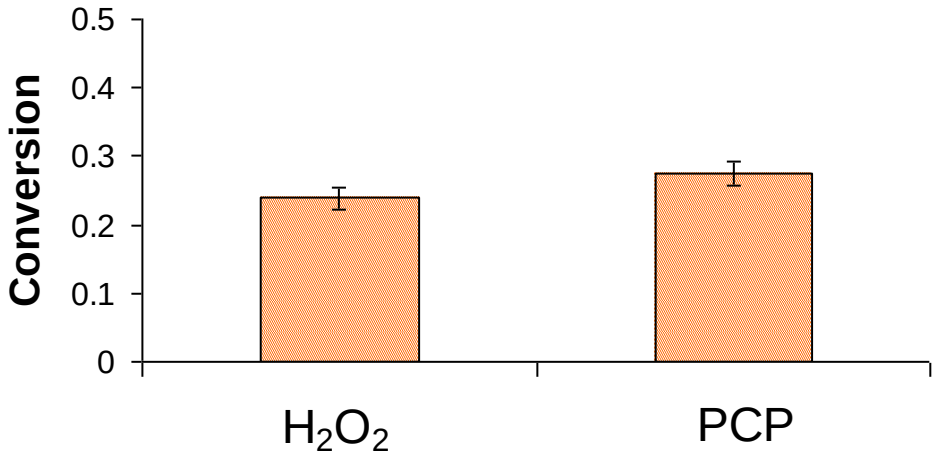

Figure 5.10. H_2O_2 and PCP conversion for membrane-immobilized Fenton reaction with 22 μmol of captured Fe(III) at pH = 6. Feed containes 150 μmol/L H_2O_2 and 20 μmol/L PCP. $\tau = 60 \pm 2$ s, water permeability = 1.7×10^{-4} cm^3 cm^{-2} bar^{-1} s^{-1}. External membrane area = 33.2 cm^2, thickness = 125 μm.

of H_2O_2, many of these oxides are capable of catalyzing the oxidative degradation of organic compounds (Huang et al. 2001). Furthermore, by using membranes impregnated with these inexpensive catalysts, additional separations for nanoparticle removal can be avoided. Our group's previous work has demonstrated the effective reductive dechlorination of contaminants via the use of zero-valent iron and bimetallic nanoparticles immobilized in the membrane domain (Xu and Bhattacharyya 2007)**.** However, a wider range of contaminants can be detoxified by using the oxidants formed from the reaction of a different iron-based nanoparticle, ferrihydrite/iron oxide, and H_2O_2. Additionally, these materials may utilize H_2O_2 more efficiently than similar materials.

Whereas other methods use elevated temperatures for ferrihydrite/iron oxide synthesis within a porous, ion exchange membrane structure functionalized via photografting (Winnik et al. 1998)**,** here, we synthesize ferrihydrite/iron oxide nanoparticles within an easily fabricated PVDF-PAA membrane at room temperature via direct precipitation of the iron species within the membrane pores. Analysis of the membranes via Mössbauer spectrometry confirmed the presence of ferrihydrite/iron oxide (Figure 5.11A). The average nanoparticle diameter was determined by SEM to be 37 ± 14 nm (Figure 5.11B). The PVDF-PAA membrane serves to limit nanoparticle aggregation, prevent nanoparticle loss, and permit the recapture of the iron ions as the nanoparticles dissolve, providing an opportunity to re-synthesize the nanoparticles in the membrane domain. H_2O_2 decomposition occurred in the presence of the membrane-immobilized ferrihydrite/iron oxide nanoparticles, confirming their reactivity towards H_2O_2.

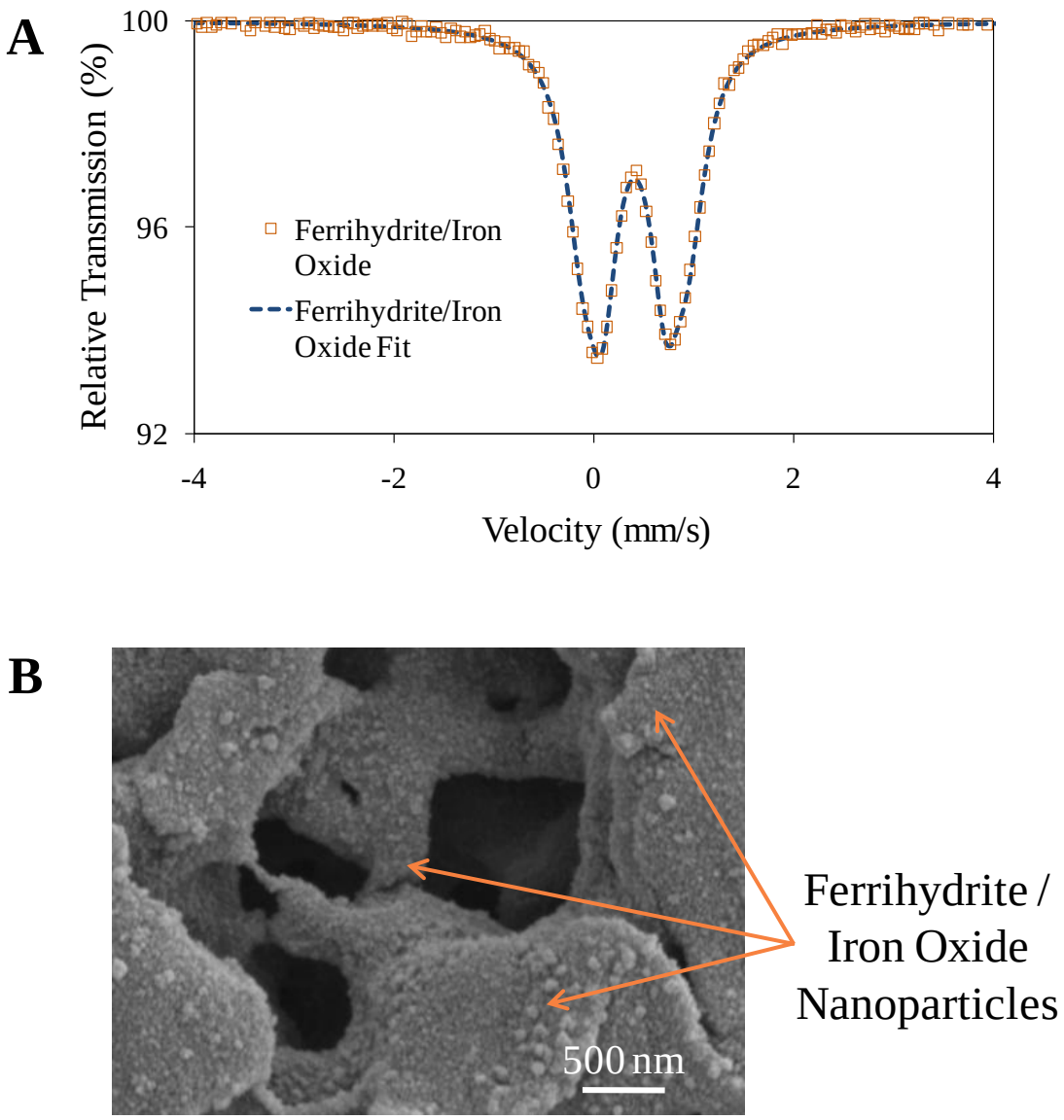

Figure 5.11. Ferrihydrite/iron oxide nanoparticles synthesized in PVDF-PAA membrane pores. (A) Mössbauer spectra of membrane-immobilized ferrihydrite/iron oxide nanoparticles. (B) SEM of immobilized ferrihydrite/iron oxide nanoparticles synthesized via direct precipitation.

Chapter 6 Modeling the Behavior of PVDF-PAA Membranes for Water Treatment

This is the first reported literature study to develop a model for free radical reactions in a stimuli-responsive (PVDF-PAA) membrane. More specifically, the goal is to model the behavior of a single pore and the reactants which convectively permeate through it via predicting the functionalized membrane's stimuli-responsive behavior, the decomposition of H_2O_2 when Fe ions are present, the conversion of Fe(II) to Fe(III), and the degradation of a target organic pollutant.

6.1 Calculation of PVDF-PAA pore dimensions

In order to accurately model the pH-responsive behavior of the PVDF-PAA membranes, it is necessary to ascertain several characteristics of the membrane pores including length, a function of tortuousity and membrane thickness, and the number of pores. Figure 6.1 illustrates a typical PVDF-PAA pore consisting of a PVDF membrane pore of radius R_2 and tortuous length, $L' = \tau_{pore} \times L$ that is lined with a uniform PAA gel of thickness $R_2 - R_1$ where τ_{pore} is the tortuosity of the pore and L (m) is the membrane thickness. It is assumed that the feed solution permeates through the center, or "core", of the pore ($0 \leq r < R_1$). The following equations are used to calculate the effective radii of the membrane pores.

The number of pores, n, was calculated using Equation 6.1.

$$n = \frac{\varepsilon \times V_{membrane}}{\pi \times R_{pore}^2 \times L'} \tag{6.1}$$

where $V_{membrane}$ (m^3) is the total membrane volume, ε is the initial porosity (%) of the unmodified membrane, and R_{pore} (m) is the radius of the pore.

Membrane tortuosity has been determined using various empirical correlations, including a popular one developed by Mackie and Meares (1955) that is based on the polymer volume fraction, 1 – ε, as shown in Equation 6.2 (Iversen et al. 1997).

$$\tau_{pore} = \frac{(2-\varepsilon)^2}{\varepsilon} \tag{6.2}$$

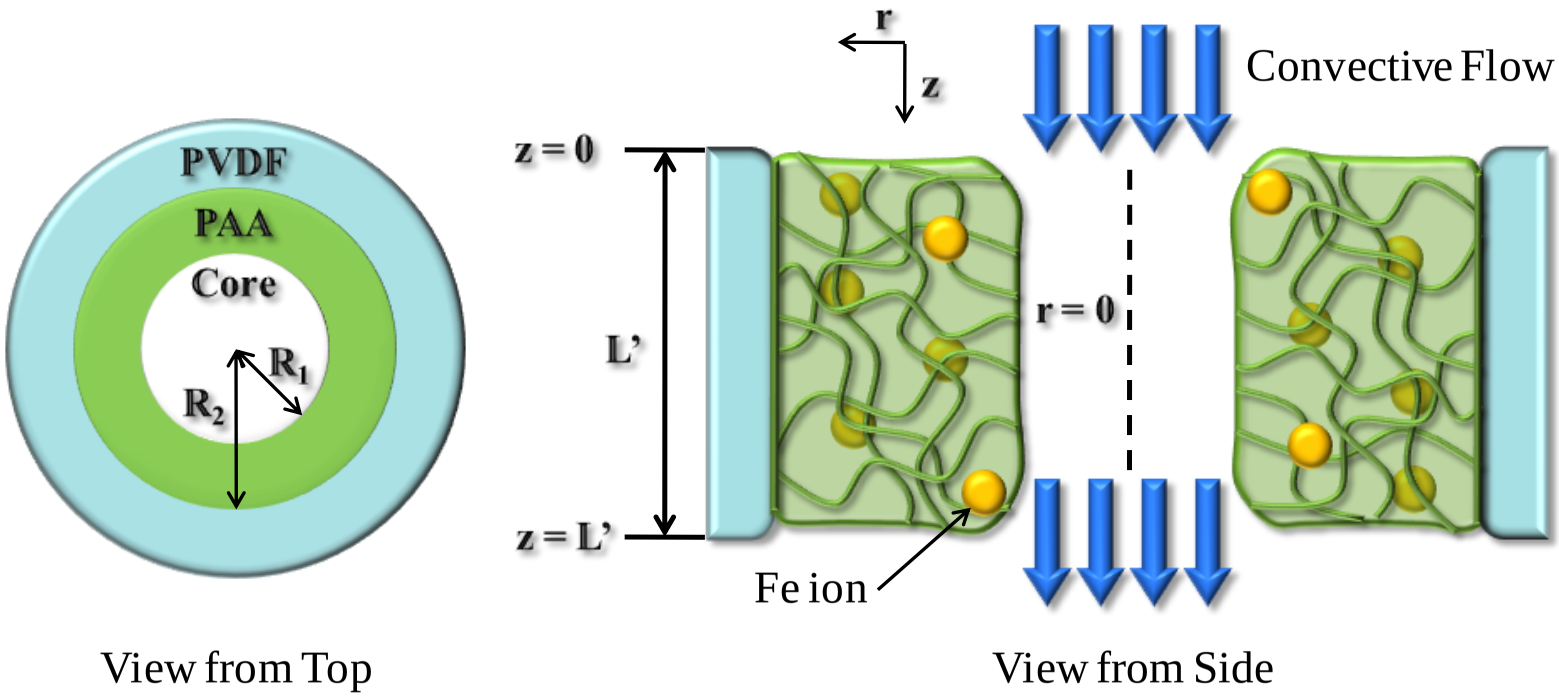

Figure 6.1. Schematic of PVDF-PAA membrane pore for modeling.

For the PVDF membrane porosity of 75 %, the calculated tortuosity is 2.08. This value has been used to model pure water flux through a hydrophobic PVDF membrane (Millipore) with pore diameter of 220 nm and 75 % porosity (Srisurichan et al. 2006). A tortuosity of 2 has also been used for modeling gas transport through hydrophobic membranes of PVDF membranes with 450 nm pore diameter (Schofield et al. 1990). However, Khayet et al. (2004) utilized gas permeation experiments to obtain an experimental value of 2.6 for the tortuosity of hydrophobic PVDF membranes (Millipore) of 450 nm pore diameter and similar porosity and thickness to the membranes used in this study. With this data, the Hagen–Poiseuille equation (Equation 6.3) can be used to calculate the effective pore radius.

$$R_{pore} = \left(\frac{8\mu}{\pi} \times \frac{Q}{\Delta P \times n} \times L' \right)^{1/4} \tag{6.3}$$

where μ is the dynamic viscosity of water (9.33×10^{-4} kg m^{-1} s^{-1} at 23 °C), Q (m^3/s) is the total volumetric flowrate through the membrane, and ΔP (Pa) is the pressure drop across the membrane thickness.

Combining Equations 6.3 and 6.1 yields

$$R_{pore} = L' \times \sqrt{\frac{8\mu}{\varepsilon \times V_{membrane}} \times \frac{Q}{\Delta P}} \tag{6.4}$$

Using a tortuosity of 2.60 and the previously-determined permeability of 596×10^{-4} cm^3 cm^{-2} s^{-1} bar^{-1} for the bare PVDF membrane (Datta et al. 2008), the calculated pore diameter is 445 nm (R_2 = 222.4 nm) which is close to the 450 nm pore diameter provided by the manufacturer. With this information, n was determined to be 6.16×10^9. Although there is undoubtedly a distribution of pore diameters for these membranes, this chapter will consider R_2 to be constant and uniform throughout the membrane. Assuming no pores are made inaccessible by PAA and the PAA coating within the PVDF membrane pores is uniform, the PVDF-PAA pores will have the same tortuosity as the unmodified membranes. After modification with PAA, $R_{pore} = R_1$ and was calculated using Q/ΔP and Equation 6.5 (derived from Equation 6.3).

$$R_1 = 1.058 \times 10^{-4} \times \left(\frac{Q}{\Delta P} \right)^{1/4} \tag{6.5}$$

6.2 Modeling of the pH-responsive behavior

Several studies have demonstrated the controlled opening and closing of PAA-modified membrane pores via pH modulation (Ito et al. 1990; Hu and Dickson 2007; Hu and Dickson 2009). The pH range in which the most drastic valve effect (a function of pore opening/closing with pH) occurs can be altered by changing the pK_a of the PAA chains/network which can be achieved by varying the concentration of monomer, concentration and type of initiator, type of solvent, and the conditions under which the polymerization takes place. As discussed in Chapter 5, increasing the pH will ionize more of the carboxylate groups, causing the PAA network to expand, thereby reducing R_1. Datta et al. (2008) studied the effects of pH variation on water flux through PVDF-PAA membranes synthesized using the same solvent, initiator, and crosslinker as were used in this study. They found that by increasing the pH from 2.4 to 10.0, the volumetric solution flux (J_V) at 1.38 bar decreased from 309×10^{-4} cm^3 cm^{-2} s^{-1} ($J_{V,max}$) to 40×10^{-4} cm^3 cm^{-2} s^{-1} ($J_{V,min}$).

$$J_V = \frac{Q}{\Delta P \times A_{membrane}} \tag{6.6}$$

where $A_{membrane}$ (m^2) is the cross-sectional area of the membrane. Using Equations 6.5 – 6.6 and $J_{V,max}$ to calculate the maximum effective pore radius, $R_{1,max}$, yields 158 nm which occurs when the volume of the PAA gel, V_{PAA}, is at a minimum, $V_{PAA,min}$. Using Equation 6.5 and $J_{V,min}$ to calculate the minimum effective pore radius, $R_{1,min}$, yields 98 nm which occurs when V_{PAA} is at a maximum, $V_{PAA,max}$. Assuming V_{PAA} expands linearly with the molar fraction of ionized carboxylate groups, this data can then be used to predict J_V as a function of pH (Equation 6.10).

$$V_{PAA} = \pi L' \times (R_2^2 - R_1^2) \tag{6.7}$$

$$V_{PAA} = V_{PAA,\min} + \frac{[COO^-]}{[COOH] + [COO^-]} (V_{PAA,\max} - V_{PAA,\min}) \tag{6.8}$$

Combining Equations 6.7 and 6.8,

$$R_1^2 = R_{1,\max}^2 + \frac{[COO^-]}{[COOH] + [COO^-]} (R_{1,\max}^2 - R_{1,\min}^2) \tag{6.9}$$

Substituting Equation 6.5 into Equation 6.9 gives

$$J_V = \left(J_{V,\max}^{1/2} - \frac{[COO^-]}{[COOH]+[COO^-]} (J_{V,\max}^{1/2} - J_{V,\min}^{1/2}) \right)^2 \quad (6.10)$$

where [COO^-] is the concentration of ionized carboxylate groups and [COOH] is the concentration of nonionized carboxylate groups. The molar fraction of ionized to nonionized carboxylate groups was calculated using Equation 6.11.

$$\frac{[COO^-]}{[COOH]+[COO^-]} = \frac{1}{1+10^{pK_a - pH}} \quad (6.11)$$

For the case where the pK_a of the PAA network is the same as that of acrylic acid, 4.25, the flux at 1.38 bar as a function of pH is shown in Figure 6.2. When compared to the experimental data obtained by Datta et al. (2008), this pK_a value incorrectly predicted J_V whereas pK_a = 5.45 resulted in the best prediction of the experimental data (7 % average relative error). This pK_a is higher than the previously reported values for PAA gels, but may have been due to differences in the aforementioned variables (crosslinker, etc) associated with this PAA network. Similarly, J_V predictions for pK_a = 5.3 and 5.7 are shown in Figure 6.2. This PAA with increased pK_a is advantageous for use in catalytic membranes at circumneutral pH since it allows for higher permeability than similar PAA coatings with lower pK_a values.

Since H^+ is not the only ion which can have an effect on the neutralization of the carboxylate groups, it is important to consider the impact of other mono- and/or multi-valent ions which are present, as discussed in Chapter 5. A PVDF-PAA membrane (see Figure 5.6) used to study the effects of divalent cation loading on solution flux contained 500 μmol of PAA repeat units in a 13.2 cm^2 surface area assuming all mass gain was in the form of PAA repeat units. Based on the total number of PAA repeat units (500 μmol) and a typical pK_a for PAA in solution (i.e. 4.5), the rate of capture of these ions began to decrease well below the theoretical capacity of the membrane. For pK_a = 4.5, 76 % of the PAA repeat units are ionized (Equation 6.8), allowing for the capture of up to 190 μmol Fe^{2+} and Ca^{2+} at pH 5.0 if each divalent cation occupied two COO^- groups after capture. Only 52 μmol Fe^{2+} and Ca^{2+} were captured as the membrane appeared to be reaching its cation exchange capacity. This represented only 27 % of the theoretical capacity. However, since this membrane was functionalized in the same manner as the one used in Figure 6.2, the pK_a was most likely 5.4 – 5.5, meaning approximately 26 % of the PAA

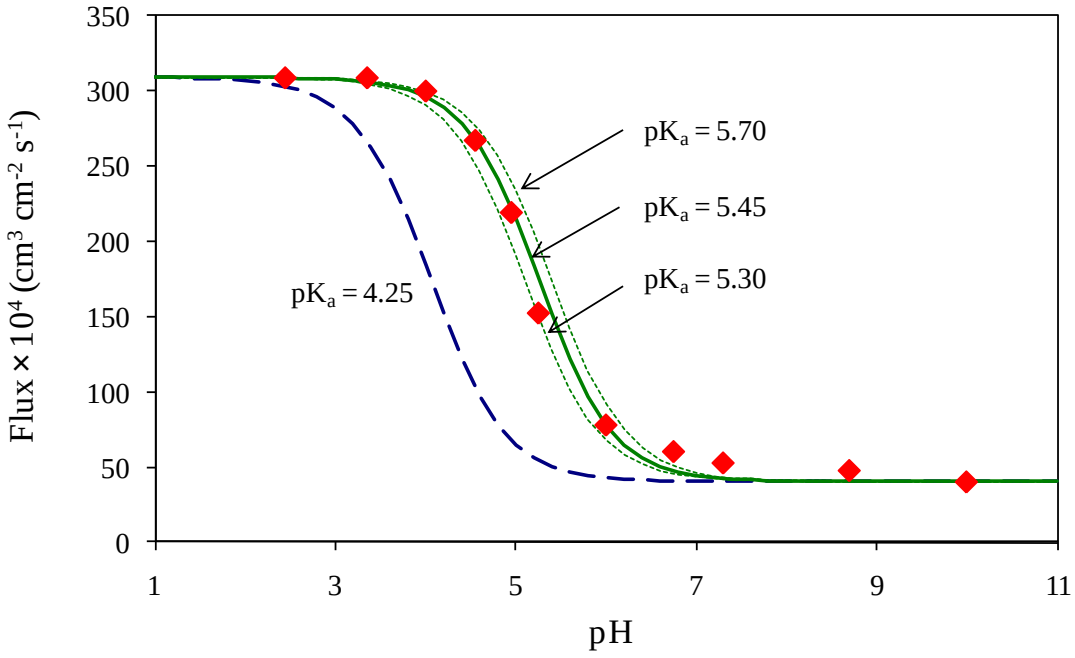

Figure 6.2. Experimental (diamonds) and predicted solution flux (lines) as a function of pH through a PVDF-PAA membrane with $J_{V,max}$ = 309 × 10^{-4} cm^3 cm^{-2} s^{-1} and $J_{V,min}$ = 40 × 10^{-4} cm^3 cm^{-2} s^{-1}. The flux for pK_a = 5.45 (solid line) is surrounded by the flux for pK_a 5.3 and 5.7 (thin dashed lines). Average relative error of 7.0 % for experimental vs model flux predicted using pK_a = 5.45. Experimental data obtained by Datta et al. (2008) at 1.38 bar.

repeat units should have been ionized (131 μmol COO^-) at pH 5.0. Therefore, the 52 μmol of captured divalent cations would actually occupy 79 %, or 104 μmol, of the available COO^- groups, which was much more reasonable. Another interesting observation was that although the pH of the feed solution was 5.0, the pH of the permeate was 4.4, corresponding to 8 % ionization of the carboxylate groups. This decrease in ionized carboxylate groups (26 to 8 %) can also be viewed as an increase in neutralized carboxylate groups from 74 to 92 %. Such neutralization could be due to the increased charge shielding associated with multivalent cations as opposed to monovalent cations. This increase corresponds to the neutralization of 90 μmol COO^- groups and equates to the capture of 45 μmol divalent cations which is similar to the actual quantity of divalent cations captured.

6.3 Modeling of H_2O_2 decomposition in the PVDF-PAA membrane pores

In order to more accurately predict the decomposition of H_2O_2 and contaminants with the PVDF-PAA-Fe membranes, where Fe is either Fe(II) or Fe(III), it is necessary to model the reactions within the membrane pores. First, a two-dimensional model for the steady-state (time-independent) degradation of H_2O_2 within the membrane pore was developed, based on Figure 6.1. Assumptions used for this model that were not previously stated included following:

- The reactive iron species are distributed uniformly throughout the PAA domain
- Reactions take place only in the PAA domain
- There is fully-developed laminar flow in the core of the membrane pore
- Reactions on the membrane surface are negligible compared to within the pores
- All pores are cylindrical and uniform in size and tortuosity
- The PAA gel on the inside of pores is of uniform thickness
- The transport of H_2O_2 and other reactants is as follows for the two domains:
    - Core domain:
        - Diffusion and convection in axial direction
        - Diffusion, but no convection in the radial direction
    - PAA domain:

- No convective transport

- There is diffusion in the radial and axial directions

- No pores are inaccessible to reactants

- The reaction conditions are isothermal

- There is no diffusion of reactants into PVDF

Operating under these assumptions, the governing equations for this model consist of balances on H_2O_2 in the open ("core") portion of the membrane pore (Equation 6.12) as well as in the PAA gel (Equation 6.13).

$$-U(r)\times\frac{\partial[H_2O_2]_{aq}}{\partial z}+\frac{D_{H2O2,aq}}{r}\frac{\partial}{\partial r}\left(r\times\frac{\partial[H_2O_2]_{aq}}{\partial r}\right)=0 \tag{6.12}$$

$$D_{H2O2,PAA}\left(\frac{\partial^2[H_2O_2]_{PAA}}{\partial^2 z}+\frac{1}{r}\frac{\partial}{\partial r}\left(r\times\frac{\partial[H_2O_2]_{PAA}}{\partial r}\right)\right)+r_{H2O2}=0 \tag{6.13}$$

where U(r) (m s^{-1})is the velocity profile of the solution permeating through the membrane pore, $[H_2O_2]_{aq}$ (mol m^{-3}) is the concentration of H_2O_2 in the aqueous-only phase or "core" of the membrane pore, $D_{H2O2,aq}$ is the diffusion coefficient of H_2O_2 in water, $[H_2O_2]_{PAA}$ (mol m^{-3}) is the concentration of H_2O_2 in the PAA domain, r_{H2O2} is the rate law governing the decomposition of H_2O_2 by the iron species in the PAA domain, and $D_{H2O2,PAA}$ is the diffusion coefficient of H_2O_2 in the hydrated PAA gel.

The boundary conditions are as follows:

1) at z = 0, $[H_2O_2]_{aq} = [H_2O_2]_{PAA} = [H_2O_2]_0$

2) at r = 0, $\frac{\partial[H_2O_2]_{aq}}{\partial r}=0$

3) at r = R_2, $\frac{\partial[H_2O_2]_{PAA}}{\partial r}=0$

4) at r = R_1, $[H_2O_2]_{aq} = [H_2O_2]_{PAA}$

where $[H_2O_2]_0$ (mol m^{-3}) is the concentration of H_2O_2 before entering the membrane pore. These differential equations were combined into one equation and, with the boundary conditions, solved using a numeric partial differential equation solver in Maple.

U(r) was calculated using Equation 6.14 as follows:

$$U(r)=U_{\max}\left(1-\left(\frac{r}{R_1}\right)^2\right) \tag{6.14}$$

where U_{max} (m/s) is the maximum fluid velocity, which is calculated using equation 6.15.

$$U_{\max} = 2 \times U_{avg} = 2 \times \frac{Q}{n \times \pi R_1^2} \tag{6.15}$$

where U_{avg} (m/s) is the average velocity through the membrane pore.

6.3.1 Determination of H_2O_2 diffusion coefficients

Since it was assumed there was no convective flow in the PAA network, diffusion is the only method by which reactants can be transported in this domain. The Wilke and Chang equation can be used to determine the diffusion coefficient of a solute, A, in a liquid solvent, B, D_{AB} ($m^2\ s^{-1}$) (Wilke and Chang 1955).

$$D_{AB} = (117.3 \times 10^{-18}) \times T \frac{(\Phi \times M_B)^{0.5}}{\mu \times v_{A,boil}^{0.6}} \tag{6.16}$$

where Φ is the association factor of the solvent (2.26 for water), M_B (g mol^{-1}) is the molecular weight of the solvent, T (K) is the temperature, and $v_{A,boil}$ ($m^3\ kmol^{-1}$) is the molar volume of the solute at its normal boiling point. The value of $v_{A,boil}$ was calculated using the Tyn and Calus method, shown in Equation 6.17 (Poling et al. 2001).

$$v_{A,boil} = 0.397 \times v_{A,critical}^{1.048} \tag{6.17}$$

where $v_{A,critical}$ ($m^3\ mol^{-1}$) is the critical volume of the solute (0.0777 $m^3\ kmol^{-1}$ for H_2O_2) (Yaws 1999). Using the calculated $v_{A,boil}$ = 0.0273 $m^3\ kmol^{-1}$ for H_2O_2, $D_{H2O2,aq}$ = 2.06 × 10^{-9} $m^2\ s^{-1}$ at 23 ˚C; however, this value deviates significantly from the literature-reported value of 1.35 × 10^{-9} $m^2\ s^{-1}$ at 20 ˚C (Borggaar.Ok 1972). Adjusting this value to its equivalent at 23 ˚C using Equation 6.18, based on the Equation 6.16, yields $D_{H2O2,aq}$ = 1.46 × 10^{-9} $m^2\ s^{-1}$.

$$D_{AB,2} = D_{AB,1} \frac{T_2}{T_1} \frac{\mu_1}{\mu_2} \tag{6.18}$$

Previous work has shown that the effective diffusion coefficient, D_{eff}, of H_2O_2 in a hydrated poly(vinyl alcohol) (PVA) hydrogel of 8 μm dry thickness (swelling factor of 2.3 in 0.1 M phosphate buffer) was 65 % lower than in phosphate buffer alone at 25 ˚C (Vanstroebiezen et al. 1993). This decrease in D_{eff} is relatively small and can most likely be attributed to the relatively open structure of the PVA gels, the low level of interaction

between H_2O_2 and the PVA gel, and the small mean size (mean diameter of 0.28 nm and mean length of 0.25 nm) of the H_2O_2 molecule (Vanstroebiezen et al. 1993; Henzler and Steudle 2000). Several correlations have been developed to describe the diffusion of solutes through hydrogel networks. These are generally based on free volume, hydrodynamic, and/or obstruction theories and can be used to describe both homogeneous and heterogeneous hydrogels (Amsden 1998). A hydrodynamic model based on scaling concepts proposed by Cukier (Equation 6.19) has been shown to agree well with literature-reported data for homogeneous polymers (Cukier 1984; Amsden 1998).

$$\frac{D_{Ag}}{D_{AB}} = \exp(-k_c \times r_S \times \varphi^{0.75}) \tag{6.19}$$

where where D_{Ag} (m^2 s^{-1}) is the diffusion coefficient of the solute in the hydrogel, r_S (Å) is the radius of the solute, φ is the volume fraction of the polymer in the gel, and k_c is an undefined constant for a specific polymer-solvent system.

The value of r_S for a given solute was determined using Equation 6.20 with the mean diameter and mean length of the solute molecule (r_S = 1.5 Å for H_2O_2).

$$\frac{\pi}{4} \times D_{solute}^2 \times L_{solute} = \frac{4}{3}\pi \times r_S^3 \tag{6.20}$$

Amsden (1998) determined the value of k_c for urea, sucrose, and RNase to be 1.12, 1.06, and 0.55, respectively. Since urea is the closest to H_2O_2 with respect to size (1.9 Å radius) and structure, k_c = 1.12 was assumed for H_2O_2 (Knepper 1994).

It should be noted that any reference to the gel/hydrogel includes the PAA polymer chains and any water present within the PAA domain. It is assumed the PAA polymer network consists of only PAA since the concentrations of crosslinker and initiator are small compared to acrylic acid. PVDF-PAA-1 is used to designate the PVDF-PAA membrane functionalized in a solution consisting of 30 wt% AA, 0.5 wt% benzoyl peroxide, 1.2 wt% TMPTA, and 70 wt% toluene used for the study of H_2O_2 degradation as a function of residence time in Chapter 5. Based on these concentrations and the complete wetting of the PVDF pores, the maximum quantity of PAA per membrane pore is 1.9×10^{-13} mol; however, the actual pickup was determined gravimetrically to be 1.4×10^{-13} mol, or ~ 74 % of the theoretical maximum. Next, the

previously reported molar volumes of PAA repeat units, ν_A = 4.86 × 10^{-5} m^3 mol^{-1} for completely ionized and 3.48 × 10^{-5} m^3 mol^{-1} for completely neutralized, were used to determine the theoretical volume occupied by the PAA chains (Hiraoka et al. 1982). Two approaches were then taken to determine the value of φ. The first was based on the permeability of PVDF-PAA-1 before iron loading and at pH 3 (4.8 × 10^{-4} cm^3 cm^{-2} s^{-1} bar^{-1}) when all carboxylate groups should be neutralized. Using Equation 6.5 yields R_1 = 67 nm, which is equivalent to a PAA hydrogel volume per pore of 4.6 × 10^{-17} m^3 and φ = 0.144. The second approach was based on the swelling behavior of PVDF-PAA-1. The water used was pH 5 with ~ 25 % of the carboxylate groups ionized based on the pK_a of the PAA chains being 5.4 - 5.5. The mass of water within the hydrogel was determined gravimetrically. ν_A was assumed to vary linearly with % ionization and was 4.25 × 10^{-5} m^3 mol^{-1}. These calculations yielded φ = 0.157, which was a variation of ~ 8 % from the φ determined using the first method. Error associated with this latter method could be due to the presence of non-"free" water in the hydrogel. Based on φ = 0.024, $D_{H2O2,PAA}$ / $D_{H2O2,aq}$ = 0.74.

6.3.2 H_2O_2 decomposition kinetics in presence of PVDF-PAA-Fe(III)

Solving Equations 6.12 and 6.13 under the assumption that $r_{H2O2} = k_2'[Fe][H_2O_2]$, [Fe] is constant, $k_2' = (1.1 \times 10^5) \times k_2$, and no axial diffusion for PVDF-PAA-1, which contained 22 μmol Fe(III) and had a flux of 1.88 × 10^{-4} cm^3 cm^{-2} s^{-1} at 10 psi, $[H_2O_2]$ variation in the radial direction was determined to be negligible, as seen in Figure 6.3. A high multiple of the established rate constant for Fe^{3+} and H_2O_2 in solution (k_2) was used to account for the effects of the increased rate of reaction of H_2O_2 with the Fe^{2+} formed from the reduction of Fe^{3+}, the potential for increased iron loading within the membrane, as well as to exaggerate the effects of H_2O_2 distribution in the radial direction. This gradient was taken from the outlet of the membrane pore, where the concentration gradient was greatest. The Peclet number, Pe, relates the characteristic diffusion time to the residence time, τ, for this system. It should be noted that for this model, the residence time is defined as the average amount of time it takes the volume of the core region of the membrane pore ($0 \leq r < R_1$) to pass through the membrane. In Chapter 5, the residence

time was defined as the total flowrate through the membrane divided by the hydrated PAA gel volume. The radial and axial Peclet numbers were calculated using Equations 6.21 and 6.22, respectively.

$$Pe_r = \frac{R_1^2 / D_{H2O2,aq}}{L' / U_{avg}} \tag{6.21}$$

$$Pe_z = \frac{L'^2 / D_{H2O2,aq}}{L' / U_{avg}} \tag{6.22}$$

For PVDF-PAA-1, Pe_r and Pe_z were 6.8×10^{-7} and 21, respectively. Since $Pe_r << Pe_z$, diffusion in the radial direction can be neglected compared to axial diffusion. Additionally, since $Pe_z >> 1$, axial diffusion is small compared to convective transport and can therefore be neglected as well (Patankar 1980). Equations 6.12 and 6.13 can then be simplified to Equation 6.23, which is for a plug-flow reactor (PFR) at steady-state.

$$U_{avg} \times \pi R_1^2 \times \frac{d[H_2O_2]}{dz} + \pi (R_2^2 - R_1^2) \times r_{H2O2} = 0 \tag{6.23}$$

Regardless of the initial ratio of Fe(II):Fe(III), it will eventually reach equilibrium and become constant with the majority of the Fe species being Fe(III), making Equation 2.2 the rate-limiting step for the decomposition of H_2O_2. Therefore, membranes containing almost all Fe(III) were used to study the kinetics of H_2O_2 decomposition. By assuming an effective concentration of Fe(III) and Fe(II) within the PAA domain of each pore, designated $[Fe(III)]_{eff}$ and $[Fe(II)]_{eff}$ (mol m^{-3}), respectively, the decomposition of H_2O_2 was assumed to follow the reactions in Equations 6.24 through 6.29.

$$[Fe]_{eff} = \frac{total \;\; Fe \;\; captured}{n \times V_{PAA}} \tag{6.24}$$

$$[Fe]_{eff} = [Fe(II)]_{eff} + [Fe(III)]_{eff} \tag{6.25}$$

$$r_1 = k_1'[Fe(II)]_{eff}[H_2O_2] \tag{6.26}$$

$$r_2 = k_2'[Fe(III)]_{eff}[H_2O_2] \tag{6.27}$$

$$r_3 = k_3[Fe(II)]_{eff}[OH\bullet] \tag{6.28}$$

$$r_8 = k_8[H_2O_2][OH\bullet] \tag{6.29}$$

The rate constant k_3, corresponds to the rate constant in Equation 2.3, k_8 corresponds to the rate constant in Equation 2.8, etc. Previous studies determined that these reactions are

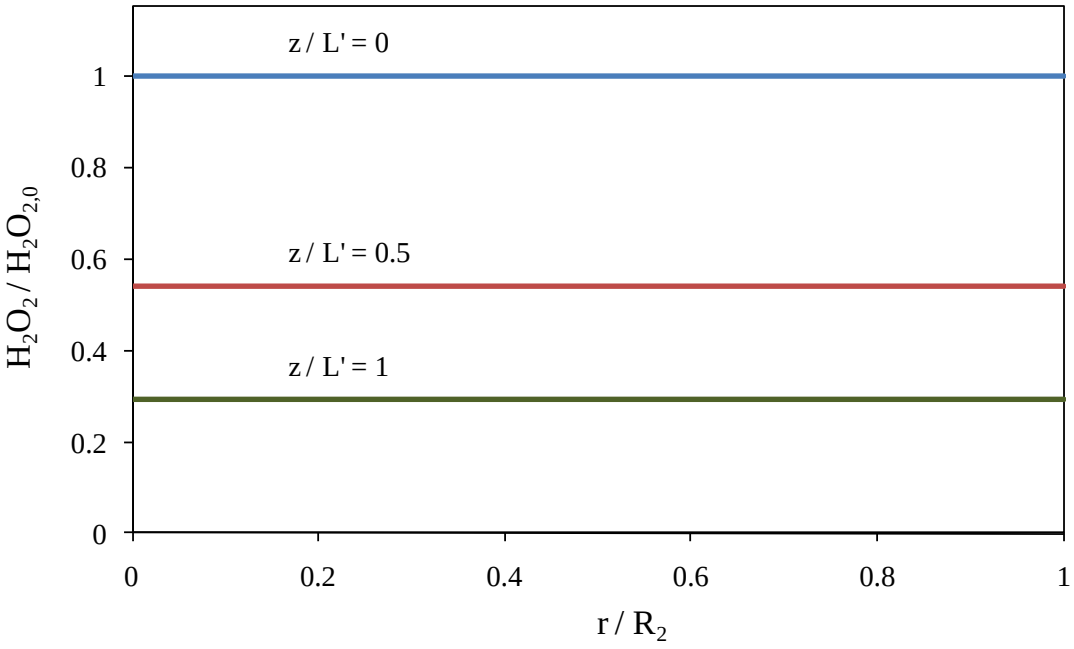

Figure 6.3. H_2O_2 variation in the radial direction for a PVDF-PAA membrane with diffusion in the radial direction and no axial diffusion. Fe loading of 22 μmol Fe(III), flux of 1.88×10^{-4} cm^3 cm^{-2} s^{-1} at 10 psi, and $k_2' = (1.1 \times 10^5) \times k_2$.

the most important for H_2O_2 decomposition in the solution phase (Ravikumar and Gurol 1994; Wang and Lemley 2001). In order to calculate the concentration of each species once the Fe(II):Fe(III) equilibrium was reached, the PFR was modeled as a large number of equally-sized continuously-stirred tank reactors (CSTRs), n_{CSTR} = 1000. In order to determine the final concentrations of H_2O_2, Fe(III), and OH•, mass balances on each species were used (Equations 6.30 through 6.37).

$$r_{H2O2} = -r_1 - r_2 - r_8 \tag{6.30}$$

$$r_{Fe(III)} = r_1 - r_2 + r_3 \tag{6.31}$$

$$r_{OH\bullet} = r_1 - r_3 - r_8 \tag{6.32}$$

$$\frac{d[H_2O_2]}{dt} \times R_2^2 - (R_2^2 - R_1^2) \times r_{H2O2} = 0 \tag{6.33}$$

$$\frac{d[H_2O_2]}{dt} = \left([H_2O_2] \times R_2^2 - [H_2O_2]_{in} \times R_1^2 - [H_2O_2]_{initial} \times (R_2^2 - R_1^2)\right) \times \frac{1}{\tau_i} \tag{6.34}$$

$$\frac{d[Fe(III)]_{eff}}{dt} = r_{Fe(III)} \tag{6.35}$$

$$\frac{d[OH\bullet]}{dt} \times R_2^2 - (R_2^2 - R_1^2) \times r_{OH\bullet} = 0 \tag{6.36}$$

$$\frac{d[OH\bullet]}{dt} = \left([OH\bullet] \times R_2^2 - [OH\bullet]_{in} \times R_1^2 - [OH\bullet]_{initial} \times (R_2^2 - R_1^2)\right) \times \frac{1}{\tau_i} \tag{6.37}$$

where $\tau_i = \tau / n_{CSTR}$ is the residence time for each CSTR, $[H_2O_2]_{in}$ and $[OH\bullet]_{in}$ are the concentrations of H_2O_2 and OH• entering the reactor, respectively, and $[H_2O_2]_{initial}$ and $[OH\bullet]_{initial}$ are the initial concentrations of H_2O_2 and OH• in the PAA gel, respectively, as shown in Figure 6.4. At Fe(II):Fe(III) equilibrium, variations between the initial and final concentrations of each species within each CSTR were very small and therefore considered negligible. Therefore, Equations 6.33 and 6.34, Equation 6.35, and Equations 6.36 and 6.37 were simplified as follows:

$$[H_2O_2] = [H_2O_2]_{in} + \frac{(R_2^2 - R_1^2)}{R_1^2} \tau_i \times r_{H2O2} \tag{6.38}$$

$$r_{Fe(III)} = 0 \tag{6.39}$$

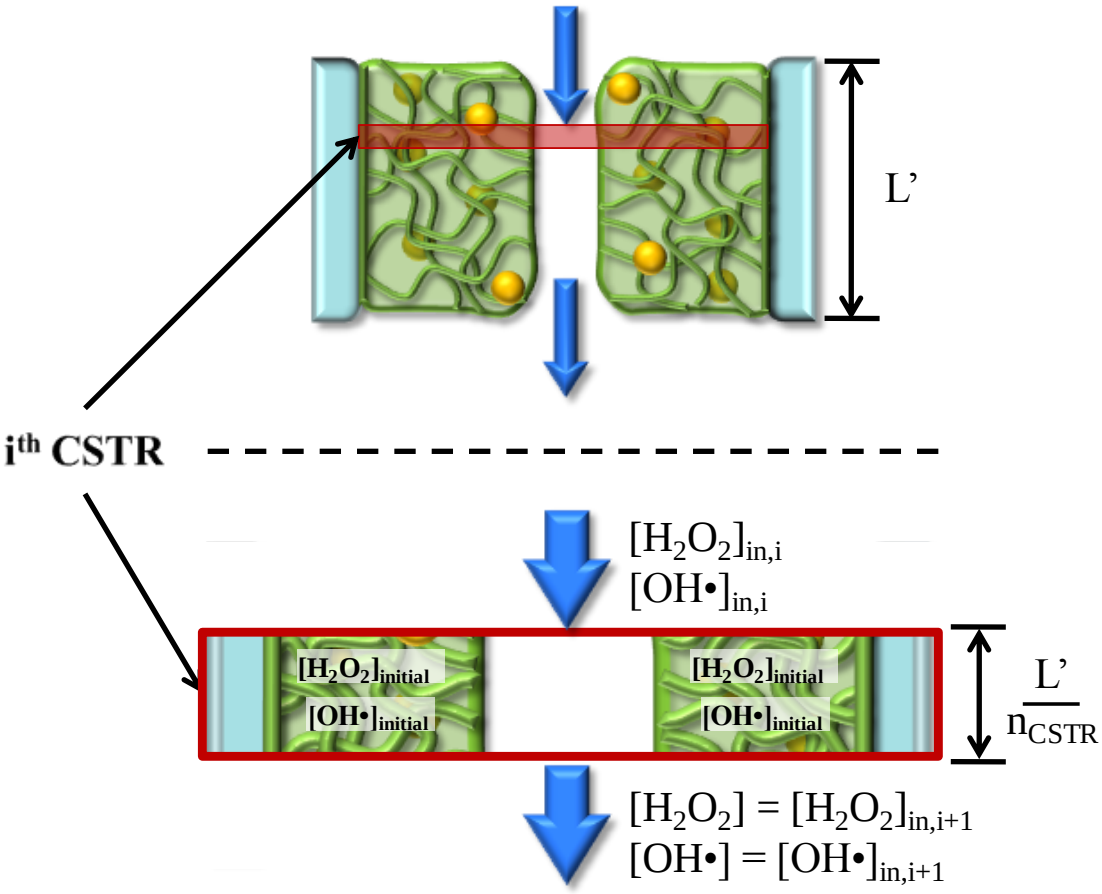

Figure 6.4. Schematic of PFR model represented as series of CSTRs.

$$[OH\bullet] = [OH\bullet]_{in} + \frac{(R_2^2 - R_1^2)}{R_1^2}\tau_i \times r_{OH\bullet} \quad (6.40)$$

Equations 6.35, 6.36, and 6.37 were used to form a balance on each species of interest in each CSTR and subsequently solved to determine the outlet concentrations of H_2O_2, Fe(III), and OH•. It should be noted that there is no inlet concentration of Fe(III) since it is immobilized in the PAA and that when the iron species have not reached a constant ratio, the change in concentration of each species with time cannot be neglected as it is in Equations 6.38 through 6.40. For the first CSTR, the initial/inlet conditions were the same as for the PFR model.

For $k_1' = k_1$ and $k_2' = k_2$, the predicted conversion of H_2O_2 was much lower than obtained experimentally, as shown in Figure 6.5. Since the decomposition of H_2O_2 is determined mostly by Equation 6.27, the optimum value of k_2' was adjusted to more accurately predict decomposition of H_2O_2 in PVDF-PAA-1. The most accurate prediction of the H_2O_2 decomposition occurred when $k_2' = 42 \times 10^{-3}$ M^{-1} $s^{-1} = 21 \times k_2$, with average relative error of 9.4 %. To ensure that the Fe(III) reaction with H_2O_2 is the dominant when the Fe(II):Fe(III) ratio is constant, the effect of varying k_1 on H_2O_2 was investigated. This was confirmed since increasing k_1' by a factor of 100 from k_1 to $100 \times k_1$ resulted in a negligible change in H_2O_2 conversion.

6.3.3 Prediction of membrane-immobilized Fe(II) to Fe(III) conversion

When these PVDF-PAA membranes are first used to capture iron ions, they are present as Fe(II). It is only after reaction with significant quantities of oxidants that the constant Fe(II):Fe(III) ratio is achieved. Therefore, it is important to investigate the nature of the conversion of the immobilized Fe(II) to Fe(III). The decomposition of H_2O_2 by a membrane initially containing 0.13 mmol Fe(II), designated PVDF-PAA-2, is shown in Figure 5.7. After ~ 185 min, the conversion of H_2O_2 was relatively constant at 0.62 ± 0.01. Based on the value of k_2' calculated above, the model-predicted value for this conversion is 0.63, which is in agreement with the experimental finding. This was done by dividing the membrane into 50 segments of equal volume and was used for the remaining simulations ($n_{CSTR} = 50$). Since the variations between the initial and final

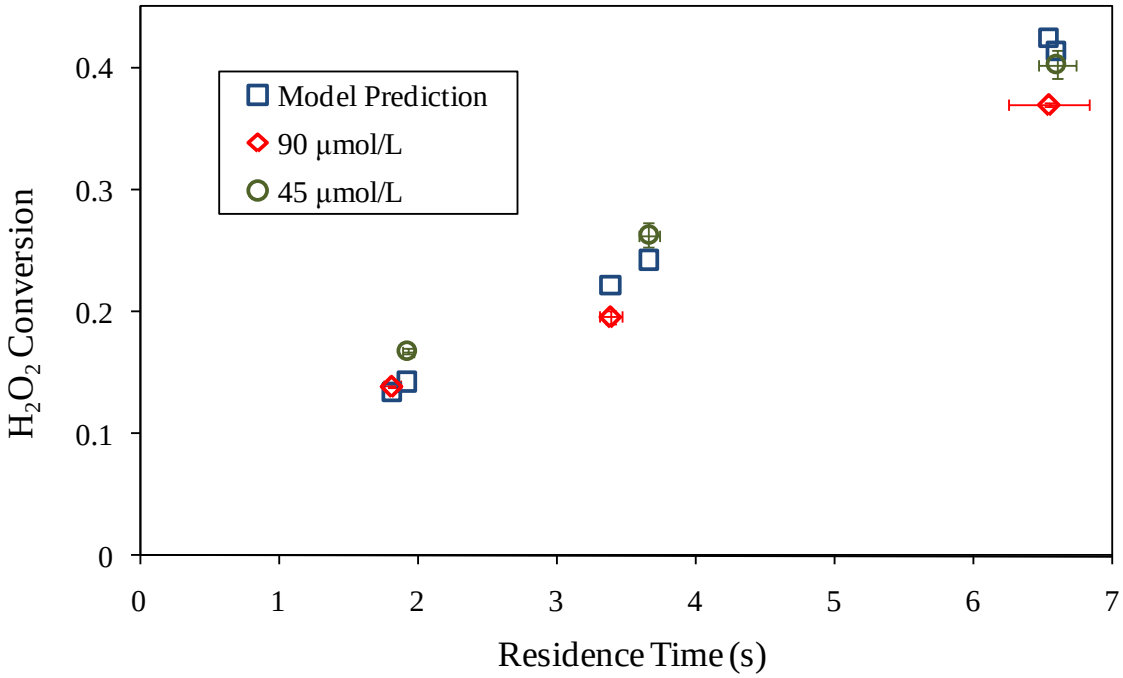

Figure 6.5. H_2O_2 conversion as a function of residence time for PVDF-PAA-1. Fe loading of 22 µmol Fe(III), $k_2' = 21 \times k_2$. Experimental data obtained for H_2O_2 feed concentrations of 90 and 45 µmol/L at pH 6. Residence time is based on volumetric flowrate (Q) and transmembrane pressure drop (ΔP). External membrane surface area = 33.2 cm^2. Error bars represent one standard deviation.

concentrations of the reactants can no longer be considered negligible, the mass balances are confined to Equations 6.34, 6.35, and 6.37. Solving these differential equations with the following initial conditions (Equations 6.41 – 6.43) after the Fe(II):Fe(III) ratio has become constant resulted in the same predicted conversion of 0.63.

$$[H_2O_2] = [H_2O_2]^* = + \frac{(R_2^2 - R_1^2) \times [H_2O_2]_{initial} + R_1^2 \times [H_2O_2]_{in}}{R_2^2} \tag{6.41}$$

$$[Fe(III)] = [Fe(III)]_{initial} \tag{6.42}$$

$$[OH\bullet] = [OH\bullet]^* = + \frac{(R_2^2 - R_1^2) \times [OH\bullet]_{initial} + R_1^2 \times [OH\bullet]_{in}}{R_2^2} \tag{6.43}$$

where $[Fe(III)]_{initial}$ is the initial concentration of Fe(III) in the current CSTR.

When the parameters for this membrane (flowrate, pressure, iron loading, etc) are used to determine the rate of H_2O_2 decomposition when the membrane initially contains only Fe(II), the amount of time before H_2O_2 appears in measurable quantities in the permeate is on the order of tens of hours. This is in sharp contrast to the almost immediate appearance of H_2O_2 in the experimental data (< 15 min). Upon further investigation, the model predicts that only approximately 1.6 to 1.7 mol Fe(II) will be converted to Fe(III) per mol of H_2O_2 consumed. However, the experimental data suggests a ratio of approximately 16 to 17, which is 10-fold higher than the predicted values. In order to account for the variables associated with this higher rate of conversion, β, a scalar quantity, was introduced into Equation 6.31, resulting in Equation 6.44.

$$r_{Fe(III)} = \beta \times r_1 - r_2 + r_3 \tag{6.44}$$

Simulations varying the value of β were conducted to determine the effects of the rate of Fe(II) conversion on the distribution of iron species throughout the membrane. The effect of varying β on the concentration of Fe(III) within the membrane pore after 90 min is shown in Figure 6.6. Although the "breakthrough" of H_2O_2 would occur at a much shorter time for larger values of β, the conversion decreases rapidly to its Fe(III) steady-state value after $Fe(III)/Fe_{tot} \approx 1$ throughout the entire membrane. It stands to reason that if the rate constant for the reaction of Fe(III) and H_2O_2 is actually higher than expected, the rate constant for the reactions of Fe(II) and H_2O_2 could be higher or lower than expected based on literature values for Fe^{2+}. This could be very significant since the exact

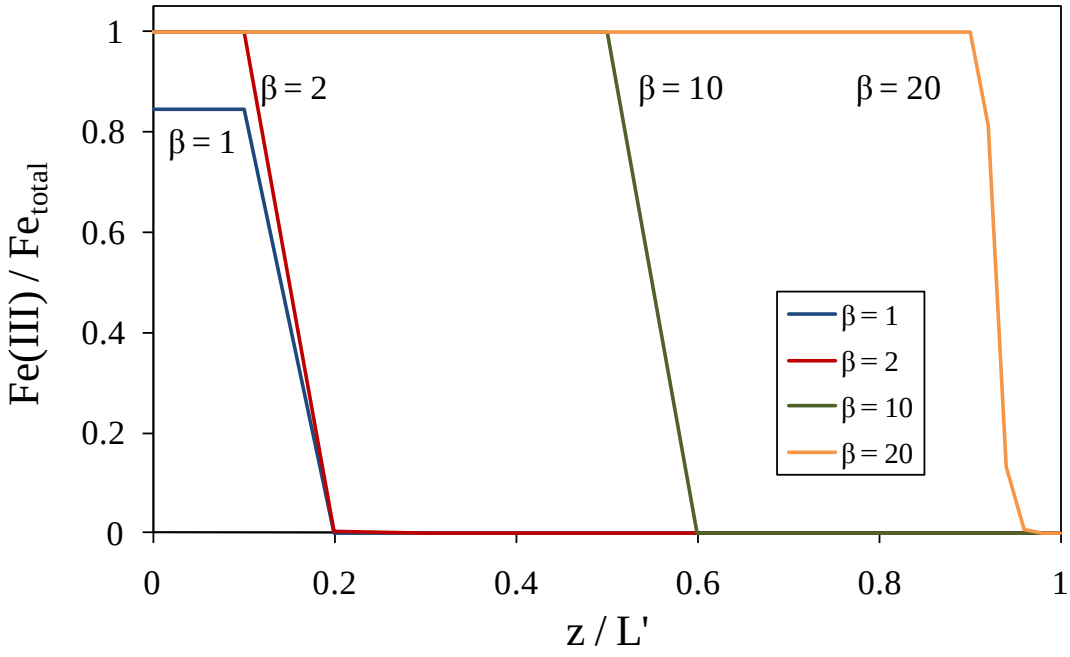

Figure 6.6. Model-simulated Fe(III)/Fe$_{total}$ distribution throughout the length of PVDF-PAA-2 after 90 min for varying β. β was introduced into $r_{Fe(III)} = \beta \times r_1 - r_2 + r_3$ to account for variations in the mols of Fe(II) converted per mol of H_2O_2 consumed. Residence time = 2 s, pH 6, at t = 0 Fe(III)/Fe$_{total}$ = 0 (all iron is present as Fe(II)), k_2' = 21 × k_2, H_2O_2 feed concentration = 69 μmol L^{-1}, J_v = 5.35 × 10^{-4} cm^3 cm^{-2} s^{-1}, ΔP = 10 psi, external membrane surface area = 33.2 cm^2.

forms of Fe(II) and Fe(III) in the PAA domain are unknown. Figure 6.7 shows the simulated concentration profile for H_2O_2 as the Fe(III)/Fe_{total} ratio is changing. The inset figure shows H_2O_2 conversion as a function of time. By decreasing the rate constant k'_1 to $k_1/10$, the transition from 100 % H_2O_2 conversion is much more gradual than in the case of $k'_1 = k_1$. This demonstrates how various factors must be accounted for in order to determine Fe(II) to Fe(III) conversion and H_2O_2 decomposition.

6.3.4 Pollutant degradation with membrane-immobilized Fe(II)/Fe(III)

When considering the degradation of a pollutant in these membrane systems, the efficiency of H_2O_2 utilization is very important. One way to control the quantity of H_2O_2 used for membrane-immobilized free radical reactions is to synthesize the H_2O_2 on-site, thereby eliminating the need for its extraneous addition. Figure 6.8 illustrates how reactive nanostructured stacked membrane systems with tunable pore size can be used to conduct environmentally important toxic organic oxidative degradation reactions through the addition of an inexpensive and abundant reactant, glucose (Datta 2007). By synthesizing H_2O_2 in the pores of the top membrane, its generation can be regulated, thus eliminating unnecessary waste. In order to achieve this, the pores of the top membrane were functionalized using a versatile polycation/polyanion layer-by-layer (LbL) assembly technique, as in Figure 2.1A for the immobilization of negatively-charged glucose oxidase (GOx), which converts glucose and oxygen to H_2O_2 and gluconic acid (Figure 6.8B). These products are convectively transported to the bottom membrane where H_2O_2 reacts with the bound iron species (iron ions or ferrihydrite/iron oxide nanoparticles) contained within a PAA network, forming the free radicals necessary for contaminant degradation (Figure 6.8D). This pH-responsiveness of the PAA network provides the opportunity for hydrodynamic control of residence time via controlled opening and closing of the pores (Figure 6.8C and D).

To demonstrate the effectiveness of the nanostructured stacked-membrane system, the oxidative degradation of TCP was carried out with a configuration consisting of the RC-LbL-GOx membrane on top of the PVDF-PAA-Fe^{2+} membrane (Figure 6.9A) (data obtained by Datta 2007). The process begins by convectively passing an oxygen-

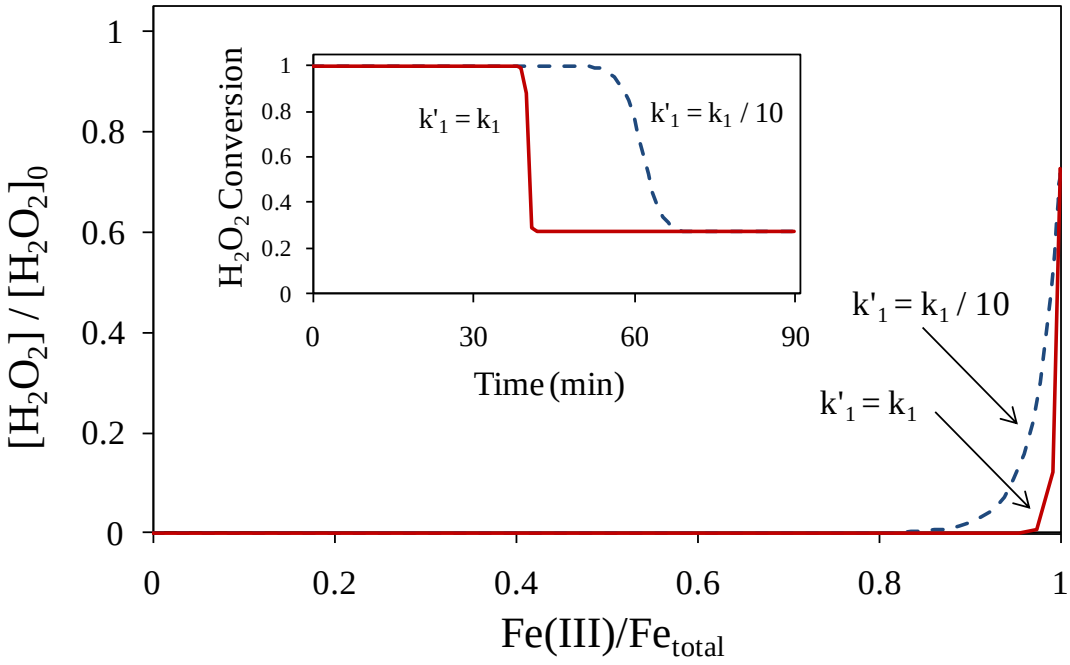

Figure 6.7. Model-simulated $[H_2O_2]/[H_2O_2]_0$ at the outlet of the membrane as a function of average $Fe(III)/Fe_{total}$ distribution throughout the length of PVDF-PAA-2 after 90 min for varying k_1 (rate law: $r_1 = k_1'[Fe(II)]_{eff}[H_2O_2]$) The inset figure shows H_2O_2 conversion with time. This rate constant was varied to account for the speciation, hence reactivity, of Fe(II) in the membrane domain. Residence time = 2 s, pH 6, at t = 0 $Fe(III)/Fe_{total}$ = 0 (all iron is present as Fe(II)), $k_2' = 21 \times k_2$, H_2O_2 feed concentration = 69 μmol L^{-1}, $J_v = 5.35 \times 10^{-4}$ cm^3 cm^{-2} s^{-1}, ΔP = 10 psi, external membrane surface area = 33.2 cm^2, and for fixed β = 50 (see Equation 6.44).

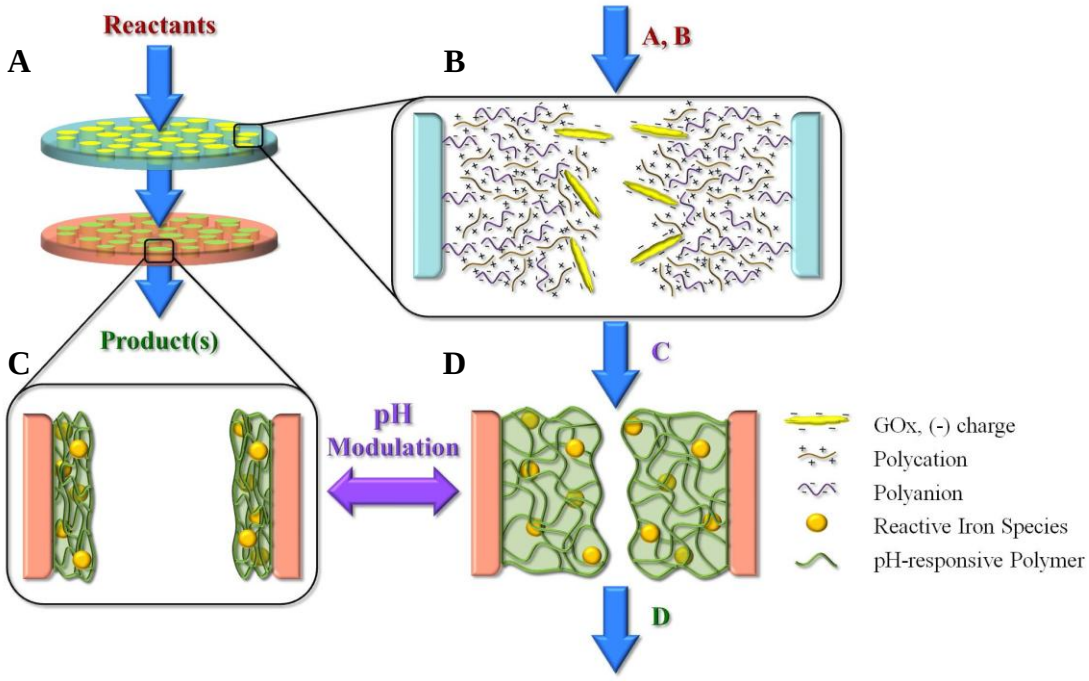

Figure 6.8. Schematic of reactive nanostructured stacked membrane system. (A) Setup of stacked membrane system consisting of two membranes of different functionality operated via convective flow. (B) Pore of top membrane with layer-by-layer polycation/polyanion assembly containing an electrostatically immobilized enzyme, GOx, for the conversion of reactants A + B → C. (C) Pore of bottom membrane consisting of pH-responsive PAA gel with immobilized iron species in collapsed state. (D) Pore of bottom membrane after exposure to increased pH causing gel to swell; reactive iron species catalyzes conversion of C → D.

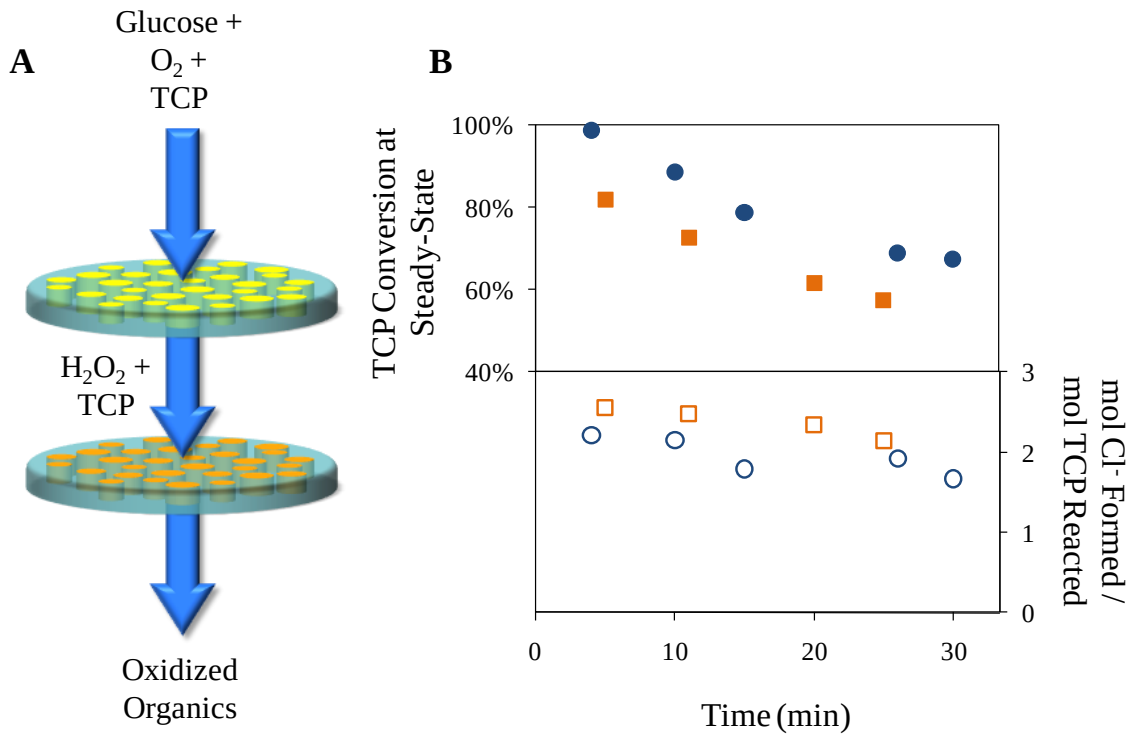

Figure 6.9. Model compound degradation from water in a reactive nanostructured stacked membrane system. (A) Schematic of stacked membrane system for degradation of TCP using glucose and oxygen. Top membrane contains GOx electrostatically immobilized in LbL assembly; bottom membrane contains Fe^{2+} immobilized in a PVDF-PAA membrane. (B) TCP conversion at steady-state and Cl^- formation as a function of time (data obtained by Datta 2007). Squares: 0.142 mmol/L TCP in feed; circles: 0.076 mmol/L TCP in feed. Maximum mol Cl^- formed / mol TCP reacted = 3. Steady state concentration of H_2O_2 from the first membrane is 0.1 mmol/L (circles) and 0.13 mmol/L (squares), Fe loading = 0.09 mmol, pH 5.5, residence time in the top membrane = 2.7 s, residence time in the bottom membrane = 2 s.

saturated solution of TCP and glucose through the top membrane where GOx converts glucose and oxygen to H_2O_2 and gluconic acid, leaving TCP unaffected. Upon entering the bottom membrane, H_2O_2 reacts with the immobilized Fe(II), generating hydroxyl radicals which react with TCP. Although it is feasible to create a single membrane with both GOx and Fe^{2+} immobilized, it is necessary to use two separate membranes so as to avoid the deactivation of the enzyme by free radicals. Maintaining positive pressure drop across the membrane stack prevents free radicals from entering the top membrane.

Using a constant residence time, the initial conversion of TCP is 100%, but decreases with time, reaching 55 – 70 % after 30 min (Figure 6.9B). This decrease in TCP conversion is characteristic of these PVDF-PAA-Fe(II) membranes as the immobilized Fe(II) is converted to Fe(III), reducing the rate of H_2O_2 decomposition and hence free radical production. As the free radical degradation of TCP progresses, various intermediates are formed and the attached chlorine atoms are released from the molecule as chloride ions. Chloride formation and TCP concentration in the permeate were monitored to ensure degradation via oxidation (Figure 6.9B). Note that although the TCP conversion initially decreases, the ratio of mol Cl^- formed to mol TCP reacted remains relatively constant (~2) through the entire experiment, indicating significant TCP degradation (maximum Cl^- released per TCP molecule is 3). The TCP conversion can be easily adjusted by varying the amount of iron loading, the rate of H_2O_2 production, the pore size via change in stimulus, and residence time through pressure modulation.

The H_2O_2 utilization efficiency for these reactions is shown in Figure 6.10. For the lower concentrations of TCP (0.076 mmol/L), the mol of TCP converted per mol of H_2O_2 reacted varied from 0.55 to 0.7 whereas it varied from 0.7 to 0.9 for the higher concentration (0.142 mmol/L). This suggests that at the higher concentration of TCP, the ratio of free radicals that react with TCP to those lost to side reactions is greater than for the lower TCP concentration. Therefore, in order to optimize the consumption of H_2O_2 for the lower concentration of TCP, either less iron or less H_2O_2 is required. Previous studies with TCE indicated that for the chelate-modified, iron-catalyzed H_2O_2 decomposition at pH 6, this efficiency was in the range of 0.07 to 0.17 even though the rate constant for OH• with TCE is only ~ 27 % lower than for OH• and TCP (both are second order as in Equation 2.17). This difference could be due to differences in the

mechanisms of oxidative degradation of the two compounds and/or the difference in reactivity between the chelated and ion exchanged iron ions.

In order to simulate TCP being the major reactant with OH•, the reaction of OH• and TCP was incorporated into the previously described kinetic model with $k_{TCP} = 5.48 \times 10^9$ M^{-1} s^{-1}. Since there will be significant competition for OH• by Fe(II), that rate of reaction of TCP with OH• was increased, substituting $k'_{TCP} = 1000 \times k_{TCP}$ for k_{TCP}. Under such conditions, the maximum mol of TCP degraded per mol of H_2O_2 consumed was 0.53 for a TCP feed concentration of 0.076 mmol/L. Increasing k_{TCP} 1000-fold again ($k'_{TCP} = 10^6 \times k_{TCP}$), to the point where the reaction of TCP with OH• is dominant compared to the reaction of Fe(II) and OH• results in a maximum ratio of 0.76. Although a large rate constant such as k'_{TCP} is very unrealistic, as mentioned previously, the rate constant for the reactions involving Fe(II) are most likely lower than literature-reported values due to the multiple variables associated with these systems. A lower rate constant for the reaction of Fe(II) and OH• would make TCP or any other contaminant more competitive for OH• relative to Fe(II).

.

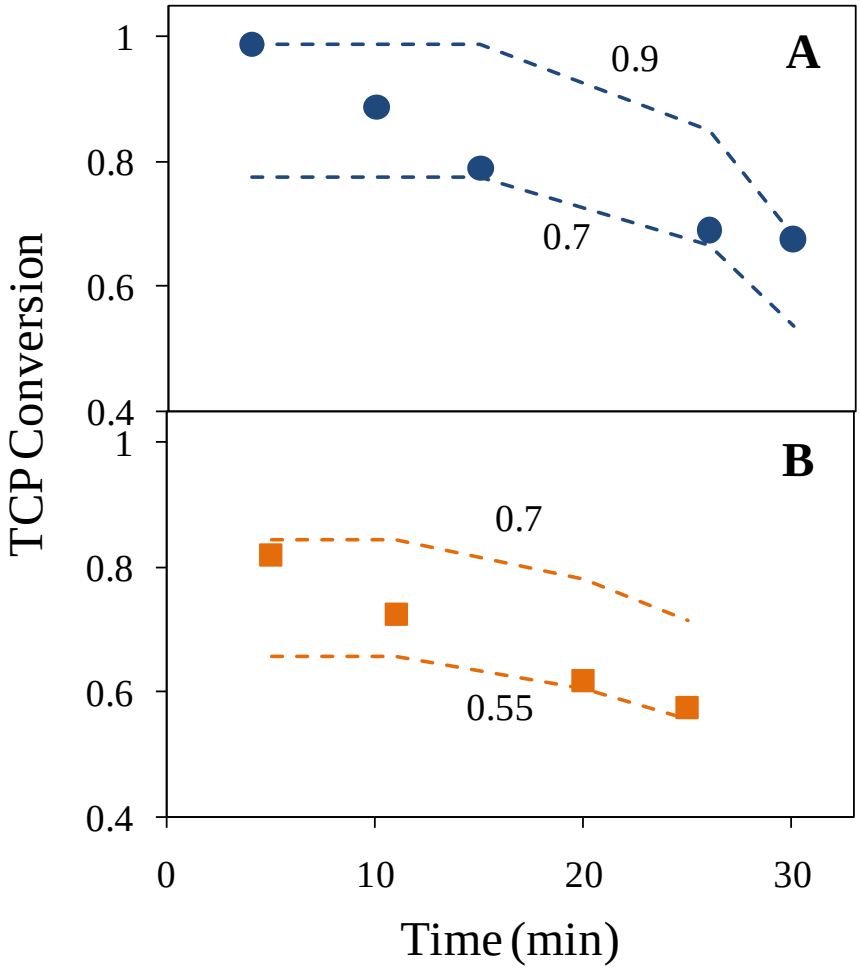

Figure 6.10. Predicted degradation of TCP with time as a function of H_2O_2 consumed. (A) TCP conversion at steady-state for 0.142 mmol/L TCP and 0.1 mmol/L H_2O_2 in feed with predicted conversion (lines) for 0.7 and 0.9 mol TCP degraded / mol H_2O_2 consumed (B) TCP conversion at steady-state for 0.076 mmol/L TCP and 0.13 mmol/L H_2O_2 in feed with predicted conversion (lines) for 0.55 and 0.7 mol TCP degraded / mol H_2O_2 consumed. Fe loading = 0.09 mmol, pH 5.5, residence time in membrane = 2 s.

Chapter 7 Extension of Membrane Immobilized Iron-Based Free Radical Reactions to Cell Inactivation

7.1 Introduction

Finding new methods to inactivate or destroy undesirable cellular organisms/tissues (i.e. bacterial, cancerous) is a continuous challenge facing scientists today. Although several oxidation-based technologies for the destruction of bacteria currently exist, there is a desire to move away from popular chlorine-based reagents due to the formation of harmful chlorinated byproducts. Such technologies include advanced oxidative processes which involve the formation of free radicals. Methods including the use of UV irradiation with H_2O_2, ozone and H_2O_2, or TiO_2 photocatalysis have been used to effectively inactivate or kill various unwanted cells such as *Escherichia coli*, *Bacillus subtilis*, and *Clostridium perfringen*s (Bayliss and Waites 1979; Wolff et al. 1986; Ireland et al. 1993; Butterfield et al. 1997). Additionally, the toxicity of free radicals to human tissue has been well established in literature (Valko et al. 2005).

The focus of this work is towards the development of a multifunctional particle for cancer therapy (nanoparticle) with an extension to water treatment for disinfection, virus inactivation, and/or toxic organic degradation (nanoparticle or microparticle). The most important reactions for these systems are the same as those used in the stacked membrane system mentioned in previous chapters. The synthesis of these nanostructures would require a combination of various functionalization and synthesis procedures (Caruso 2001). An illustration of such a nanoparticle is shown in Figure 7.1. The center of the particle contains an inert nanoparticle which serves as its structural basis. This nanoparticle core could also be used as a contrast agent for non-invasive, *in vivo* monitoring of the particle distribution or, if magnetic, used to separate the particles from solution for water treatment applications. The core is surrounded by a positively-charged polyelectrolyte (PE) layer with electrostatically-immobilized GOx (similar to the LbL assembly mentioned in earlier chapters). As glucose diffuses into this region, it will generate H_2O_2 which, upon diffusing outward, will react with the immobilized reactive iron species, such as Fe(II), Fe(III), or Fe_xO_y, forming free radicals (as in the membrane

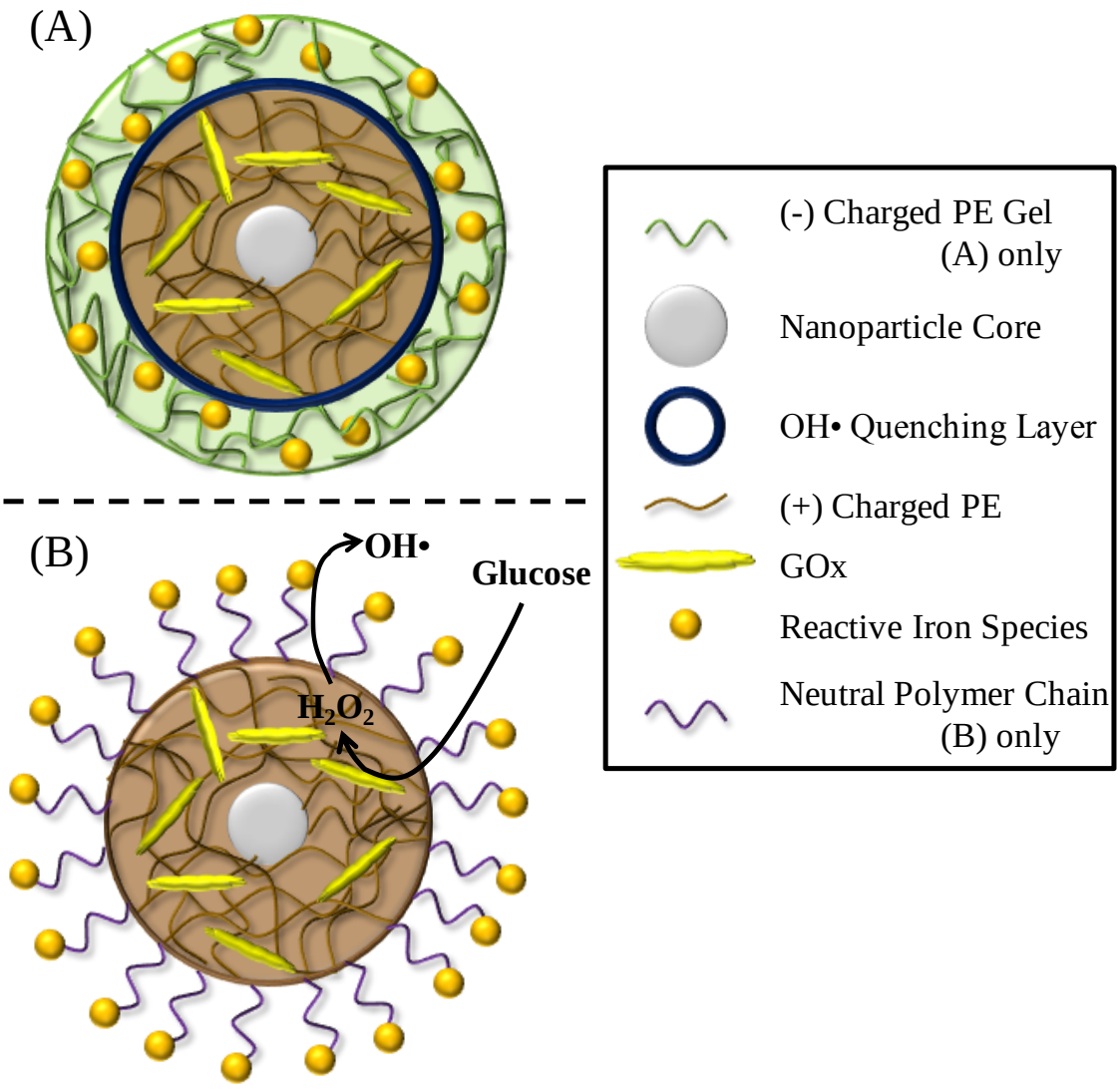

Figure 7.1. Illustration of functionalized particles for the generation of free radicals in close proximity to unwanted cells (i.e. bacterial, cancerous) and/or water treatment. The center of the particle has an inert nanoparticle core surrounded by a positively-charged polyelectrolyte (PE) layer with electrostatically-immobilized GOx. The outer layer consists of either (A) a negatively-charged PE gel with immobilized reactive iron species or (B) neutral polymer chains extending away from the particle with the iron species attached to its end.

immobilized free radical reactions). These free radicals will then degrade the neighboring unwanted cells/pollutants. The OH• quenching layer in Figure 7.1A is designed to protect GOx from the free radicals since the reactive iron species may be in close proximity to the GOx. The neutral polymer chain in Figure 7.1B would not necessarily be entirely neutral, but could have functional group/moieties at either end via which attachment to the PE layer and/or the reactive iron species would be possible. Thus, the iron species would be far enough away from the GOx that damage to the enzyme via free radical exposure would be minimal. If this particle (of the correct size) were to be used for targeted delivery to cancerous tissue, free radical generation before reaching the tumor site, where it would be retained by the enhanced permeability and retention effect, would be undesirable (Maeda et al. 2009). In this case, the negatively-charged PE gel in Figure 7.1A could be pH-responsive and designed to be in a swollen state at normal physiological pH (7.4), creating a larger diffusion pathlength for the reactants. Upon entering the tumor region, it would collapse slightly since the extracellular pH of tumors was found to be below 7.2 in 80 % of studies (Lee et al. 2008), thereby reducing the diffusion pathlength of the reactants. Additionally, the extracellular pH of tumor tissue has been found to decrease in transient hyperglycemic patients upon ingestion of glucose (Leeper et al. 1994). This would simultaneously provide more glucose for conversion to H_2O_2 and the lower pH would result in the further collapse of the pH-responsive gel, resulting in greater accessibility to the reactive iron species.

In this study, the potential for using immobilized free radical reactions for the inactivation/killing of cells was investigated. These preliminary studies were conducted by exposing both adherent and non-adherent mammalian cells to PVDF-PAA-Fe^{2+} membranes in the presence of H_2O_2.

7.2 Materials and methods

7.2.1 Materials

Dulbecco's Modified Eagle's Medium (DMEM), and fetal bovine serum (FBS) were purchased from ATCC. Sodium dodecyl sulfate (SDS), dimethylformamide (DMF),

and (3-(4,5-Dimethylthiazol-2-yl)-2,5-diphenyl tetrazolium bromide (MTT reagent) were purchased from Sigma Aldrich. Iscove's Modified Dulbecco's Medium (IMDM) (1X) (no phenol red), Calcein AM, and ethidium homodimer were purchased from Invitrogen.

7.2.2 Cell lines

Human myeloid leukaemic cells (HL-60, CCL-224) were obtained from the laboratory of Dr. Daunert at the University of Kentucky and were originally purchased from ATCC. All HL-60 cells were cultured in IMDM with 20 vol % FBS and passaged every 2-3 days.

Mouse bone marrow cells (D1 pluripotent mesenchymal cells, CRL-12424) were obtained from the laboratory of Dr. Hilt at the University of Kentucky and were originally purchased from ATCC. All D1 cells were cultured in DMEM with 10 vol % FBS and passaged every 3-4 days.

7.2.3 Non-adherent (HL-60) cell studies

In order to determine the effect of membrane immobilized iron-based free radical reactions on non-adherent cell types, preliminary studies on the toxicity of these systems to HL-60 cells were conducted. First, six 3.5 cm^2 circular pieces of PVDF-PAA membranes were soaked in a deoxygenated, 1 mM MES-buffered solution containing 3 mM $FeCl_2$ at pH 5.5 – 5.8 to capture Fe^{2+}. After 3 h, the PVDF-PAA-Fe^{2+} membranes were added to deoxygenated DIUF water to prevent oxidation. These membranes were then placed in 12-well plates (3.8 cm^2 surface area per well) and secured with metal washers around the perimeter of each membrane to keep them immobilized. These washers were autoclaved, stored in EtOH, and dried thoroughly before use. Next, the wells were seeded with 1 mL of a solution containing 10^6 cells/mL and either 0 or 100 μM H_2O_2. The cell suspension containing H_2O_2 was prepared immediately before use so as to minimize any potential damage to the cells before addition to the wells. A control experiment containing no membrane, washer, or H_2O_2 was conducted simultaneously. All experiments were conducted in triplicate. The well plate was then placed in an incubator

at 37 ˚C and rotated several times every 2 min to keep the concentration of live and dead cells uniform throughout the well. After 30 min, the MTT assay was used to determine cell viability. A summary of the nomenclature used when reporting results is shown in Table 7.1.

7.2.4 MTT assay

The MTT assay is a widely-used, quantitative, colorimetric method for the measurement of cytotoxicity (Mosmann 1983). MTT solution is added to the well containing the cells of interest and MTT, which is yellow in color, is reduced to formazan by mitochondrial reductase in living cells, forming dark blue crystals (Mosmann 1983). The MTT solution was prepared by dissolving 5 mg/mL MTT in phosphate-buffered saline (PBS) and subsequently sterile-filtered. For this study, 0.5 mL of the HL-60 cell suspension was removed from the center of each well and transferred to a 24-well plate. This was followed by the addition of 0.125 mL MTT solution and the well plate was placed in an incubator at 37 °C for 3 h. A row of control wells containing only media and MTT solution were also added. The well plate was removed and 0.5 mL of lysing buffer consisting of 20 wt % SDS, 50 wt % DMF in DI water at pH 4.7 was added to each well to lyse the cells and dissolve the formazan product. After 24 h in an incubator at 37 ˚C, the well plate was removed and solution was transferred to a 96-well plate for analysis via absorbance at 570 nm.

7.2.5 Surface-adherent (D1) cell studies

In order to determine the effect of membrane immobilized iron-based free radical reactions on surface-adherent cell types, preliminary studies on the toxicity of these systems to D1 cells were conducted. These experiments were performed similarly to those outlined in Section 7.2.3. However, the D1 cells were seeded (2.5×10^4 cells/cm^2) 0.5 h before the addition of H_2O_2 to allow them to settle. After the addition of 100 μM H_2O_2, the well plates were put in an incubator at 37 ˚C for 4 h. Next, the cells were immediately analyzed using the live/dead assay.

Table 7.1. Summary of notation used for cell studies. "X" indicates what was present.

Designation	**Media**	**Cells**	**Washer**	**Other**
Blank	X			
Control	X	X		
PVDF-PAA-Fe^{2+}	X	X	X	PVDF-PAA-Fe^{2+} membrane
PVDF-PAA-Na^{+}	X	X	X	PVDF-PAA-Na^{+} membrane
PVDF	X	X	X	Hydrophobic PVDF membrane

7.2.6 Live/Dead assay

The cells in each well were stained using calcein AM and ethidium homodimer. Calcein AM enters the living cells where it is cleaved by cytoplasmic esterase, yielding calcein, which fluoresces green (excitation ~495 nm / emission ~515 nm) (Papadopoulos et al. 1994). Ethidium homodimer is impermeable to the membranes of living cells and will therefore only enter dead cells, where it stains DNA and fluoresces red (excitation ~495 nm / emission ~635 nm). Images of the stained cells were obtained using a Nikon Microscope with NIS Elements Software.

7.2.7 Statistical analysis

ANOVA analysis of data was performed using GraphPad InStat software. For $p < 0.05$, a post-comparison analysis was performed using a Tukey Multiple Comparison Test.

7.3 Effect of H_2O_2 on HL-60 cells

Before investigating the effects of the membrane immobilized iron-based free radical reactions on these mammalian cells, it was necessary to determine how the presence of H_2O_2 would affect their viability. If the concentration of H_2O_2 was too high, the cells would be severely damaged before ever being exposed to the free radicals whereas if the concentration was too low, the free radicals would be generated at an insufficient rate. Previous work has investigated the mechanisms by which the cellular functions of proliferating mammalian cells are affected by exposure to H_2O_2 (Davies 1999), the findings of which are summarized in Table 7.2. It is interesting to note that although concentrations of 120 to 150 μM H_2O_2 initially inhibited the growth of the mammalian fibroblasts tested, they exhibited an adaptive response after only 4-6 h and were eventually able to return to normal function. Similar responses have been reported for bacteria (20 – 30 min) and yeast cells (~ 45 min) (Demple and Halbrook 1983; Christman et al. 1985; Davies et al. 1995). Since different cell types will respond

Table 7.2. Summary of effect of H_2O_2 on proliferating mammalian cells (fibroblasts) as determined by Davies (1999).

[H_2O_2] (μM)	**H_2O_2 (μmol) / 10^7 Cells**	**Effect on Cell**
3 – 15	0.1 – 0.5	Growth stimulation
120 – 150	2 – 5	Temporary growth arrest
250 – 400	9 – 14	Permanent growth arrest
500 – 1000	15 – 30	Cell apoptosis
5000 - 10000	150 - 300	Cell membrane disintegration

differently to the same H_2O_2 exposure, the findings related to the mammalian fibroblasts were used only as a guide. Based on this information, a concentration of 100 μM H_2O_2 was chosen for use in these studies.

To determine the effect of H_2O_2 on HL-60 cells, 10^5 cells/mL were exposed to 100 μM H_2O_2 for 19 h. The MTT assay absorbance, a function of cell viability, is shown in Figure 7.2. After 19 h of exposure to the H_2O_2, there was a significant statistical difference between the absorbance of the control well and the following wells: control + H_2O_2, blank, and blank + H_2O_2. This, and the finding that there was no statistical difference between the MTT assay absorbance of the latter three, indicated that exposure to 100 μM H_2O_2 for 19 h caused enough oxidative stress to either inhibit the reduction of MTT to formazan within the cell or induce cell apoptosis. In order to eliminate the possibility that H_2O_2 was interfering with the MTT assay, an immediate assay was performed on 10^5 cells/mL in media and 10^5 cells/mL in media with 100 μM H_2O_2. Since there was no statistical difference in absorbances, the effect of this concentration of H_2O_2 on formazan formation in the living cells and subsequent dissolution of the formazan product were determined to be negligible. As a result of these findings, the concentration of cells was increased to 10^6 cells/mL and exposure time to H_2O_2 was decreased.

7.4 Effect of membrane immobilized iron-based free radical reactions on HL-60 cells

In order to determine the effect of the membrane immobilized iron-based free radical reactions on HL-60 cells, cell viability was tested after 30 min exposure to a PVDF-PAA-Fe^{2+} membrane with and without 100 μM H_2O_2 (Figure 7.3). The exposure of the cells to these conditions showed no significant variation in MTT assay absorbance from the control. This lack of difference in cell viability suggested that the cells were not exposed to a significant quantity of free radicals. Since the majority of the PAA was in the PVDF pores and the transport of free radicals is diffusion-limited, the cells would need to be close enough to the source of free radicals to have a significant effect on overall cell viability. This presented a problem since the cells were distributed throughout the solution. A more noticeable effect could potentially be brought about by reducing the

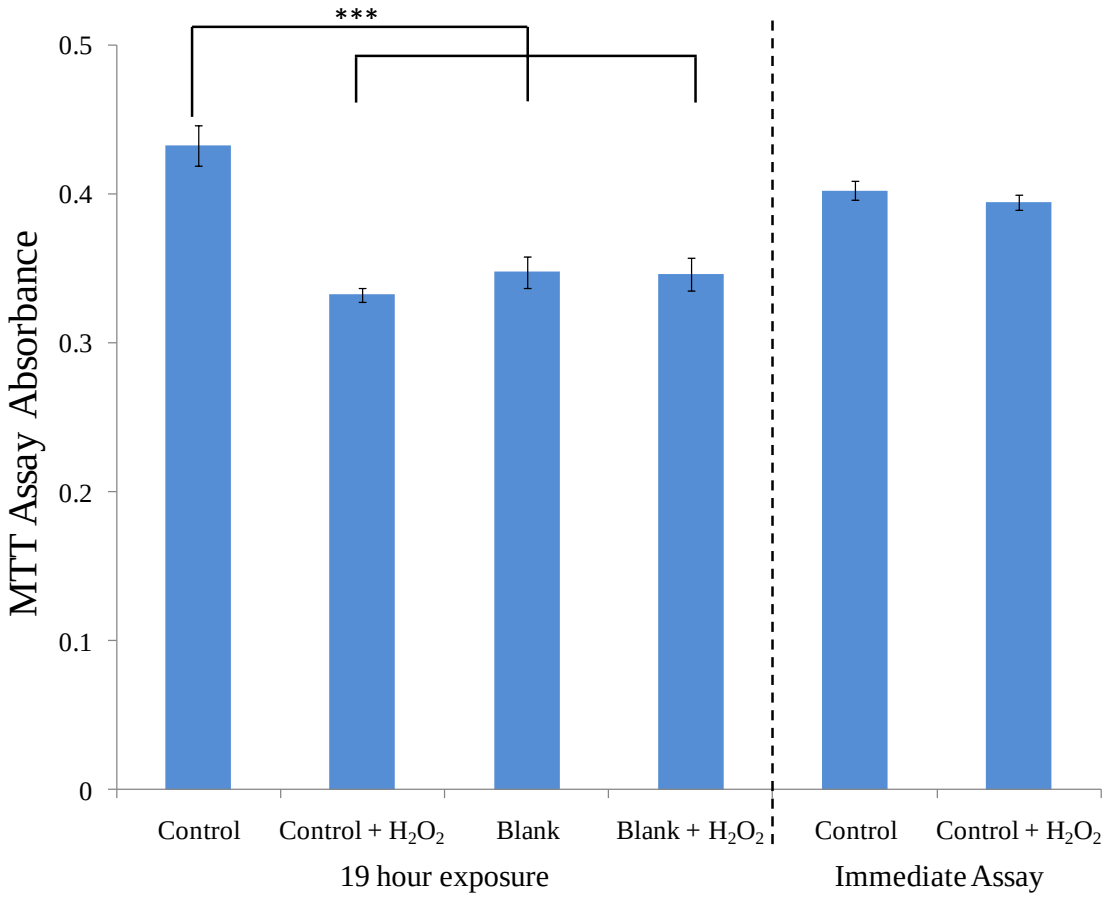

Figure 7.2. MTT assay absorbance for determining the effect of H_2O_2 on HL-60 cells. The left side of the graph illustrates effect of 100 µM H_2O_2 after 19 h exposure with an additional 3 h for MTT assay. The right side of the graph illustrates the effect of 100 µM H_2O_2 added immediately before the 3 h MTT assay. Control: indicates only cells and media were added to the well. Error bars represent one standard deviation. ***$p < 0.001$

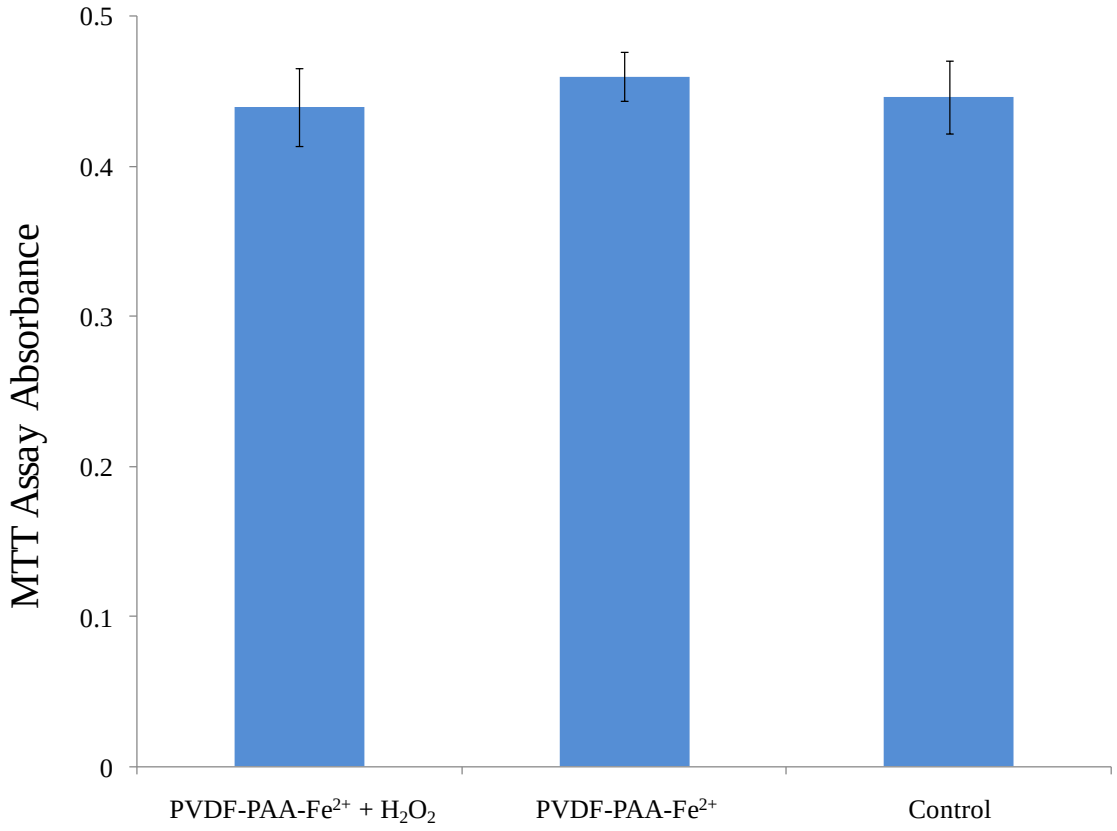

Figure 7.3. MTT assay absorbance for determining the effect of membrane-immobilized free radical reactions on HL-60 cells. Reactions were carried out for 30 min. "H_2O_2" indicates the presence of 100 μM H_2O_2. Error bars represent one standard deviation.

concentration of cells and therefore increasing the number of free radicals to which each cell is exposed. However, a more effective approach would be to anchor the cells to the membrane surface, thereby keeping them in close proximity to the source of free radicals.

7.5 Effect of membrane immobilized iron-based free radical reactions on D1 cells

By using an adherent cell line, the cells could attach to the membrane surface, where they would have the highest possible exposure to the free radicals generated by the reaction of the immobilized iron ions and H_2O_2. Since the adhesion and proliferation of mammalian cells on surfaces is of great importance to areas ranging from tissue engineering to biosensors, several investigators have studied how to promote and prevent such interactions through surface modification (Berg et al. 2004). Previous work has demonstrated how the modification of untreated polystyrene surfaces with carboxyl and hydroxyl groups promotes cell adhesion (Teare et al. 2000). As such, polyelectrolytes have also been used to modify surfaces to make them cytophilic or even cytophobic (Liu and Ito 2002; Mendelsohn et al. 2003). PAA has been used to increase charge density in thin films, thereby imparting greater cytophilicity to surfaces such as polystyrene (Jung et al. 2008). Although hydrophobic PVDF is not ideal for cell attachment, the PVDF-PAA membrane could be a more favorable substrate. Assuming there is only PAA in the pores of the PVDF-PAA membrane and not covering the surface, a significant portion of the exposed membrane surface area would be PAA (> 66 % for R_2 = 225 nm, R_1 = 75 nm, and $\varepsilon = 0.75$). The carboxyl groups of this exposed PAA could provide attachment sites for the adherent cells.

The effect of the membrane immobilized free radical reactions on adherent D1 cells was determined by following the procedure outlined in Section 7.2.5. Although MTT assay has been used for the analysis of adherent cells, some of the reagents used are incompatible with the PVDF-PAA membrane, so this procedure was avoided. Representative fluorescent and/or brightfield images of the membranes and controls after the live/dead assay are shown in Figure 7.4. Due to the inability to keep the membranes perfectly flat on the bottom of the plate, only portions of some of the images were in focus. In some cases, a redish hue was seen and was a result of the background

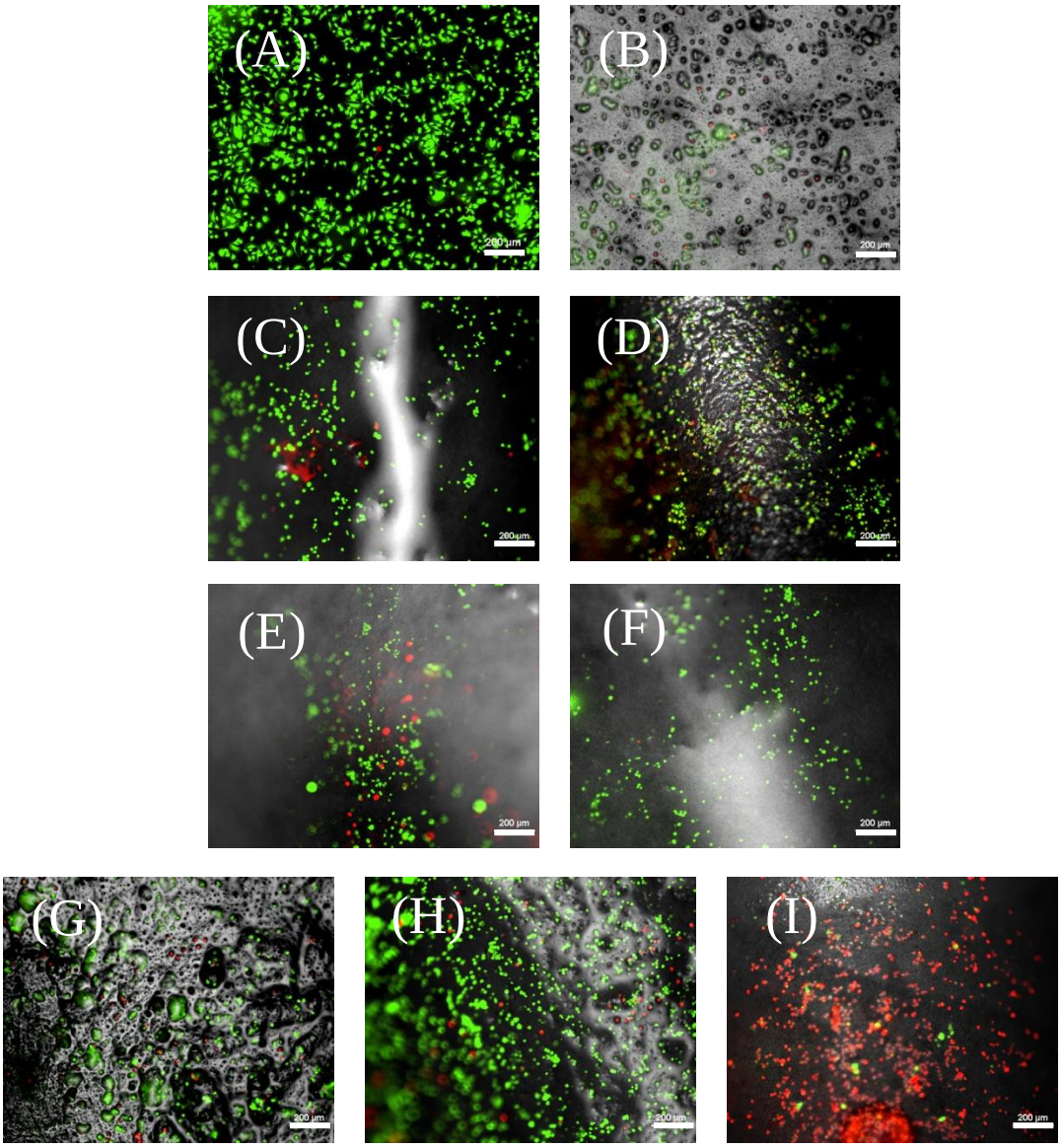

Figure 7.4. Membrane immobilized free radical exposure study. All images (except A) consist of live/dead fluorescence images overlaid on brightfield images taken after 4 h exposure. (A) TCPS Control (no brightfield), (B) PVDF, (C-D) PVDF-PAA-Na^{+}, (E-F) PVDF-PAA-Na^{+} + H_2O_2, (G-I) PVDF-PAA-Fe^{2+} + H_2O_2. Refer to Table 7.1 for notation. Scale bar represents 200 μm.

fluorescence of PVDF. Note that the following discussion is based on qualitative results. Despite the hydrophobicity of PVDF membrane, several cells were present on its exterior, but mainly in confined domains (Figure 7.4 B). The cells showed greater affinity towards the PVDF-PAA-Na^+ membranes, appearing on unconfined areas as well as confined areas (Figure 7.4 C-D). Even when cells on PVDF-PAA-Na^+ membranes were exposed to H_2O_2, there did not appear to be widespread cell death (Figure 7.4 E-F). Images of the cells exposed to the PVDF-PAA-Fe^{2+} membranes with H_2O_2 indicate that the cell death was inconsistent across the membrane surface (Figure 7.4 G-I). This could be due to non-uniform distribution of PAA (and therefore Fe^{2+}/Fe^{3+}) near the surface since this distribution may not be as controlled as it is through the majority of the membrane pore.

7.6 Conclusions

The viability of adherent and non-adherent mammalian cells after exposure to membrane immobilized iron-based free radical reactions was investigated as a preliminary step to determining the applicability of such reactions to the inactivation of various types of unwanted cells. These preliminary results were promising, but also raised several questions. To improve upon this process, the PAA gel with the immobilized reactive iron species (ions and/or nanoparticles) would be only on the outside of the material being used so the target cells would be exposed to a larger percentage of the free radicals that are formed. Therefore, a particle-based approach, such as those outlined at the beginning of the chapter, would be more ideal.

Chapter 8 Application of Solution-Based and Membrane Immobilized Oxidative and Reductive Technologies for Site Remediation

This chapter focuses on the implementation of the previously-discussed oxidative and reductive platforms for the remediation of TCE from groundwater at the Paducah Gaseous Diffusion Plant in Paducah, KY. Before applying these technologies to actual contaminated groundwater, some issues remain and fundamental studies are needed to address them. To gain approval of these studies, a treatability study workplan outlining the lab-scale and pilot-plant studies required to evaluate these technologies entitled "Iron - Based Treatability Study: Use of Nano-aggregates, Membrane Immobilized Nanoparticles, and Green Chemistry" was submitted to the Department of Energy (Lewis et al. 2011). For brevity, the reductive dechlorination of toxic organic compounds was not discussed in this dissertation; however, several references are available regarding the use of zero-valent iron (Fe^0) nanoparticles/aggregates and bimetallic Fe/Pd nanoparticles/aggregates for such applications (Choe et al. 2001; Tee et al. 2005; Xu and Bhattacharyya 2005; Cheng et al. 2007; He et al. 2007; Lewis et al. 2009; Meyer et al. 2009). Figure 8.1 gives an overview of the technologies outlined in this treatability study.

8.1 Experimental approach and design

This treatability study will consist of three tiers of testing to evaluate which technologies are best suited for potential *in situ* and *ex-situ* remediation of TCE from groundwater in the Northwest Plume. Tier 1 will evaluate the effectiveness of Fe^0 and Fe/Fe_xO_y particle aggregates for the reductive and oxidative, respectively, degradation of TCE in groundwater. Tier 2 will evaluate the performance of Fe^0, Fe/Pd and Fe/Fe_xO_y nanoparticles immobilized within a cut-up polymeric membrane for degradation of TCE in groundwater. Tier 3 will evaluate the effectiveness of the nanoparticles from Tier 2 immobilized within a polymeric membrane module for degradation of TCE in groundwater. All testing will be done with groundwater from the Northwest Plume. Tiers 1 and 2 will be evaluated for potential *in situ* application by first conducting column tests with simulated groundwater flow. All tiers will be tested at an on-site pump-and-treat

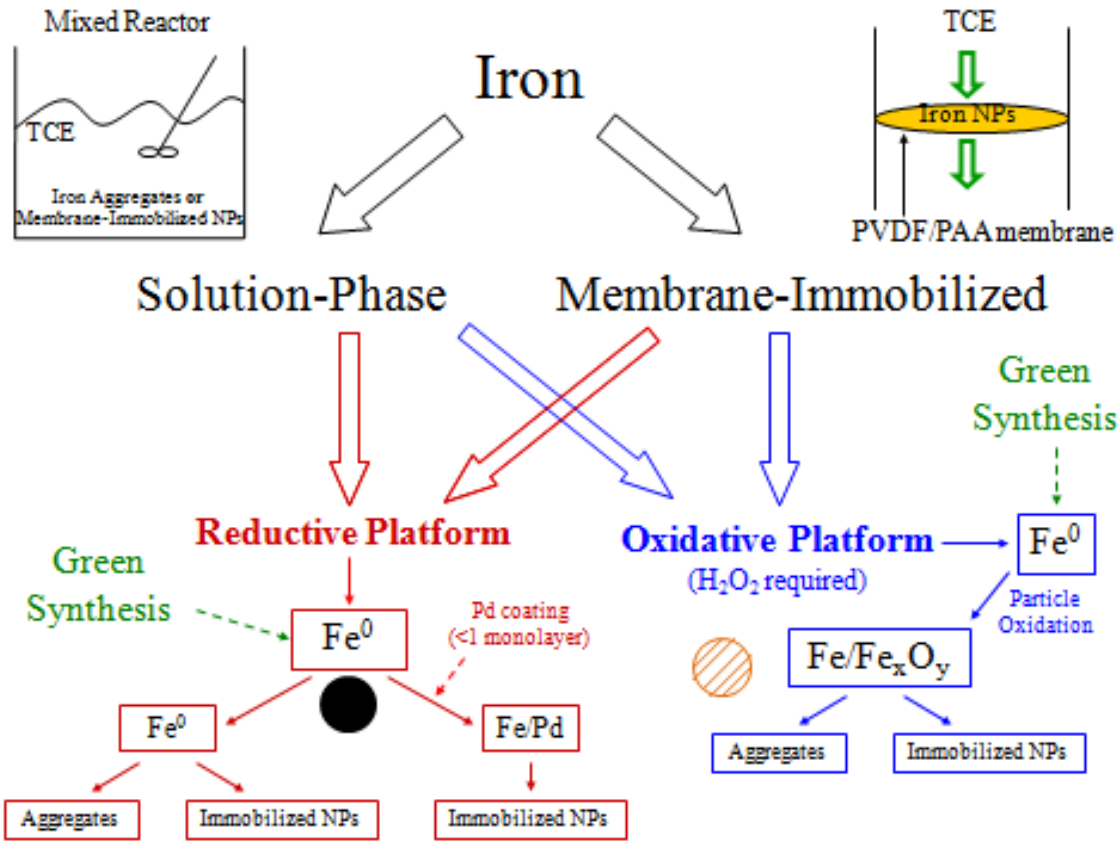

Figure 8.1. Overview of iron platforms to be used in this treatability study.

facility for potential long-term *ex-situ* application. The effect of conventional versus green synthesis of the iron particles on particle reactivity will also be investigated. For the oxidative approaches the main goal will be to minimize H_2O_2 consumption.

8.1.1 Experimental approach

Tier 1

The goal of Tier 1 is to determine the most suitable composition and method of synthesis for the iron aggregates which are to be used for the degradation of TCE from groundwater from the Northwest Plume. These aggregate particles will consist of either Fe^0 for the reductive degradation of TCE or Fe/Fe_xO_y and H_2O_2 for the oxidative degradation of TCE. The effect of conventional versus green synthesis on iron aggregate reactivity may be investigated. In order to confirm the composition and size of these aggregates, several characterization techniques will be used, including SEM, TEM, and DLS.

During initial Tier 1 testing, lab-scale experiments will be conducted through the use of horizontal columns containing RGA gravel and groundwater from the Northwest Plume operated under simulated groundwater flow conditions of 1-3 ft/day. TCE, chloride, chlorinated intermediates (if necessary), and H_2O_2 (if applicable), pH, and ORP will be monitored during experimentation with and without the reactive iron aggregates. Samples will be taken from sampling ports along the horizontal axis of the column. In order to determine the most effective treatment(s), several performance parameters will be monitored including dosing, longevity, transport, and efficiency of reactant utilization at constant conditions for all treatment technologies. Each technology will be evaluated for its efficiency of TCE degradation to determine whether it will be used for *ex-situ*, pilot plant testing at an on-site pump-and-treat facility. If the technology proves to be effective, it will then be considered for future *in situ* treatment of the contaminated aquifer. Figure 8.2 illustrates the technology selection process using a common iron platform.

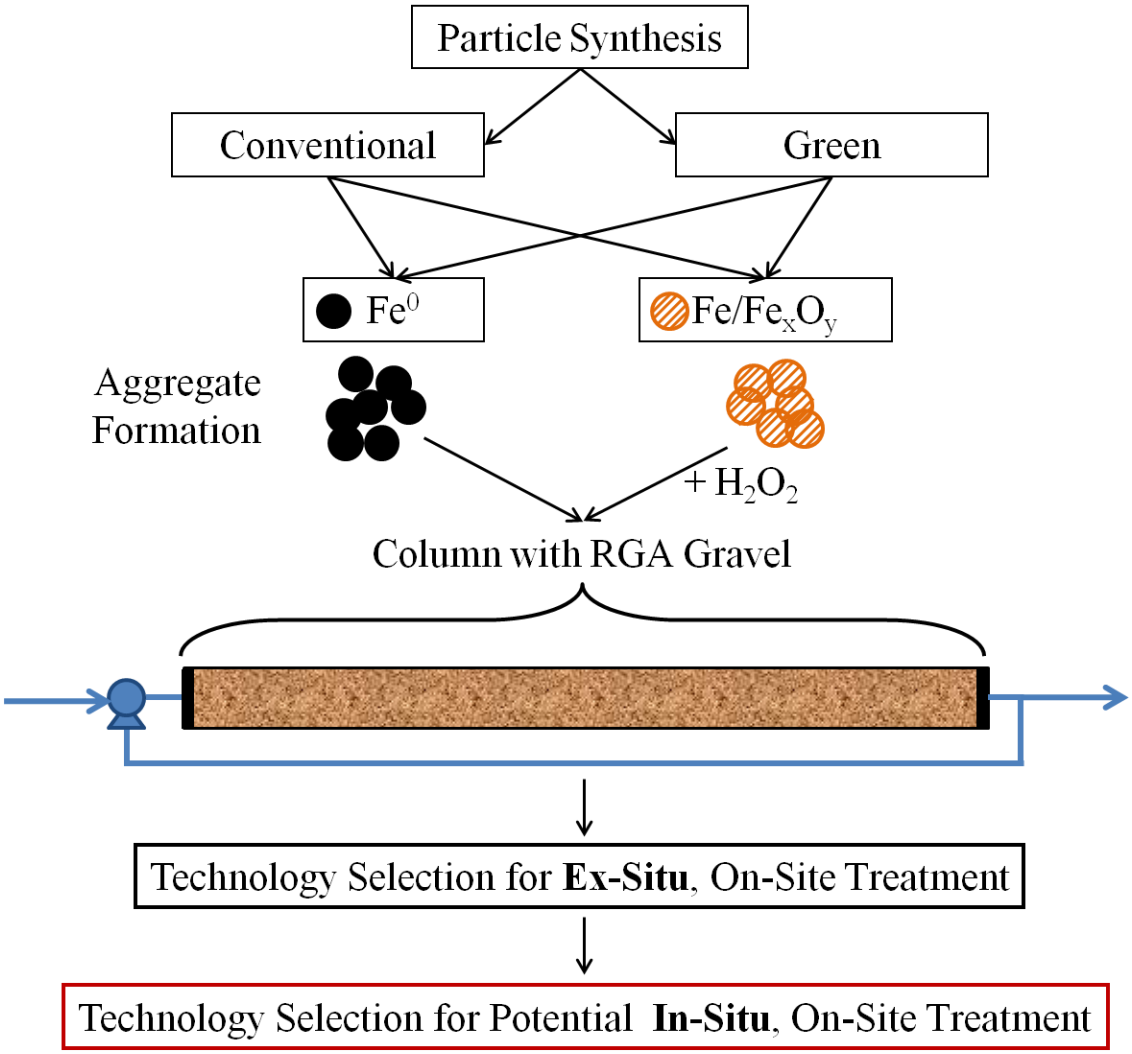

Figure 8.2. Overview of iron platforms to be tested and diagram of primary testing equipment for Tier 1.

Tier 2

The focus of Tier 2 is to determine the most suitable composition and method of synthesis for the cut-up, polymeric membrane-bound iron-based nanoparticles which are to be used for the degradation of TCE from groundwater from the Northwest Plume. These nanoparticles will consist of either Fe^0 or Fe/Pd for the reductive degradation of TCE and Fe/Fe_xO_y and H_2O_2 for the oxidative degradation of TCE. The effect of conventional versus green synthesis on iron aggregate reactivity may be investigated. Obviously the cut-up membrane size will affect NP loading per membrane. In order to confirm the composition and size of these immobilized nanoparticles, several characterization techniques will be used, including SEM, TEM, and DLS.

During initial Tier 2 testing, lab-scale experiments will be conducted through the use of horizontal columns containing RGA gravel and groundwater from the Northwest Plume operated under simulated groundwater flow conditions of 1-3 ft/day. TCE, chloride, chlorinated intermediates (if necessary), and H_2O_2 (if applicable) concentrations, pH, and ORP will be monitored during experimentation with and without the addition of the cut-up membranes containing the immobilized nanoparticles. Samples will be taken from sampling ports along the horizontal axis of the column. In order to determine the most effective treatment(s), several performance parameters will be monitored including dosing, longevity, transport, and efficiency of reactant utilization at constant conditions for all treatment technologies. Each technology will be evaluated for its efficiency of TCE degradation to determine whether it will be used for *ex-situ* testing at an on-site pump-and-treat facility. If the technology proves effective, it will then be considered for future *in situ* treatment of the contaminated aquifer. Figure 8.3 illustrates the technology selection process.

As an alternative to adding commercially-produced H_2O_2 to the immobilized Fe/Fe_xO_y nanoparticles, the potential for green on-site enzymatic generation of H_2O_2 will be investigated. By using GOx enzyme immobilized within the pores of a cut-up polymeric membrane, the H_2O_2 necessary for the oxidative reactions will be generated *ex-situ* and/or *in situ* via the addition of glucose. Although the addition of gluose to the groundwater could provide benefits associated with bioaugmentation, studying these effects will not be a primary focus of this treatability study.

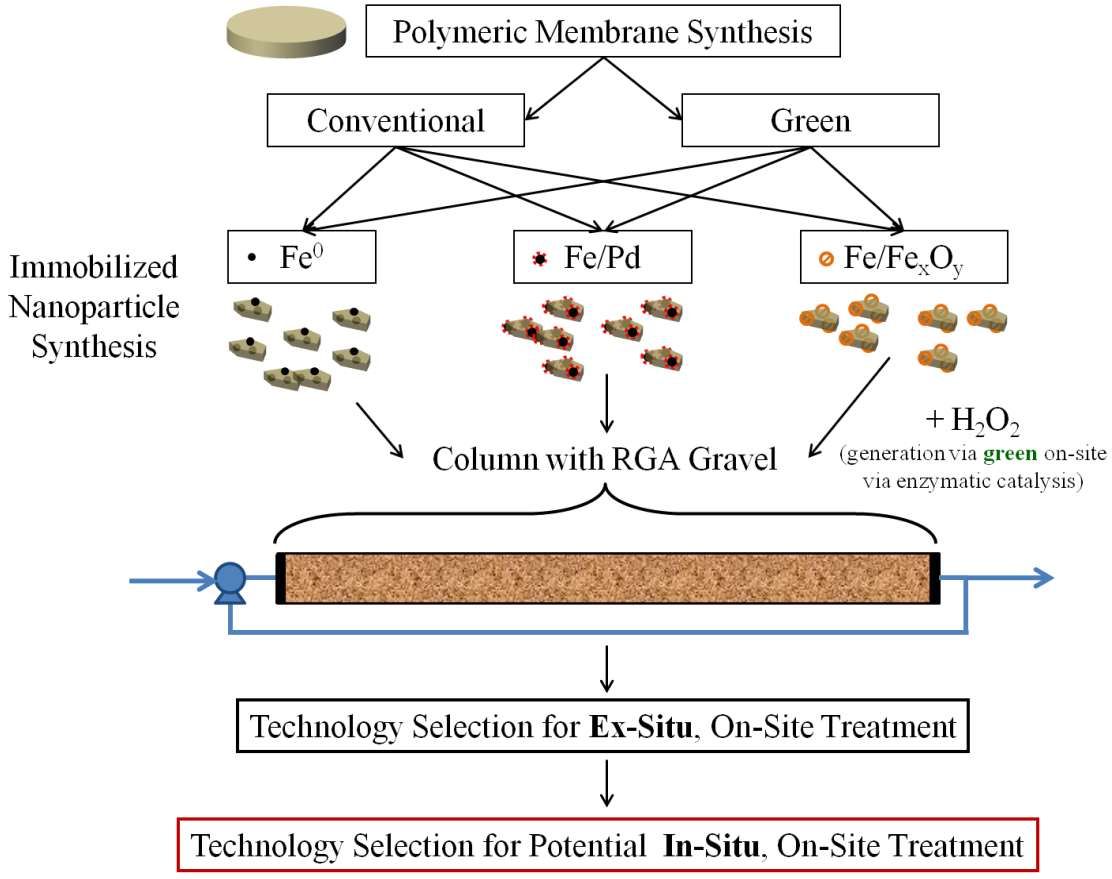

Figure 8.3. Overview of iron platforms to be tested and diagram of primary testing equipment for Tier 2.

Tier 3

The goal of Tier 3 is to determine the most suitable composition and method of synthesis for the polymeric membrane-bound iron-based nanoparticles which are to be used for the degradation of TCE from groundwater from the Northwest Plume. Obviously the biggest advantage of membrane immobilization is to maintain high NP reactivity by preventing aggregation. These nanoparticles will consist of either Fe^0 or Fe/Pd for the reductive degradation of TCE or Fe/Fe_xO_y and H_2O_2 for the oxidative degradation of TCE. The effect of conventional versus green synthesis on iron reactivity may be investigated. This system will consist of a membrane module containing the immobilized nanoparticles through which the groundwater will travel under pressure-driven flow. This system will be operated under convective flow through the membrane, providing increased access to the nanoparticles immobilized within the membrane pores and thus potentially higher rates of TCE degradation. In order to confirm the composition and size of these immobilized nanoparticles, several characterization techniques will be used, including SEM, TEM, and DLS.

Testing will first be conducted in lab-scale convective flow (dead-end filtration) cells using groundwater from the Northwest Plume. TCE, chloride, chlorinated intermediates (if necessary), and H_2O_2 (if applicable) concentrations, pH, and ORP will be monitored during experimentation. Each of the iron platforms will be evaluated for its efficiency of TCE degradation to determine whether it will be used for *ex-situ* testing at an on-site pump-and-treat facility. Since the main focus of this work will be on use with a pump-and-treat system, the groundwater for laboratory testing will be pretreated similarly to the way it is at the pump-and-treat site. If the technology proves effective, it will then be considered for long-term *ex-situ* treatment of the contaminated groundwater. Since the nanoparticles will be immobilized within the cut-up membrane pieces, they will not be released into the aquifer. Figure 8.4 illustrates the technology selection process.

8.1.2 Variables affecting performance

There are several variables which can affect the performance of the reductive and oxidative reactions associated with these iron-based platforms. These include pH,

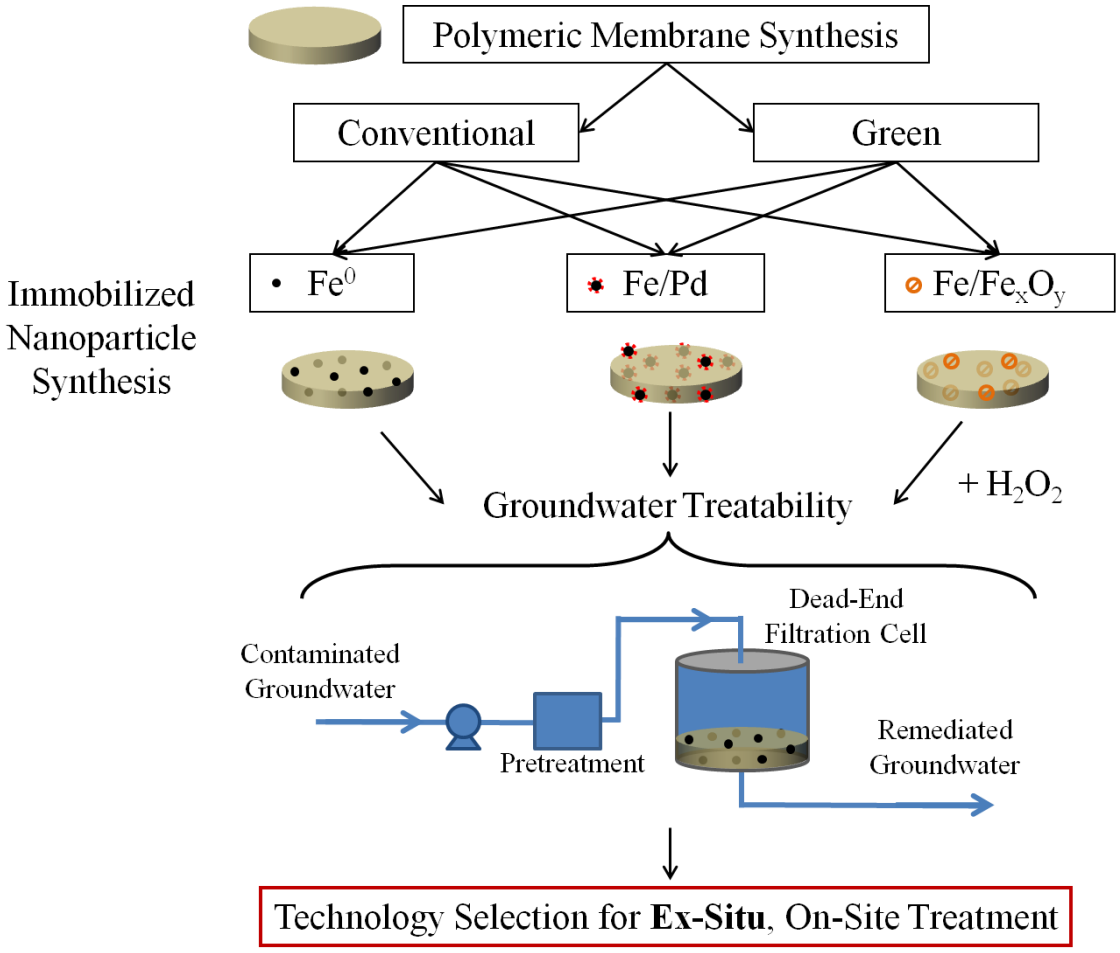

Figure 8.4. Overview of iron platforms to be tested and diagram of primary testing equipment for Tier 3.

dissolved oxygen, hardness, natural organic carbon, contaminant concentration, groundwater flowrate, and alkalinity. Our lab studies using water from the Paducah site have indicated that hardness and alkalinity have an insignificant effect on TCE dechlorination for the platforms used in the reductive pathway (Meyer et al. 2009). Since the majority of these variables cannot be altered in the aquifer, these studies will mainly focus on the effects of varying groundwater flowrate, and potentially dissolved oxygen, on the performance of the selected iron-based platforms. Table 8.1 shows the variables that could affect performance.

8.2 Equipment design and experimental procedures

This section describes the equipment and systems used to implement this treatability study. Included are general procedures for operation of the equipment, sampling and analysis, and a description of the equipment to be used.

8.2.1 Design criteria

To conduct the treatability study based on the experimental approach and variables presented in Section 8.1.2, the equipment and procedures outlined in this section will be used. Since one of the objectives of this treatability study is to determine whether the iron platforms presented in Tiers 1 and 2 could find application for the *in situ* remediation of TCE, columns packed with RGA gravel and groundwater from the Northwest Plume will be utilized to simulate groundwater flow through the RGA. Similarly, dead-end filtration cells will be used to simulate the effectiveness of a larger, commercial membrane module containing the iron platforms outlined in Tier 3 for potential long-term *ex-situ* treatment. The chemical analysis of the groundwater which will aid in determining important process parameters have been previously reported (Clausen and Richards, 1994).

Table 8.1. Variables affecting performance of iron-based platforms.

Variable	Comment
Iron Content	Higher reactive surface area and loadings of iron media will increase rate of TCE degradation
Flow Rate	Longer residence times (lower flow rate) should produce greater TCE removal
Influent pH	pH will affect rates of reaction for both oxidative and reductive platforms
$H_2 O_2$	Needed only for oxidative pathway
Influent TCE concentration	Higher contaminant concentrations will require longer contact times for degradation
Water Chemistry	Inorganic and organic material could affect the iron-based platforms in a negative or positive manner
Influent ORP	Reductive or oxidative conditions will determine effectiveness of the iron-based platforms

8.2.2 Process description

For laboratory-scale testing of these iron platforms, various sets of equipment will be required. These include: horizontal columns (Tiers 1 and 2), dead-end filtration cells (Tier 3), mixed vessel reactors (Tiers 1 and 2, post-selection), and membrane modules (Tier 3, post-selection).

Tiers 1 and 2

Horizontal columns will be used for simulating groundwater flow through an aquifer representative of the one at the Paducah Gaseous Diffusion Plant. It will contain RGA gravel and groundwater spiked with TCE from the Northwest Plume (Figure 8.5). The column will be constructed so it can be operated by either continuously introducing fresh groundwater spiked with TCE (1-10000 ppb) to the column from a separate feed container or circulating the same batch of groundwater through the column multiple times. This provides a means to control the contact time with the reactants while keeping the same groundwater flowrate of 1-3 ft/day.

Column injections of the iron aggregates (Tier 1) or cut-up membranes (0.04 – 0.1 cm^2) with immobilized nanoparticles (Tier 2) will be made using concentrated solutions (slurries) of these reactants. For the multiple injection/sampling ports will allow for the monitoring of the previously outlined parameters upgradient and downgradient of the selected iron platform injections.

After selecting the best platform(s), they will be tested at an on-site pump-and-treat facility in a mixed reactor vessel. This will be a sidestream treatment system where pretreated groundwater will enter a mixed vessel containing the iron aggregates or cut-up membranes. No additional chemicals will need to be added to the vessel except for H_2O_2 to be used with the Fe/Fe_xO_y-based platforms. Groundwater will flow through the vessel for removal of TCE. The outlet of the vessel will contain a porous mat to prevent the iron aggregates and cut-up membranes from leaving the reactor in the effluent.

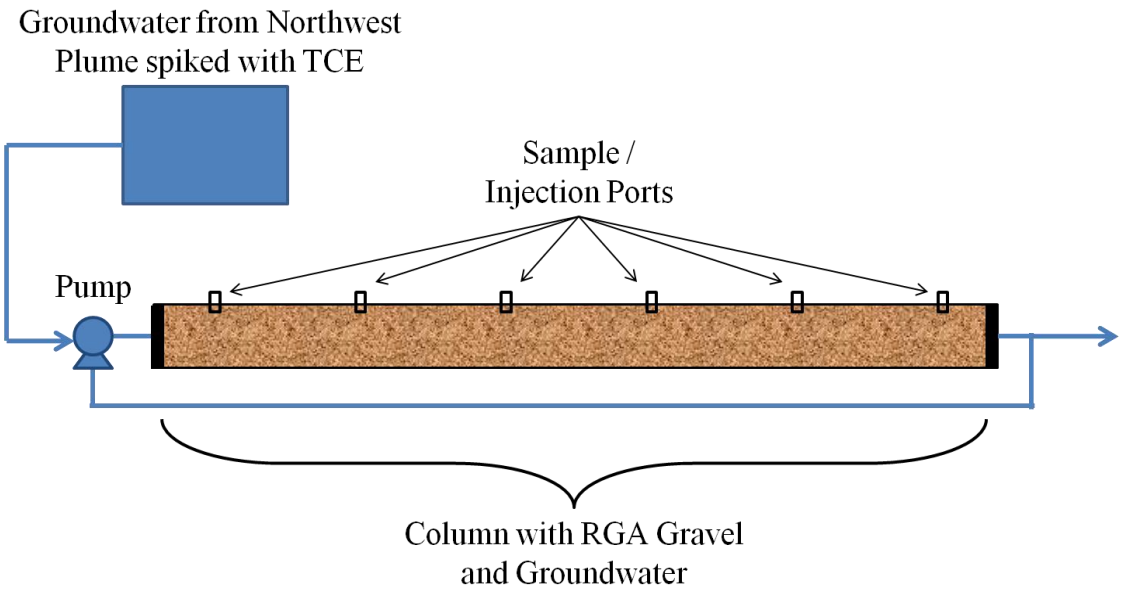

Figure 8.5. Schematic of column packed with RGA gravel for Tiers 1 and 2 testing.

Tier 3

In order to determine the most suitable iron platform for use in the functionalized membranes containing immobilized nanoparticles operated under convective flow, dead-end filtration cells will be used to conduct the initial testing. The membranes containing immobilized nanoparticles will be sealed in the bottom of the filtration apparatus and the pretreated groundwater from the Northwest Plume with added TCE will be permeated through the membrane. In the case of immobilized Fe/Fe_xO_y nanoparticles, H_2O_2 will be added to produce the necessary free radicals for contaminant degradation. The feed solutions will be permeated through the cell by pressure. As the solution permeates, it will be collected and analyzed for chloride, TCE, and H_2O_2 (if applicable).

8.2.3 Equipment description

Columns

The horizontal columns to be used for simulating groundwater flow will consist of cylindrical plastic tubing filled with RGA gravel and groundwater from the Northwest Plume. The column will be several feet long and contain an injection/sampling port every 0.5-1.0 ft. The column will be constructed so it can be operated by either continuously introducing fresh groundwater spiked with TCE (100-10000 ppb) to the column from a separate feed container or circulating the same batch of groundwater through the column multiple times. This provides a means to control the contact time with the reactants while keeping the same groundwater flowrate of 1-3 ft/day. The groundwater flowrate will be controlled by either a peristaltic or similar pump. These columns will be similar to those described by Meyer et al. (2009) and Lewis et al. (2009) for use in simulating groundwater flow for oxidative and reductive dechlorination of TCE (Figure 4.18). Control experiments will be conducted to determine the effect of column material on adsorption of TCE. If TCE adsorption to the column is determined to have a non-quantifiable effect on TCE dechlorination experiments, a virgin column will be used for each column experiment.

Dead-end membrane filtration cells

The dead-end filtration cells will be used to conduct the initial testing of the membranes used in Tier 3. These will be stainless steel and/or glass convective flow cells with membrane surface areas of either 14.7 cm^2 or 33.2 cm^2. The membranes containing immobilized nanoparticles will be sealed in the bottom of the filtration apparatus. The feed solution will pass through the membrane via pressure-driven flow, which is obtained by pressurizing the cell with compressed gas (N_2 or air) or by a pump. Figure 8.4 contains an illustration of a dead-end filtration cell.

Mixed reactor vessel

The mixed reactor vessel for on-site testing as described in Section 8.2 will contain the necessary reactants and have an injection port for the addition of any consumables necessary for the degradation of TCE (i.e. H_2O_2). Additional ports will be used for monitoring important variables (pH, etc.). This vessel will be continuously stirred and the outlet will be covered with a porous mat to prevent particle loss.

Membrane module

The membrane module for the on-site testing portion of Tier 3 will be a commercial module and incorporate a membrane of approximately 100-200 ft^2. After iron functionalization we expect to get about 100 – 200 g of Fe per module.

Polymeric membranes with immobilized nanoparticles

This section describes the methods to be used for preparation of the reactive materials used in Tiers 2 and 3. These materials will be prepared off-site. Once the membranes are prepared with the desired immobilized nanoparticles, they will be either cut-up into small pieces for testing in Tier 2 or cut to the desired size for use with the dead-end filtration cell in Tier 3. For the second phase of Tier 3 testing (on-site) a larger membrane sheet will be functionalized and inserted into the membrane module described earlier. In order to confirm the composition and size of these immobilized nanoparticles, several characterization techniques will be used, including SEM, TEM, and DLS.

Polymeric membrane synthesis

PVDF membranes are extensively used in water industries. The PVDF/PAA membranes for use in Tiers 2 and 3 will be prepared off-site using the following methods. PVDF membranes will be coated with PAA by *in situ* polymerization of acrylic acid. Although various membrane materials can be used for this application, PVDF has been chosen for its high chemical and thermal stabilities. The polymerization reaction will be carried out using an aqueous "green approach". Aqueous phase *in situ* polymerization of acrylic acid (green chemistry) will utilize a polymerization solution contained 30 wt% acrylic acid (monomer), ethylene glycol (cross-linker, added in a 1:10 molar ratio of EG to acrylic acid), and 1 wt% potassium persulfate (initiator). We have a well established procedure to use this approach.

For polymerization, a PVDF membrane will be dipped in the polymerization solution for 2 min, sandwiched between 2 teflon or glass plates and placed in an oven at 90 °C for 4 h. Nitrogen gas will be continuously supplied to remove oxygen, which acts as an inhibitor for the polymerization reaction. In order to ensure the proper wetting, hydrophilized PVDF membranes will be used for the aqueous-phase polymerization. This aqueous-based method for the *in situ* polymerization of PAA within PVDF pores is well-established in literature (Lewis, Smuleac et al. 2009).

Membrane immobilized Fe^0 nanoparticle synthesis

Nanoparticle immobilization within the membrane pores will be achieved using the following or similar methods. The PVDF/PAA membrane will be immersed in $FeCl_2$, or similar ferrous salt, solution (typically 180 mg/L Fe^{2+}) at a pH of 5.5 for ~4 h. Nitrogen gas will be bubbled to minimize Fe^{2+} oxidation. For the conventional synthesis of Fe^0 nanoparticles, the reduction of Fe^{2+} with $NaBH_4$ will ensure Fe^0 nanoparticle formation and the membranes will be stored in ethanol to prevent oxidation. For the green synthesis of Fe^0 nanoparticles, the reduction of Fe^{2+} with polyphenols and/or ascorbic acid will ensure Fe^0 nanoparticle formation and the membranes will be stored in ethanol to prevent oxidation. Another important aspect of Fe NPs use is long term stability. Our current results indicate that the Fe NPs synthesized by green chemistry (tea

extract) have considerably higher (because of polyphenol capping from tea) stability compared to borohydride synthesis particles.

Membrane immobilized Fe/Pd nanoparticle synthesis

To synthesize Fe/Pd nanoparticles in the PVDF/PAA membrane, a PVDF/PAA membrane with Fe^0 nanoparticles synthesized by either green or conventional methods will be used. The secondary metal, Pd, will be deposited on the Fe^0 nanoparticles by immersing the membrane in a K_2PdCl_4 solution containing ethanol/water (90:10 vol% mixture), preventing the oxidation of the highly reactive Fe nanoparticles. This will create the desired core-shell nanoparticles. The membranes will be stored in ethanol to prevent oxidation.

Membrane immobilized Fe/Fe_xO_y nanoparticle synthesis

To synthesize Fe/Fe_xO_y nanoparticles in the PVDF/PAA membrane, a PVDF/PAA membrane with Fe^0 nanoparticles synthesized by either green or conventional methods will be used. The membrane will be transferred to deionized water where it will be purged with air at a rate of ~40 mL/min for 1-10 h to form the desired immobilized Fe/Fe_xO_y nanoparticles.

Iron aggregates

This section describes the general methods used to prepare the iron aggregates for Tier 1 testing. These materials will be prepared off-site. In order to confirm the composition and size of these aggregates, several characterization techniques will be used, including SEM, TEM, and DLS.

Fe^0 aggregate synthesis

An aqueous $FeCl_2$, or similar ferrous salt, solution will be prepared at a pH of 4.5-5.5 to prevent oxidation of the dissolved Fe^{2+}. For conventional reduction to Fe^0, $NaBH_4$ will be used whereas polyphenols (such as tea extract) or similar compounds will be used for green reduction to Fe^0 during mixing. For the conventional reduction method, capping agents such as CMC (carboxymethyl cellulose, a common food additive) may be used.

The use of green chemistry eliminates the need for CMC. These reactions will be carried out under N_2 atmosphere to prevent aggregate oxidation. The reduced Fe will be allowed to settle before decanting off the excess solution. The remaining slurry will be filtered using continuous additions of ethanol to minimize particle oxidation.

Fe/Fe_xO_y aggregate synthesis

To convert the Fe^0 aggregates to Fe/Fe_xO_y, they will be transferred to deionized water where it will be purged with air at a rate of ~40 mL/min for 1-10 h.

Chapter 9 Conclusions

The purpose of this work was to better understand iron-catalyzed H_2O_2 decomposition reactions at near-neutral pH when either immobilized in a stimuli-responsive membrane domain or chelated in solution, how they can be used to conduct interfacial reactions in membrane and solution-based systems for the degradation of toxic organic compounds, and to develop quantitative models for the prediction of reactant behavior in both systems.

9.1 Key Advancements to Science and Engineering

The key advancements to science and engineering achieved in this work were as follows.

- The degradation of a toxic organic compound in both dissolved and droplet phases in aqueous systems can be achieved at near-neutral pH and can be modeled through a combination of mass transfer and reaction kinetics correlations
- A significant advancement towards a new generation of ultrafiltration membranes through the creation of a tunable iron-functionalized platform for the catalytic decomposition of H_2O_2 and subsequent toxic compound degradation
- Kinetic modeling of the membrane immobilized H_2O_2 decomposition reactions can be used to better understand the consumption of reactants in the process, providing the information necessary for more efficient utilization of reactants

9.2 Specific Accomplishments

The specific accomplishments for the solution phase and membrane immobilized iron-based free radical reactions were as follows.

9.2.1 Solution phase, iron-based free radical reactions

- Hydroxyl radical generation and Fe(II) to Fe(III) conversion were quantified for solution-based iron-catalyzed H_2O_2 decomposition reactions. Reactions with Fe(III) demonstrated better efficiency for hydroxyl radical formation that similar reactions with Fe(II)
- The modified Fenton reaction was effective for the degradation of TCE in groundwater samples and in simulated groundwater aquifers at near-neutral pH
- A chelating agent, citrate, can be used to control the rate of H_2O_2 decomposition by iron ions at near-neutral pH
- The effective degradation of TCE droplets through the use of standard and modified Fenton reactions were established
- A kinetic model for the prediction of TCE droplet degradation incorporating solution and interfacial reactions and mass transfer was developed

9.2.2 Membrane immobilized, iron-based free radical reactions

- The composition and structure of a PVDF-PAA membrane were investigated.
- Modulations in pH and/or divalent cation concentration can be used to induce a stimuli-repsonsive change in membrane permeability
- Although PVDF-PAA-immobilized Fe(III) decomposes H_2O_2 at a slower rate than immobilized Fe(II), it is more stable in the presence of Ca^{2+} and therefore may be more suitable for long-term use
- The decomposition of H_2O_2 through the use of Fe(III) immobilized in PVDF-PAA membranes was predicted using both CSTR and PFR models. Both models indicated a ~ 20-fold higher reaction rate for Fe(III) and H_2O_2 than expected based on literature-reported values.
- Degradation of PCP was achieved using membrane-immobilized H_2O_2 decomposition operated under convective flow. This system allows for modulation of conversion by changing iron loading, residence time, and/or H_2O_2 concentration

- Iron oxide/ferrihydrite nanoparticles were synthesized within the pores of PVDF-PAA membranes through a simple technique
- A model for the determining the decomposition of H_2O_2 in an iron-functionalized membrane as a function of time and position within the membrane pore was developed

References

Ahuja, D. K., L. G. Bachas, et al. (2007). "Modified Fenton reaction for trichlorophenol dechlorination by enzymatically generated H2O2 and gluconic acid chelate." Chemosphere **66**(11): 2193-2200.

Amarante, D. (2000). "Applying in situ chemical oxidation." Pollution Engineering **32**(2): 40-42.

Amsden, B. (1998). "Solute diffusion within hydrogels. Mechanisms and models." Macromolecules **31**(23): 8382-8395.

Anzai, J., A. Ueno, et al. (1983). "Photocontrolled Permeation of Alkali Cations through Polyvinyl-Chloride) Crown Ether Membrane." Makromolekulare Chemie-Rapid Communications **4**(11): 731-734.

Baes, C. F. and R. E. Mesmer (1976). The hydrolysis of cations. New York, Wiley.

Barb, W. G., J. H. Baxendale, et al. (1949). "Reactions of Ferrous and Ferric Ions with Hydrogen Peroxide." Nature **163**(4148): 692-694.

Bayliss, C. E. and W. M. Waites (1979). "Combined Effect of Hydrogen-Peroxide and Ultraviolet-Irradiation on Bacterial-Spores." Journal of Applied Bacteriology **47**(2): 263-269.

Beckman, J. S., T. W. Beckman, et al. (1990). "Apparent Hydroxyl Radical Production by Peroxynitrite - Implications for Endothelial Injury from Nitric-Oxide and Superoxide." Proceedings of the National Academy of Sciences of the United States of America **87**(4): 1620-1624.

Benitez, F. J., J. Beltran-Heredia, et al. (1999). "Chemical decomposition of 2,4,6-trichlorophenol by ozone, Fenton's reagent, and UV radiation." Industrial & Engineering Chemistry Research **38**(4): 1341-1349.

Berg, M. C., S. Y. Yang, et al. (2004). "Controlling mammalian cell interactions on patterned polyelectrolyte multilayer surfaces." Langmuir **20**(4): 1362-1368.

Bhattacharyya, D. and D. A. Butterfield (2003). New insights into membrane science and technology polymeric and biofunctional membranes. Membrane science and technology series,. Amsterdam ; Boston, Elsevier**:** 1 online resource (xxii, 415 p.).

Borggaar.Ok (1972). "Polarographic Determination of Diffusion-Coefficients of Hydrogen-Peroxide and Iron Chelates and Rate Constants of Hydroxyl Radical Reactions." Acta Chemica Scandinavica **26**(8): 3393-3394.

Brady, J. E. and G. E. Humiston (1982). General chemistry, principles and structure. New York, Wiley.

Brown, P. P. and D. F. Lawler (2003). "Sphere drag and settling velocity revisited." Journal of Environmental Engineering-ASCE **129**(3): 222-231.

Bruening, M. L., D. M. Dotzauer, et al. (2008). "Creation of functional membranes using polyelectrolyte multilayers and polymer brushes." Langmuir **24**(15): 7663-7673.

Brunet, R., M. M. Bourbigot, et al. (1984). "Oxidation of Organic-Compounds through the Combination Ozone-Hydrogen Peroxide." Ozone-Science & Engineering **6**(3): 163-183.

Butterfield, I. M., P. A. Christensen, et al. (1997). "Water disinfection using an immobilised titanium dioxide film in a photochemical reactor with electric field enhancement." Water Research **31**(3): 675-677.

Caruso, F. (2001). "Nanoengineering of particle surfaces." Advanced Materials **13**(1): 11-22.

Charcosset, C. (2006). "Membrane processes in biotechnology: An overview." Biotechnology Advances **24**(5): 482-492.

Cheng, R., J. L. Wang, et al. (2007). "Comparison of reductive dechlorination of p-chlorophenol using Fe-0 and nanosized Fe-0." Journal of Hazardous materials **144**(1-2): 334-339.

Choe, S., S. H. Lee, et al. (2001). "Rapid reductive destruction of hazardous organic compounds by nanoscale Fe-0." Chemosphere **42**(4): 367-372.

Christman, M. F., R. W. Morgan, et al. (1985). "Positive Control of a Regulon for Defenses against Oxidative Stress and Some Heat-Shock Proteins in Salmonella-Typhimurium." Cell **41**(3): 753-762.

Clapp, P. A., D. F. Evans, et al. (1989). "Spectrophotometric Determination of Hydrogen-Peroxide after Extraction with Ethyl-Acetate." Analytica Chimica Acta **218**(2): 331-334.

Cornell, R. M. and U. Schwertmann (2003). The iron oxides : structure, properties, reactions, occurrences, and uses. Weinheim, Wiley-VCH.

Cukier, R. I. (1984). "Diffusion of Brownian Spheres in Semidilute Polymer-Solutions." Macromolecules **17**(2): 252-255.

Dai, J. and M. L. Bruening (2002). "Catalytic nanoparticles formed by reduction of metal ions in multilayered polyelectrolyte films." NanoLetters **2**(5): 497-501.

Datta, S. (2007). Functionalized Poylmeric Membranes for Bioseparation and Biocatalysis. College of Engineering. Lexington, KY, University of Kentucky. **Ph.D.**

Datta, S., C. Cecil, et al. (2008). "Functionalized membranes by layer-by-layer assembly of polyelectrolytes and in situ polymerization of acrylic acid for applications in enzymatic catalysis." Industrial & Engineering Chemistry Research **47**(14): 4586-4597.

Davies, J. M. S., C. V. Lowry, et al. (1995). "Transient Adaptation to Oxidative Stress in Yeast." Archives of Biochemistry and Biophysics **317**(1): 1-6.

Davies, K. J. A. (1999). "The broad spectrum of responses to oxidants in proliferating cells: A new paradigm for oxidative stress." Iubmb Life **48**(1): 41-47.

De Laat, J. and H. Gallard (1999). "Catalytic decomposition of hydrogen peroxide by Fe(III) in homogeneous aqueous solution: Mechanism and kinetic modeling." Environmental Science & Technology **33**(16): 2726-2732.

Demple, B. and J. Halbrook (1983). "Inducible Repair of Oxidative DNA Damage in Escherichia-Coli." Nature **304**(5925): 466-468.

Djuric, Z., D. W. Potter, et al. (2001). "Comparison of iron-catalyzed DNA and lipid oxidation." Journal of Biochemical and Molecular Toxicology **15**(2): 114-119.

Dorfman, L. M., G. E. Adams, et al. (1973). Reactivity of the hydroxyl radical in aqueous solutions. [NSRDS-NBS 46]. [Washington, D.C.], U.S. Dept. of Commerce, National Bureau of Standards**:** vi-59.

Dotzauer, D. M., J. Dai, et al. (2006). "Catalytic membranes prepared using layer-by-layer adsorption of polyelectrolyte/metal nanoparticle films in porous supports." NanoLetters **6**(10): 2268-2272.

Dubinsky, S., G. S. Grader, et al. (2004). "Thermal degradation of poly(acrylic acid) containing copper nitrate." Polymer Degradation and Stability **86**(1): 171-178.

Duke, F. R., M. Weibel, et al. (1969). "Glucose Oxidase Mechanism . Enzyme Activation by Substrate." Journal of the American Chemical Society **91**(14): 3904-3909.

Engwall, M. A., J. J. Pignatello, et al. (1999). "Degradation and detoxification of the wood preservatives creosote and pentachlorophenol in water by the photofenton reaction." Water Research **33**(5): 1151-1158.

Espro, C., F. Arena, et al. (2001). "On the potential of the multifunctional three phase catalytic membrane reactor in the selective oxidation of light alkanes by Fe2+-H2O2 Fenton system." Catalysis Today **67**(1-3): 247-256.

Espro, C., F. Frusteri, et al. (2000). "Selective oxidation of propane on a Nafion-based catalytic membrane mediated by FeII-H2O2 Fenton system." Journal of Molecular Catalysis A: Chemical **159**(2): 359-364.

Fang, F. C. (2004). "Antimicrobial reactive oxygen and nitrogen species: Concepts and controversies." Nature Reviews Microbiology **2**(10): 820-832.

Fernandez, J., J. Bandara, et al. (1998). "Efficient photo-assisted Fenton catalysis mediated by Fe ions on Nafion membranes active in the abatement of non-biodegradable azo-dye." Chemical Communciations(14): 1493-1494.

Fernandez, J., V. Nadtochenko, et al. (2003). "Testing and performance of immobilized Fenton photoreactions via membranes, mats, and modified copolymers." International Journal of Photoenergy **5**(2): 107-113.

Fogler, H. S. (1999). Elements of chemical reaction engineering. Upper Saddle River, N.J., Prentice Hall PTR.

Fritzmann, C., J. Lowenberg, et al. (2007). "State-of-the-art of reverse osmosis desalination." Desalination **216**(1-3): 1-76.

Fukushima, M. and K. Tatsumi (2001). "Degradation pathways of pentachlorophenol by photo-Fenton systems in the presence of iron(III), humic acid, and hydrogen peroxide." Environmental Science & Technology **35**(9): 1771-1778.

Gabriel, E. M. and G. E. Gillberg (1993). "Insitu Modification of Microporous Membranes." Journal of Applied Polymer Science **48**(12): 2081-2090.

Haag, W. R. and C. C. D. Yao (1992). "Rate Constants for Reaction of Hydroxyl Radicals with Several Drinking-Water Contaminants." Environmental Science & Technology **26**(5): 1005-1013.

Haber, F. and J. Weiss (1934). "The Catalytic Decomposition of Hydrogern Peroxide by Iron Salts." Proceedings of the Royal Society **A147**: 332-351.

Halliwell, B. and M. Whiteman (2004). "Measuring reactive species and oxidative damage in vivo and in cell culture: how should you do it and what do the results mean?" British Journal of Pharmacology **142**(2): 231-255.

Harriott, P. (1962). "Mass Transfer to Particles .1. Suspended in Agitated Tanks." AIChE Journal **8**(1): 93-101.

He, F., D. Y. Zhao, et al. (2007). "Stabilization of Fe-Pd nanoparticles with sodium carboxymethyl cellulose for enhanced transport and dechlorination of trichloroethylene in soil and groundwater." Industrial & Engineering Chemistry Research **46**(1): 29-34.

Henzler, T. and E. Steudle (2000). "Transport and metabolic degradation of hydrogen peroxide in Chara corallina: model calculations and measurements with the pressure probe suggest transport of H2O2 across water channels." Journal of Experimental Botany **51**(353): 2053-2066.

Hermanek, M., R. Zboril, et al. (2007). "Catalytic efficiency of iron(III) oxides in decomposition of hydrogen peroxide: Competition between the surface area and crystallinity of nanoparticles." Journal of the American Chemical Society **129**(35): 10929-10936.

Hestekin, J. A., L. G. Bachas, et al. (2001). "Poly(amino acid)-functionalized cellulosic membranes: Metal sorption mechanisms and results." Industrial & Engineering Chemistry Research **40**(12): 2668-2678.

Hinds, B. J., N. Chopra, et al. (2004). "Aligned multiwalled carbon nanotube membranes." Science **303**(5654): 62-65.

Hiraoka, K., H. Shin, et al. (1982). "Density-Measurements of Poly(Acrylic Acid) Sodium-Salts." Polymer Bulletin **8**(7-8): 303-309.

Ho, W. S. W. and K. K. Sirkar (1992). Membrane handbook. New York, Van Nostrand Reinhold.

Hollman, A. M. and D. Bhattacharyya (2004). "Pore-assembled multilayers of charged polypeptides in microporous membranes for ion separation." Langmuir **20**(13): 5418-5424.

Hu, K. and J. M. Dickson (2007). "Development and characterization of poly(vinylidene fluoride)-poly(acrylic acid) pore-filled pH-sensitive membranes." Journal of Membrane Science **301**(1-2): 19-28.

Hu, K. and J. M. Dickson (2009). "In vitro investigation of potential application of pH-sensitive poly(vinylidene fluoride)-poly(acrylic acid) pore-filled membranes for controlled drug release in ruminant animals." Journal of Membrane Science **337**(1-2): 9-16.

Huang, H. H., M. C. Lu, et al. (2001). "Catalytic decomposition of hydrogen peroxide and 2-chlorophenol with iron oxides." Water Research **35**(9): 2291-2299.

Inczedy, J. (1976). Analytical applications of complex equilibria. Chichester, Eng., E. Horwood.

Ireland, J. C., P. Klostermann, et al. (1993). "Inactivation of Escherichia-Coli by Titanium-Dioxide Photocatalytic Oxidation." Applied and Environmental Microbiology **59**(5): 1668-1670.

Ishihara, K., N. Hamada, et al. (1984). "Photoinduced Swelling Control of Amphiphilic Azoaromatic Polymer Membrane." Journal of Polymer Science Part a-Polymer Chemistry **22**(1): 121-128.

Ito, Y., S. Kotera, et al. (1990). "Control of Pore-Size of Polycarbonate Membrane with Straight Pores by Poly(Acrylic Acid) Grafts." Polymer **31**(11): 2157-2161.

Iversen, S. B., V. K. Bhatia, et al. (1997). "Characterization of microporous membranes for use in membrane contactors." Journal of Membrane Science **130**(1-2): 205-217.

Jirage, K. B., J. C. Hulteen, et al. (1997). "Nanotubule-based molecular-filtration membranes." Science **278**(5338): 655-658.

Joo, S. H., A. J. Feitz, et al. (2005). "Quantification of the oxidizing capacity of nanoparticulate zero-valent iron." Environmental Science & Technology **39**(5): 1263-1268.

Jung, H., B. Kwak, et al. (2008). "Attachment of cells to poly(styrene-co-acrylic acid) thin films with various charge densities." Colloids and Surfaces a-Physicochemical and Engineering Aspects **313**: 562-566.

Karppi, J., S. Akerman, et al. (2010). "Adsorption of metal cations from aqueous solutions onto the pH responsive poly(vinylidene fluoride grafted poly(acrylic acid) (PVDF-PAA) membrane." Journal of Polymer Research **17**(1): 71-76.

Karr, C. (1978). Analytical methods for coal and coal products. New York, Academic Press.

Keenan, C. R. and D. L. Sedlak (2008). "Factors affecting the yield of oxidants from the reaction of nanoparticulate zero-valent iron and oxygen." Environmental Science & Technology **42**(4): 1262-1267.

Kennedy, C. A. and W. C. Lennox (1997). "A pore-scale investigation of mass transport from dissolving DNAPL droplets." Journal of Contaminant Hydrology **24**(3-4): 221-246.

Khayet, M., K. C. Khulbe, et al. (2004). "Characterization of membranes for membrane distillation by atomic force microscopy and estimation of their water vapor transfer coefficients in vacuum membrane distillation process." Journal of Membrane Science **238**(1-2): 199-211.

Kidambi, S. and M. L. Bruening (2005). "Multilayered polyelectrolyte films containing palladium nanoparticles: synthesis, characterization, and application in selective hydrogenation." Journal of Materials Chemistry **17**(2): 301-307.

Kinoshita, T., M. Sato, et al. (1986). "Photocontrol of Polypeptide Membrane Functions by Cis-Trans Isomerization in Side-Chain Azobenzene Groups." Macromolecules **19**(1): 51-55.

Klein, E. (2000). "Affinity membranes: a 10-year review." Journal of Membrane Science **179**(1-2): 1-27.

Klein, G. W., K. Bhatia, et al. (1975). "Reaction of Oh with Benzoic-Acid - Isomer Distribution in Radical Intermediates." Journal of Physical Chemistry **79**(17): 1767-1774.

Knepper, M. A. (1994). "The Aquaporin Family of Molecular Water Channels." Proceedings of the National academy of Sciences of the United States of America **91**(14): 6255-6258.

Kohanski, M. A., D. J. Dwyer, et al. (2010). "How antibiotics kill bacteria: from targets to networks." Nature Reviews Microbiology **8**(6): 423-435.

Kosaka, K., H. Yamada, et al. (1998). "Comparison among the methods for hydrogen peroxide measurements to evaluate advanced oxidation processes: Application of a spectrophotometric method using copper(II) ion and 2.9 dimethyl-1,10-phenanthroline." Environmental Science & Technology **32**(23): 3821-3824.

Kumar, A., A. Srivastava, et al. (2007). "Smart polymers: Physical forms and bioengineering applications." Progress in Polymer Science **32**(10): 1205-1237.

Kwan, W. P. and B. M. Voelker (2003). "Rates of hydroxyl radical generation and organic compound oxidation in mineral-catalyzed Fenton-like systems." Environmental Science & Technology **37**(6): 1150-1158.

Ladhe, A. R., P. Frailie, et al. (2009). "Thiol-functionalized silica–mixed matrix membranes for silver capture from aqueous solutions: Experimental results and modeling." Journal of Membrane Science **326**(2): 460-471.

Laine, D. F. and I. F. Cheng (2007). "The destruction of organic pollutants under mild reaction conditions: A review." Microchemical Journal **85**(2): 183-193.

Lee, E. S., Z. G. Gao, et al. (2008). "Recent progress in tumor pH targeting nanotechnology." Journal of Controlled Release **132**(3): 164-170.

Lee, S. B., D. T. Mitchell, et al. (2002). "Antibody-based bio-nanotube membranes for enantiomeric drug separations." Science **296**(5576): 2198-2200.

Lee, Y. and W. Lee (2010). "Degradation of trichloroethylene by Fe(II) chelated with cross-linked chitosan in a modified Fenton reaction." Journal of Hazardous materials **178**(1-3): 187-193.

Leeper, D. B., K. Engin, et al. (1994). "Human Tumor Extracellular Ph as a Function of Blood-Glucose Concentration." International Journal of Radiation Oncology Biology Physics **28**(4): 935-943.

Letant, S. E., B. R. Hart, et al. (2003). "Functionalized silicon membranes for selective bio-organism capture." Nature Materials **2**(6): 391-396.

Lewis, S., A. Lynch, et al. (2009). "Chelate-Modified Fenton Reaction for the Degradation of Trichloroethylene in Aqueous and Two-Phase Systems." Environmental Engineering Science **26**(4): 849-859.

Lewis, S., V. Smuleac, et al. (2011). Iron - Based Treatability Study: Use of Nano-aggregates, Membrane Immobilized Nanoparticles, and Green Chemistry. Lexington, KY, University of Kentucky.

Lewis, S., V. Smuleac, et al. (2009). "Iron-Functionalized Membranes for Nanoparticle Synthesis and Reactions." Separation Science and Technology **44**(14): 3289-3311.

Li, K., M. I. Stefan, et al. (2007). "Trichloroethene degradation by UV/H2O2 advanced oxidation process: Product study and kinetic modeling." Environmental Science & Technology **41**(5): 1696-1703.

Li, W., H. Li, et al. (2009). "Preparation and investigation of PVDF/PMMA/TiO2 composite film." Journal of Materials Science **44**(11): 2977-2984.

Li, Y., L. G. Bachas, et al. (2005). "Kinetic studies of trichlorophenol destruction by chelate-based Fenton reaction." Environmental Engineering Science **22**(6): 756-771.

Li, Y. C., L. G. Bachas, et al. (2007). "Selected chloro-organic detoxifications by polychelate (Poly(acrylic acid)) and citrate-based Fenton reaction at neutral pH environment." Industrial & Engineering Chemistry Research **46**(24): 7984-7992.

Liang, L., X. D. Feng, et al. (1999). "Temperature-sensitive membranes prepared by UV photopolymerization of N-isopropylacrylamide on a surface of porous hydrophilic polypropylene membranes." Journal of Membrane Science **162**(1-2): 235-246.

Lin, S. S. and M. D. Gurol (1998). "Catalytic decomposition of hydrogen peroxide on iron oxide: Kinetics, mechanism, and implications." Environmental Science & Technology **32**(10): 1417-1423.

Liou, R.-M., S.-H. Chen, et al. (2004). "Catalytic oxidation of pentachlorophenol in contaminated soil suspensions by Fe^{+3}-resin/H_2O_2." Chemosphere **55**(9): 1271-1280.

Liu, H. C. and Y. Ito (2002). "Cell attachment and detachment on micropattern-immobilized poly(N-isopropylacrylamide) with gelatin." Lab on a Chip **2**(3): 175-178.

Lu, Y., Y. Mei, et al. (2006). "Thermosensitive core-shell particles as carriers for Ag nanoparticles: Modulating the catalytic activity by a phase transition in networks." Angewandte Chemie-International Edition **45**(5): 813-816.

Mackay, D. (2006). Handbook of physical-chemical properties and environmental fate for organic chemicals. Boca Raton, FL, CRC/Taylor & Francis.

Mackie, J. S. and P. Meares (1955). "The Diffusion of Electrolytes in a Cation-Exchange Resin Membrane .1. Theoretical." Proceedings of the Royal Society of London Series a-Mathematical and Physical Sciences **232**(1191): 498-509.

Maeda, H., G. Y. Bharate, et al. (2009). "Polymeric drugs for efficient tumor-targeted drug delivery based on EPR-effect." European Journal of Pharmaceutics and Biopharmaceutics **71**(3): 409-419.

Masten, S. J. and J. Hoigne (1992). "Comparison of Ozone and Hydroxyl Radical-Induced Oxidation of Chlorinated Hydrocarbons in Water." Ozone-Science & Engineering **14**(3): 197-214.

Mendelsohn, J. D., S. Y. Yang, et al. (2003). "Rational design of cytophilic and cytophobic polyelectrolyte multilayer thin films." Biomacromolecules **4**(1): 96-106.

Merkel, T. C., B. D. Freeman, et al. (2002). "Ultrapermeable, reverse-selective nanocomposite membranes." Science **296**(5567): 519-522.

Meyer, D. E., S. Hampson, et al. (2009). "A Study of Groundwater Matrix Effects for the Destruction of Trichloroethylene Using Fe/Pd Nanoaggregates." Environmental Progress & Sustainable Energy **28**(4): 507-518.

Miller, D. M., G. R. Buettner, et al. (1990). "Transition-Metals as Catalysts of Autoxidation Reactions." Free Radical Biology and Medicine **8**(1): 95-108.

Montgomery, J. H. (1996). Groundwater chemicals desk reference. Boca Raton, Fla., CRC Lewis Publishers.

Mopper, K. and X. L. Zhou (1990). "Hydroxyl Radical Photoproduction in the Sea and Its Potential Impact on Marine Processes." Science **250**(4981): 661-664.

Morgan, P. and R. J. Watkinson (1992). "Factors Limiting the Supply and Efficiency of Nutrient and Oxygen Supplements for the Insitu Biotreatment of Contaminated Soil and Groundwater." Water Research **26**(1): 73-78.

Mosmann, T. (1983). "Rapid Colorimetric Assay for Cellular Growth and Survival - Application to Proliferation and Cyto-Toxicity Assays." Journal of Immunological Methods **65**(1-2): 55-63.

Munson, B. R., D. F. Young, et al. (1998). Fundamentals of fluid mechanics. New York, Wiley.

Ng, A. N. L. and A. S. Kim (2007). "A mini-review of modeling studies on membrane bioreactor (MBR) treatment for municipal wastewaters." Desalination **212**(1-3): 261-281.

Noble, R. D. and S. A. Stern (1995). Membrane separations technology : principles and applications. Amsterdam ; New York, Elsevier.

Omenn, G. S. (2006). "Grand challenges and great opportunities in science, technology, and public policy." Science **314**(5806): 1696-1704.

Pandiyan, T., O. M. Rivas, et al. (2002). "Comparison of methods for the photochemical degradation of chlorophenols." Journal of Photochemistry and Photobiology a-Chemistry **146**(3): 149-155.

Papadopoulos, N. G., G. V. Z. Dedoussis, et al. (1994). "An Improved Fluorescence Assay for the Determination of Lymphocyte-Mediated Cytotoxicity Using Flow-Cytometry." Journal of Immunological Methods **177**(1-2): 101-111.

Park, H. B., C. H. Jung, et al. (2007). "Polymers with cavities tuned for fast selective transport of small molecules and ions." Science **318**(5848): 254-258.

Parra, S., L. Henao, et al. (2004). "Synthesis, testing, and characterization of a novel Nafion membrane with superior performance in photoassisted immobilized Fenton catalysis." Langmuir **20**(13): 5621-5629.

Patankar, S. V. (1980). Numerical heat transfer and fluid flow. New York, McGraw-Hill.

Patnaik, P. (2003). Handbook of Inorganic Chemicals, McGraw-Hill.

Pignatello, J. J., D. Liu, et al. (1999). "Evidence for an additional oxidant in the photoassisted Fenton reaction." Environmental Science & Technology **33**(11): 1832-1839.

Pignatello, J. J., E. Oliveros, et al. (2006). "Advanced oxidation processes for organic contaminant destruction based on the Fenton reaction and related chemistry." Critical Reviews in Environmental Science and Technology **36**(1): 1-84.

Poling, B. E., J. M. Prausnitz, et al. (2001). Properties of Gases and Liquids, McGraw-Hill.

Ravikumar, J. X. and M. D. Gurol (1994). "Chemical Oxidation of Chlorinated Organics by Hydrogen-Peroxide in the Presence of Sand." Environmental Science & Technology **28**(3): 394-400.

Reber, N., A. Kuchel, et al. (2001). "Transport properties of thermo-responsive ion track membranes." Journal of Membrane Science **193**(1): 49-58.

Reichert, C., W. H. Hoell, et al. (2004). "Mass transfer enhancement in stirred suspensions of magnetic particles by the use of alternating magnetic fields." Powder Technology **145**(2): 131-138.

Ritchie, S. M. C., L. G. Bachas, et al. (1999). "Surface modification of silica- and cellulose-based microfiltration membranes with functional polyamino acids for heavy metal sorption." Langmuir **15**(19): 6346-6357.

Rivett, M. O., S. Feenstra, et al. (2001). "A controlled field experiment on groundwater contamination by a multicomponent DNAPL: creation of the emplaced-source and overview of dissolved plume development." Journal of Contaminant Hydrology **49**(1-2): 111-149.

Roy-Perreault, A., B. H. Kueper, et al. (2005). "Formation and stability of polychlorinated biphenyl Pickering emulsions." Journal of Contaminant Hydrology **77**(1-2): 17-39.

Russell, H. H., J. E. Matthews, et al. (1992). TCE removal from contaminated soil and ground water. Ground water issue. [Ada, Okla.], United States Environmental Protection Agency, Office of Research and Development, Office of Solid Waste and Emergency Response : Superfund Technology Support Center for Ground Water, Robert S. Kerr Environmental Research Laboratory.

Schild, H. G. (1992). "Poly (N-Isopropylacrylamide) - Experiment, Theory and Application." Progress in Polymer Science **17**(2): 163-249.

Schofield, R. W., A. G. Fane, et al. (1990). "Gas and Vapor Transport through Microporous Membranes .2. Membrane Distillation." Journal of Membrane Science **53**(1-2): 173-185.

Seol, Y. and I. Javandel (2008). "Citric acid-modified Fenton's reaction for the oxidation of chlorinated ethylenes in soil solution systems." Chemosphere **72**(4): 537-542.

Sexton, J. L. (2006). Lithologic and stratigraphic compilation of nearsurface sediments for the Paducah Gaseous Diffusion Plant. Lexington, KY, University of Kentucky. **Masters Thesis**.

Sgarlata, C., G. Arena, et al. (2008). "Heavy metal separation with polymer inclusion membranes." Journal of Membrane Science **323**(2): 444-451.

Shah, T. N., J. C. Goodwin, et al. (2005). "Development and characterization of a microfiltration membrane catalyst containing sulfonated polystyrene grafts." Journal of Membrane Science **251**(1-2): 81-89.

Shannon, M. A., P. W. Bohn, et al. (2008). "Science and technology for water purification in the coming decades." Nature **452**(7185): 301-310.

Shao, L. and J. L. Lutkenhaus (2010). "Thermochemical properties of free-standing electrostatic layer-by-layer assemblies containing poly(allylamine hydrochloride) and poly(acrylic acid)." Soft Matter **6**(14): 3363-3369.

Shi, W., Y. Shen, et al. (2008). "Functionalized anodic aluminum oxide (AAO) membranes for affinity protein separation." Journal of Membrane Science **325**(2): 801-808.

Singh, N., J. Wang, et al. (2008). "Surface initiated atom transfer radical polymerization: a new method for preparation of polymeric membrane adsorbers." Journal of Membrane Science **309**(1-2): 64-72.

Smuleac, V., D. A. Butterfield, et al. (2006). "Layer-by-layer-assembled microfiltration membranes for biomolecule immobilization and enzymatic catalysis." Langmuir **22**(24): 10118-10124.

Spohr, R., N. Reber, et al. (1998). "Thermal control of drug release by a responsive ion track membrane observed by radio tracer flow dialysis." Journal of Controlled Release **50**(1-3): 1-11.

Srisurichan, S., R. Jiraratananon, et al. (2006). "Mass transfer mechanisms and transport resistances in direct contact membrane distillation process." Journal of Membrane Science **277**(1-2): 186-194.

Stamatialis, D. F., B. J. Papenburg, et al. (2008). "Medical applications of membranes: Drug delivery, artificial organs and tissue engineering." Journal of Membrane Science **308**(1-2): 1-34.

Stookey, L. L. (1970). "Ferrozine - A new spectrophotometric reagent for iron." Analytical Chemistry **42**(7): 779-781.

Struse, A. M., R. L. Siegrist, et al. (2002). "Diffusive transport of permanganate during in situ oxidation." Journal of Environmental Engineering-Asce **128**(4): 327-334.

Stuart, M. A. C., W. T. S. Huck, et al. (2010). "Emerging applications of stimuli-responsive polymer materials." Nature Materials **9**(2): 101-113.

Sun, Y. F. and J. J. Pignatello (1992). "Chemical Treatment of Pesticide Wastes - Evaluation of Fe(Iii) Chelates for Catalytic Hydrogen-Peroxide Oxidation of 2,4-D at Circumneutral Ph." Journal of Agricultural and Food Chemistry **40**(2): 322-327.

Teare, D. O. H., N. Emmison, et al. (2000). "Cellular attachment to ultraviolet ozone modified polystyrene surfaces." Langmuir **16**(6): 2818-2824.

Tee, Y. H., E. Grulke, et al. (2005). "Role of Ni/Fe nanoparticle composition on the degradation of trichloroethylene from water." Industrial & Engineering Chemistry Research **44**(18): 7062-7070.

Teel, A. L., C. R. Warberg, et al. (2001). "Comparison of mineral and soluble iron Fenton's catalysts for the treatment of trichloroethylene." Water Research **35**(4): 977-984.

Valko, M., H. Morris, et al. (2005). "Metals, toxicity and oxidative stress." Current Medicinal Chemistry **12**(10): 1161-1208.

Vanstroebiezen, S. A. M., F. M. Everaerts, et al. (1993). "Diffusion-Coefficients of Oxygen, Hydrogen-Peroxide and Glucose in a Hydrogel." Analytica Chimica Acta **273**(1-2): 553-560.

Vasudevan, T., S. Das, et al. (2009). "Pore-functionalized polymer membranes for preconcentration of heavy metal ions." Talanta **78**(1): 171-177.

Voelker, B. M. and B. Sulzberger (1996). "Effects of fulvic acid on Fe(II) oxidation by hydrogen peroxide." Environmental Science & Technology **30**(4): 1106-1114.

Vogel, T. M., C. S. Criddle, et al. (1987). "Transformations of Halogenated Aliphatic-Compounds." Environmental Science & Technology **21**(8): 722-736.

Wandera, D., S. R. Wickramasinghe, et al. (2010). "Stimuli-responsive membranes." Journal of Membrane Science **357**(1-2): 6-35.

Wang, Q. Q. and A. T. Lemley (2001). "Kinetic model and optimization of 2,4-D degradation by anodic Fenton treatment." Environmental Science & Technology **35**(22): 4509-4514.

Watts, R. J., J. Howsawkeng, et al. (2005). "Destruction of a carbon tetrachloride dense nonaqueous phase liquid by modified Fenton's reagent." Journal of Environmental Engineering-Asce **131**(7): 1114-1119.

Watts, R. J., S. Kong, et al. (1994). "Oxidation of Sorbed Hexachlorobenzene in Soils Using Catalyzed Hydrogen-Peroxide." Journal of Hazardous materials **39**(1): 33-47.

Watts, R. J. and A. L. Teel (2005). "Chemistry of modified Fenton's reagent (catalyzed H2O2 propagations-CHP) for in situ soil and groundwater remediation." Journal of Environmental Engineering-ASCE **131**(4): 612-622.

Watts, R. J. and A. L. Teel (2006). "Mechanism for the destruction of carbon tetrachloride and chloroform DNAPLs by modified Fenton's reagent." Journal of Contaminant Hydrology **85**(3-4): 229-246.

Watts, R. J. and A. L. Teel (2006). "Treatment of Contaminated Soils and Groundwater Using ISCO." Practice Periodical of Hazardous, Toxic, and Radioactive Waste Management **10**(1): 2-9.

Welch, K. D., T. Z. Davis, et al. (2002). "Deleterious iron-mediated oxidation of biomolecules." Free Radical Biology and Medicine **32**(7): 577-583.

Wilke, C. R. and P. Chang (1955). "Correlation of Diffusion Coefficients in Dilute Solutions." AIChE Journal **1**(2): 264-270.

Winnik, F. M., A. Morneau, et al. (1998). "Polyacrylic acid pore-filled microporous membranes and their use in membrane-mediated synthesis of nanocrystalline ferrihydrite." Canadian Journal of Chemistry **76**(1): 10-17.

Wolff, S. P., A. Garner, et al. (1986). "Free-Radicals, Lipids and Protein-Degradation." Trends in Biochemical Sciences **11**(1): 27-31.

Xu, J. and D. Bhattacharyya (2005). "Membrane-based bimetallic nanoparticles for environmental remediation: Synthesis and reactive properties." Environmental Progress **24**(4): 358-366.

Xu, J. and D. Bhattacharyya (2007). "Fe/Pd nanoparticle immobilization in microfiltration membrane pores: Synthesis, characterization, and application in the dechlorination of polychlorinated biphenyls." Industrial & Engineering Chemistry Research **46**(8): 2348-2359.

Xu, J. and D. Bhattacharyya (2008). "Modeling of Fe/Pd nanoparticle-based functionalized membrane reactor for PCB dechlorination at room temperature." Journal of Physical Chemistry C **112**(25): 9133-9144.

Xu, J., A. Dozier, et al. (2005). "Synthesis of nanoscale bimetallic particles in polyelectrolyte membrane matrix for reductive transformation of halogenated organic compounds." Journal of Nanoparticle Research **7**(4-5): 449-467.

Yamauchi, T., E. Kokufuta, et al. (1993). "Electrically Controlled Protein Permeation through a Polyelectrolyte Gel Membrane." Abstracts of Papers of the American Chemical Society **205**: 105-COLL.

Yang, W. C., R. Xie, et al. (2008). "Preparation and characterization of dual stimuli-responsive microcapsules with a superparamagnetic porous membrane and thermo-responsive gates." Journal of Membrane Science **321**(2): 324-330.

Yaron-Marcovich, D., I. Dror, et al. (2007). "Behavior and stability of organic contaminant droplets in aqueous solutions." Chemosphere **69**(10): 1593-1601.

Yashima, E., J. Noguchi, et al. (1995). "Photocontrolled Chiral Recognition by [4-(Phenylazo)Phenyl] Carbamoylated Cellulose and Amylose Membranes." Macromolecules **28**(24): 8368-8374.

Yasunaga, N. and J. Hirotsuji (2008). "Efficient decomposition of trichloroethylene (TCE) in groundwater by ozone-hydrogen peroxide treatment." Ozone-Science & Engineering **30**(2): 127-135.

Yaws, C. L. (1999). Chemical Properties Handbook, McGraw-Hill.

Nomenclature

Chapter 4

C_D	drag coefficient (dimensionless)
$D_{TCE\text{-}water}$	diffusion coefficient (m^2/s)
Fe	total quantity of all iron species (mmol)
$(H_2O_2)_0$	initial total quantity of hydrogen peroxide (mmol)
$[H_2O_2]$	hydrogen peroxide concentration (mmol/L)
$[H_2O_2]_0$	initial hydrogen peroxide concentration (mmol/L)
k_c	mass transfer coefficient (m/s)
k'_{TCE}	fitted first-order rate constant for constant [OH•] model (s^{-1})
k''_{TCE}	observed rate constant for varying [OH•] model (dimensionless)
M_{TCE}	molecular weight of TCE (g/mol)
n	number of TCE droplets (dimensionless)
[OH•]	hydroxyl radical concentration (mmol/L)
R	droplet radius (m)
Re	Reynolds number (dimensionless)
S	surface area of single droplet (m^2)
Sc	Schmidt number (dimensionless)
Sh	Sherwood number (dimensionless)
TCE_0	initial total quantity of TCE (mmol)
$[TCE]_{aq}$	aqueous-phase TCE concentration (mmol/L)
$[TCE]_{aq,0}$	initial aqueous-phase TCE concentration (mmol/L)
$[TCE]_{sat}$	TCE saturation concentration (mmol/L)
U	velocity of droplet relative to surrounding fluid (m/s)
V	reactor volume (L)
W_r	mass flux in radial direction (mmol s^{-1} m^{-2})
α	proportionality constant relating [OH•] and $d[H_2O_2]/dt$ (Equations 4.19, 4.20) (s)

δ	droplet coundary layer thickness (m)
ν	kinematic viscosity of water (m^2/s)
ρ_{TCE}	density of TCE (g/m^3)

Chapters 5 and 6

D_{AB}	diffusion coefficient of a solute, A, in a liquid solvent, B, ($m^2\ s^{-1}$)
D_{Ag}	diffusion coefficient of the solute in the hydrogel ($m^2\ s^{-1}$)
$D_{H2O2,aq}$	diffusion coefficient of H_2O_2 in water ($m^2\ s^{-1}$)
$D_{H2O2,PAA}$	diffusion coefficient of H_2O_2 in the hydrated PAA gel ($m^2\ s^{-1}$)
$[H_2O_2]_0$	concentration of H_2O_2 before entering the membrane pore (mol m^{-3})
$[H_2O_2]_{aq}$	concentration of H_2O_2 in the membrane pore's non-gel portion (mol m^{-3})
$[H_2O_2]_{in}$	concentration H_2O_2 entering the reactor (mol m^{-3})
$[H_2O_2]_{initial}$	initial concentrations of H_2O_2 in the PAA gel (mol m^{-3})
$[H_2O_2]_{PAA}$	concentration of H_2O_2 in the PAA domain (mol m^{-3})
J_V	volumetric solution flux ($cm^3\ cm^{-2}\ s^{-1}$)
$J_{V,max}$	maximum volumetric solution flux ($cm^3\ cm^{-2}\ s^{-1}$)
$J_{V,min}$	minimum volumetric solution flux ($cm^3\ cm^{-2}\ s^{-1}$)
L	membrane thickness (m)
L'	tortuous pore length (m)
M_B	molecular weight of the solvent (g mol^{-1})
$[OH\bullet]_{in}$	concentration OH• entering the reactor (mol m^{-3})
$[OH\bullet]_{initial}$	initial concentrations of OH• in the PAA gel (mol m^{-3})
Pe	Peclet number (dimensionless)
Q	total volumetric flowrate through the membrane ($m^3\ s^{-1}$)
R_1	effective radius of core region of PVDF-PAA pore (m)
$R_{1,max}$	maximum effective radius of core region of PVDF-PAA pore (m)
$R_{1,min}$	minimum effective radius of core region of PVDF-PAA pore (m)
R_2	effective radius of unmodified PVDF pore (m)
r_{H2O2}	rate law governing the decomposition of H_2O_2 (mol $m^{-3}\ s^{-1}$)
R_{pore}	pore radius (m)

r_S	radius of the solute (Å)
U_{avg}	average fluid velocity (m s^{-1})
U_{max}	maximum fluid velocity (m s^{-1})
U(r)	velocity profile of the solution permeating through membrane pore (m s^{-1})
$V_{membrane}$	total membrane volume (m^3)
V_{PAA}	volume of PAA gel in one PVDF-PAA membrane pore (m^3)
$V_{PAA,max}$	maximum volume of PAA gel in one PVDF-PAA membrane pore (m^3)
$V_{PAA,min}$	minimum volume of PAA gel in one PVDF-PAA membrane pore (m^3)
ΔP	pressure drop across the membrane thickness (Pa)
ε	initial porosity of the unmodified membrane (%)
μ	dynamic viscosity of water (kg m^{-1} s^{-1})
$\nu_{A,boil}$	molar volume of the solute at its normal boiling point (m^3 $kmol^{-1}$)
$\nu_{A,critical}$	critical volume of the solute (m^3 $kmol^{-1}$)
φ	volume fraction of the polymer in the gel (dimensionless)
Φ	association factor of a given solvent (dimensionless)
τ	residence time (s)
τ_{pore}	pore tortuosity (dimensionless)

Vita

Scott Romak Lewis was born on the 22nd of July, 1985 in Huntington, WV. He was raised in Ashland, KY where he graduated from Paul G. Blazer HS in 2003. He received his B.S. degree in Chemical Engineering from the University of Kentucky in 2006 after which he began pursuing his Ph.D. in Chemical Engineering under the guidance of Prof. Dibakar Bhattacharyya at the University of Kentucky.

Awards/Honors:

- NSF-IGERT Fellow - (Fall 2007 – present)
- Graduate Certificate in Bioactive Interfaces and Devices. Focus: novel bioactive architectures, cell/protein interactions at interfaces, and integration in devices. (August 2010)
- 3rd Place in Division (formation, preparation, synthesis) for work entitled Iron-Polymer Composite Membranes for Oxidative Reactions". Scott Lewis, J. Amundson, E. Coker, A. Montague, S. Daunert, and D. Bhattacharyya at NAMS/ICIM Annual Meeting in Washington, D.C. (July 2010)
- Received Elias Klein Founders' travel award for NAMS 2010 meeting (July 2010)
- 3rd Place in Division for work entitled "Iron-Functionalized MF Membranes for Hydroxyl Radical Reactions". Scott Lewis, A. Montague, S. Daunert, and D. Bhattacharyya at NAMS Annual Meeting in Charleston, SC (June 2009)

Publications:

- Lewis, S.; Bhattacharyya, D. "Modeling Approach to Free Radical Reactions in the Membrane Domain" *to be submitted to J. Phys. Chem. C (2011)*.
- Lewis, S.; Datta, S.; Gui, M.; Coker, E.; Huggins, F.; Daunert, S.; Bachas, L.; Bhattacharyya, D. "Reactive Nanostructured Membranes for Water Purification" (in press) *PNAS*.
- Lewis, S.; Smuleac, V.; Montague, A.; Bachas, L.; Bhattacharyya, D. "Iron-Functionalized Membranes for Nanoparticle Synthesis and Reactions" (2009) *Separation Science and Technology*, 44 (14): 3289-3311.

- Lewis, S.; Lynch, A.; Bachas, L.; Hampson, S.; Ormsbee, L.; Bhattacharyya, D. "Chelate-Modified Fenton Reaction for the Degradation of Trichloroethylene in Aqueous and Two-Phase Systems" (2009) *Environmental Engineering Science*, 26 (4): 849-859.

Professional Conference Presentations (Poster/Oral):

- "Iron-Based Functionalized Materials for Free Radical-Mediated Toxic Organic Degradation". Scott Lewis, M. Gui, L. Bachas, D. Sedlak, L. Ormsbee, and D. Bhattacharyya. National Institute of Environmental Health Sciences / Superfund Research Program Annual Meeting, Portland, OR, November 2010 – Poster

- "Overview of Iron-Functionalized Oxidative Membrane Platforms for Water Treatment". Scott Lewis, E. Coker, S. Daunert, and D. Bhattacharyya. American Institute of Chemical Engineers Annual Meeting, Salt Lake City, UT, November 2010 – Oral

- "Iron-Polymer Composite Membranes for Oxidative Reactions". Scott Lewis, J. Amundson, E. Coker, A. Montague, S. Daunert, and D. Bhattacharyya. North American Membrane Society / International Conference on Inorganic Membranes (NAMS/ICIM) Annual Meeting, Washington, D.C., July 2010 – Oral and Poster

- "Functionalized Membranes for Iron Capture and Subsequent Free Radical Reactions". Scott Lewis, A. Montague, S. Daunert, and D. Bhattacharyya. American Institute of Chemical Engineers (AIChE) Annual Meeting, Nashville, TN, November 2009 – Oral

- "Toxic Organic Destruction Using Iron-Functionalized Materials". Scott Lewis, V. Smuleac, Y. Li, J. Xu, L. Bachas, L. Ormsbee, S. Daunert, and D. Bhattacharyya. National Institute of Environmental Health Sciences / Superfund Research Program (NIEHS/SRP) Annual Meeting, New York, NY, November 2009 – Poster

- "Chelate-Modified and Membrane-Immobilized Fenton Reactions for Remediation". Scott Lewis, A. Montague, V. Smuleac, S. Daunert, L. Bachas, and D. Bhattacharyya. 8th World Congress of Chemical Engineering (WCCE8), Montreal, QC, Canada, August 2009 – Poster

- "Iron-Functionalized MF Membranes for Hydroxyl Radical Reactions". Scott Lewis, A. Montague, S. Daunert, and D. Bhattacharyya. NAMS Annual Meeting, Charleston, SC, June 2009 – Oral and Poster

- "Toxic Organic Degradation by Immobilized Nanoparticles and Free Radical Reactions". Scott Lewis, V. Smuleac, J. Xu, L. Bachas, and D. Bhattacharyya.

National Association of Remedial Project Managers (NARPM) Annual Meeting, Atlanta, GA, June 2009 – Poster

- "TCE Droplet Degradation and Membrane-Immobilized Fenton Reaction". Scott Lewis, Y. Li, L. Bachas, L. Ormsbee, S. Daunert, and D. Bhattacharyya. NIEHS/SBRP Annual Meeting, Pacific Grove, CA, December 2008 – Poster

- "Chelate-Modified Hydroxyl Radical Reactions for Detoxification of Chlorinated Organics: Experimental Results and Model Development". Scott Lewis, Y. Li, A. Montague, S. Daunert, L. Bachas, and D. Bhattacharyya. AIChE Annual Meeting, Philadelphia, PA, November 2008 – Oral

- "Environmentally Important Oxidative and Reductive Reactions with Functionalized Membranes". Scott Lewis, Y. Li, J. Xu, S. Daunert, L. Bachas, and D. Bhattacharyya. International Congress on Membranes and Membrane Science (ICOM), Honolulu, HI, July 2008 – Poster

- "Chloro-Organic Degradation by Nanosized Metallic Systems and by Hydroxyl Radical Reaction". Scott Lewis, D. Meyer, Y.C. Li, S. Datta, L. Bachas, J. Xu, and D. Bhattacharyya. NIEHS/SBRP Annual Meeting, Durham, NC, December 2007 – Poster

- "Chelate-Modified Fenton Reaction for the Destruction of Trichloroethylene in Two-Phase Systems". Scott Lewis, Y. Li, D. Ahuja, L. Bachas, and D. Bhattacharyya. AIChE Annual Meeting, Salt Lake City, UT, November 2007 – Oral

- "Nanotechnology and Oxidative Techniques for Remediation". Scott Lewis, D. Meyer, Y. Li, J. Xu, L. Bachas, D. Bhattacharyya. Kentucky Research Consortium for Energy and the Environment Scientific and Technical Symposium, Lexington, KY, October 2007 – Oral

- "Destruction of Chlorinated Organics from Contaminated Water by Chelate-Modified Fenton Reaction". Scott Lewis, Y. Li, D. Ahuja, L. Bachas, and D. Bhattacharyya. Engineering Conferences International (ECI) - Water Treatment and Re-Use II, Tomar, Portugal, February 2007 – Poster